U.S.NRC
United States Nuclear Regulatory Commission
Protecting People and the Environment

Assessment of Graphite Properties and Degradation Including Source Dependence

August 2021

PREPARED FOR:

U.S. NUCLEAR REGULATORY COMMISSION
CONTRACT NO. NRC-HQ-25-14-E-0004
TASK ORDER NO. 31310018F019

PREPARED BY:

NUMARK Associates Inc.
M. Srinivasan, B. Marsden, W. von Lensa, L. Cronise, R. Turk in conjunction with the U.S. Nuclear Regulatory Commission

PROGRAM MANAGERS:

Office of Nuclear Regulatory Research, U.S. Nuclear Regulatory Commission
M. Gordon, R. Iyengar

This report does not contain or imply legally binding requirements, nor does it establish or modify any regulatory guidance or positions of the U.S. Nuclear Regulatory Commission, and it is not binding on the Commission.

EXECUTIVE SUMMARY

This report contains research information related to nuclear graphite properties that are significant for nonlight-water high-temperature reactors (HTRs). This research is part of a collection of reference information that the U.S. Nuclear Regulatory Commission (NRC) will use to inform licensing decisions and regulatory guidance for the construction of nonlight-water HTRs. The NRC anticipates HTRs to use nuclear-grade graphite in many core components. The properties of graphite and the resistance of graphite to HTR environments are heavily influenced by the source material and fabrication method. This report contains experimental data on properties important to the performance of graphite components for a variety of graphites used in previously operated and currently operating gas-cooled reactors and graphites proposed for the Next Generation Nuclear Plant project.

This report reviews how the source material and processing parameters impact strength, Young's modulus, thermal conductivity, coefficient of thermal expansion, and fracture toughness of unirradiated graphites. It also examines how these variables affect graphite degradation as a result of irradiation. Because of the scarcity of publicly available data on irradiated graphites and their uncertainties, as well as incomplete manufacturing and microstructural information, it is very difficult to discern the influence of these variables on the properties of irradiated graphite.

American Society for Testing and Materials (ASTM) nuclear graphite specifications D7219, "Standard Specification for Isotropic and Near-isotropic Nuclear Graphites," and D7301, "Standard Specification for Nuclear Graphite Suitable for Components Subjected to Low Neutron Irradiation Dose," have addressed concerns arising from variations in raw material and other mix formulations for graphite manufacture, the processing methods used, and the purity needs for meeting particular challenges in an HTR environment. ASTM specifications have also addressed concerns about the variability in properties that are observed between component-sized billets and within billets, by including specific requirements for sampling and testing.

This report contains information on the limited research conducted on laboratory-scale graphites with variations in processing that have been irradiated and properties determined. There is no evidence, however, that the results of these experiments have played any role in optimizing graphite manufacturing on a commercial scale. To bridge this gap, the appendices contain a thorough evaluation of thermal and mechanical properties before and after irradiation of four modern nuclear-grade graphites.

TABLE OF CONTENTS

LIST OF FIGURES

LIST OF TABLES

ACKNOWLEDGMENTS

ABBREVIATIONS AND ACRONYMS

°C	degrees Celsius
°F	degrees Fahrenheit
AG	against-grain
AGL	Anglo Great Lakes
AGR	advanced gas reactor
ARDC	advanced reactor design criteria
ASME	American Society of Mechanical Engineers
ASTM	American Society for Testing and Materials
AVR	Arbeitsgemeinschaft Versuchsreaktor
BAEL	British Acheson Electrodes Limited
BET	Brunauer–Emmett–Teller
C	Celsius
Ca	calcium
CO_2	carbon dioxide
CR	chemical regime
CTE	coefficient of (linear) thermal expansion
DC	design criteria
DCP	delayed coking process
DDN	design data need(s)
DOD	degree of disorder
DOE	U.S. Department of Energy
dpa	displacements per atom
DR	diffusion regime
EGCA	European Carbon and Graphite Association
F	Fahrenheit
Fe	iron
g/cm^3	grams per cubic centimeter
GA	General Atomics, Inc.
GCC	graphite core component
GDC	general design criterion/criteria
GPa	gigapascal
GR	gaseous phase transfer regime
HTGR	high-temperature gas-cooled reactor
HTR	high-temperature reactor
HTTR	high-temperature engineering test reactor
IAEA	International Atomic Energy Agency
IAEA-TECDOC	IAEA Technical Document [a category of IAEA publication]
ISO	International Standards Organization
JAEA	Japanese Atomic Energy Agency
kilocalorie per calorie	kJ/cal
kilojoule per mole	kJ/mol
LWR	light-water reactor
MAGNOX	magnesium alloy graphite moderated gas-cooled uranium oxide reactor

MHTGR	modular high-temperature gas-cooled reactor
μm	micrometer
μΩm	micro-ohm meter
mb	millibarn
mm	millimeter
Mg/m^3	mega gram per cubic meter
MPa	megapascal
nm	nanometer
NGNP	Next Generation Nuclear Plant
NRC	U.S. Nuclear Regulatory Commission
Ω/m	ohm per meter
Pa	pascal
PBMR	pebble bed modular reactor, Pebble Bed Modular Reactor (Pvt), Ltd.
PDC	principal design criterion/criteria
PGA	Pile Grade A (graphite)
PGB	Pile Grade B (graphite)
PIRT	phenomena identification and ranking table
POCO	a graphite manufacturer
ppm	parts per million
PSD	particle size distribution
QI	quinoline insoluble
RG	regulatory guide
SARRDL	specified acceptable system radionuclide release design limit
SFR	sodium-cooled fast reactor
SGL	Sigri Great Lakes
SRC	solvent refined coal
t	ton
THTR	thorium high-temperature reactor
U.K.	United Kingdom
U.S.	United States
UCAR	Union Carbide
UHTREX	ultra-high-temperature reactor experiment (reactor)
vol.%	volume percent
W/m°K	Watts per meter degree Kelvin
wt.%	weight percent
XRD	x-ray diffraction
XRF	x-ray fluorescence

1   INTRODUCTION

This document describes the results of focused research to obtain and review experimental data and operational experience relevant to the performance of graphite in high-temperature gas-cooled reactors (HTGRs). This report contains information on significant properties of several past and present nuclear graphites and a discussion of primary drivers for variations observed in these properties. It assesses the effects of the source material and processing parameters upon unirradiated graphite properties (e.g., strength, Young's modulus, fracture toughness, and the coefficient of thermal expansion (CTE). It also assesses the impact of the source material and processing parameters upon graphite degradation mechanism environments (e.g., irradiation effects, resistance to moisture, and oxygen ingress).

1.1   Background

Because of the nature of graphite manufacture, graphite's crystalline structure and distributed porosity vary from batch to batch and within a batch. Also, variations from billet to billet, and within billets, are also common. As a result, variability in properties is commonly observed. Additionally, pertaining to the use of graphites in nuclear reactors, irradiation alters the structure of the graphite body by changing both the physical dimensions of crystalline graphite and the porosity. Such microstructural changes result in difference between the irradiated properties and the unirradiated properties. The American Society of Mechanical Engineers (ASME) Boiler and Pressure Vessel Code, Section III, "Rules for Construction of Nuclear Facility Components," Division 5, "High Temperature Reactors" (ASME, 2017), requires variations in graphite properties to be considered in the design of the graphite core components (GCCs) and the graphite core assembly, as discussed in the U.S. Nuclear Regulatory Commission's (NRC's) assessment of the ASME Boiler and Pressure Vessel Code (NRC, 2020).

In assembling and studying graphite properties, this research was informed by several regulatory and design requirements for HTGRs contained in regulatory, consensus code, and consensus materials standards documents. These included, for example, the following:

- NRC Regulatory Guide (RG) 1.232, "Guidance for Developing Principal Design Criteria for Non-Light-Water Reactors"

- ASME Boiler and Pressure Vessel Code, Section III, Division 5 (ASME, 2017)

- American Society for Testing and Materials (ASTM) D7219-08, "Standard Specification for Isotropic and Near-isotropic Nuclear Graphites"

- ASTM D7301-08, "Standard Specification for Nuclear Graphite Suitable for Components Subjected to Low Neutron Irradiation Dose"

The literature survey and documents accessed included the sources shown in Figure 1-1.
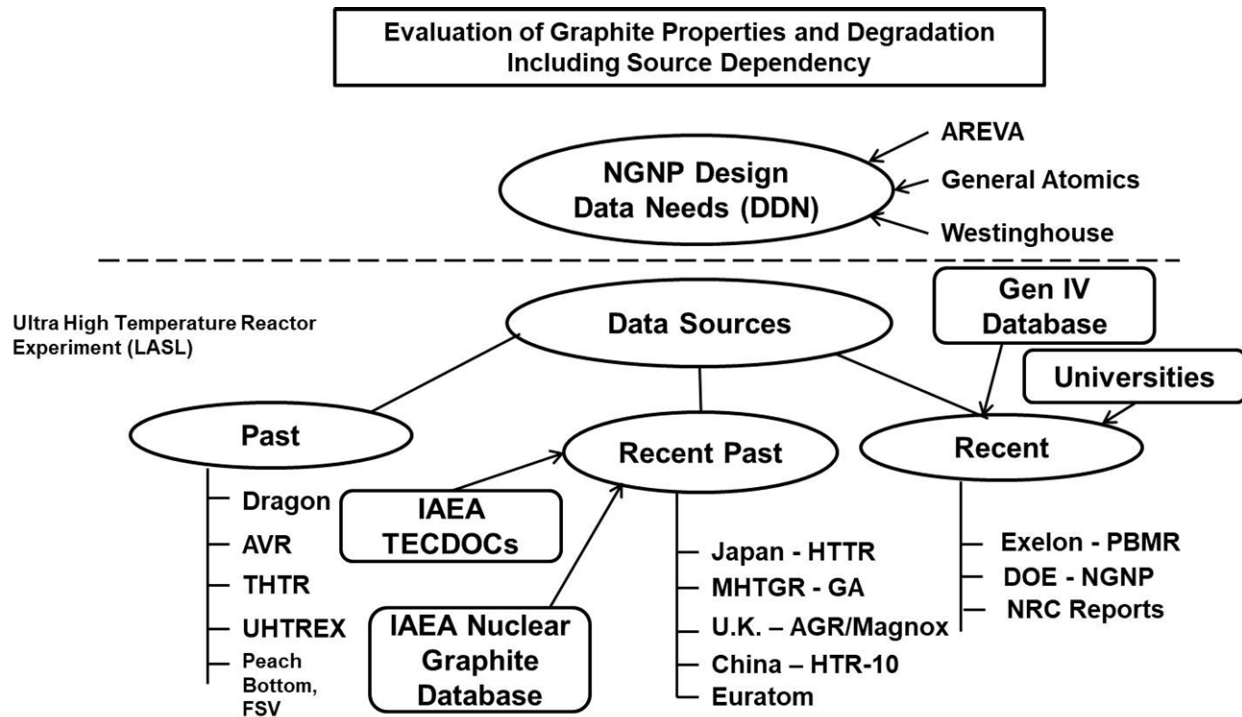
Figure 1-1 Information sources used in this research for evaluating the effect of source and processing parameters upon graphite properties

The data sources used for this research, as shown in Figure 1-1, consisted of industry reports; reports generated by various national laboratories; technical reports and conference proceedings generated by the International Atomic Energy Agency (IAEA), the NRC, and the Office for Nuclear Regulation—United Kingdom; presentations made at various International Nuclear Graphite Specialists Meetings; and research reports and technical journals published by universities.

1.2   Basis for studying specific properties

Graphite properties were chosen for study in this research based on a number of factors that drive assurance of reactor safety under all operational conditions. IAEA Safety Standards require a nuclear power plant to ensure the following fundamental safety functions for all plant states (IAEA, 2016):

- control of reactivity
- removal of heat from the reactor and from the fuel
- confinement of radioactive material, shielding against radiation, and control of planned radioactive releases, as well as limitation of accidental radioactive releases

Thus, for an HTGR graphite core, designed features include the following:

- core stability, durability
- unobstructed coolant pathways

- unobstructed control rod access
- unobstructed fuel rod and fuel movement

These design aspects are important from a safety perspective and must be addressed throughout the life of the reactor. Therefore, this research examines the important graphite properties related to these design features for the operational life of the reactor.

Subpart A, "Graphite Materials," of Subsection HH, "Class A Nonmetallic Core Support Structures," of ASME Boiler and Pressure Vessel Code, Section III, contains design requirements for GCCs and the graphite core assembly. Basically, the design rules require the assurance of the functionality of the core by ensuring the following:

- unhindered movement of control rods and fuel rods
- continued adequate cooling of the fuel and the core
- continued ability to charge and discharge fuel

The methodology for the safety assessment of the core requires a demonstration of the following:

- no component failure
- geometrical stability of the structure
- material properties bounded by a database

All of the above are thus determined by graphite properties and the changes that occur to these properties as a function of the graphite component location in the core, time-dependent temperature, and fluence. These variables also include potential chemical reactions between the graphite component and the impurities or the constituents of the gas coolant, or the liquid coolant in the case of molten salt reactors.

Typical components with design-specific property requirements include the following:

- moderator blocks
- reflector blocks (side, top, bottom)
- fuel blocks
- support columns
- dowels, keys
- tube housing fuel pins (in a prismatic design)

An important aspect in analyzing graphite properties is the different focus it requires from analyzing metals and alloys in their application in nuclear reactors. Graphite is a special ceramic, manufactured in quite a different manner than the metals and alloys, which are typically formed by melting and casting. Typical powder metallurgical techniques are not directly applicable because the bonding is not established through the formation of a liquid phase, or liquid phase sintering. Nuclear graphite manufacture involves heat treatment at

temperatures equal to or exceeding 2,800 degrees Celsius (C) (5,072 degrees Fahrenheit (F)). Inhomogeneity is intrinsic in its manufacture and the resulting product.

The analysis of physical, mechanical, thermal, and chemical properties of graphite thus is different from that of metals and alloys. Table 1-1 shows a few fundamental differences between steels and graphite that are necessary to acknowledge in analyzing graphite properties.

Table 1-1 Fundamental differences in the properties and behavior of steel and graphite

Steel	Nuclear graphite (Ceramic)
Region of linear elastic stress-strain behavior	Always nonlinear stress-strain behavior
Yield stress can be defined	Yield stress is not definable
High tensile strength, fracture strain, and fracture toughness	Low tensile strength, fracture strain, and fracture toughness
Small scatter of the strength data	Large scatter of the strength data
Strength decreases with increasing temperature	Strength increases with increasing temperature
Relief of peak stresses due to plasticity	Relief of peak stresses by microcracking
Local peak stresses are uncritical	Local peak stresses can cause damage
Crack initiation depends on the primary stress	Crack initiation depends on the total stress
Material properties are dependent on thermal neutron flux	Material properties are independent of thermal neutron flux
Fast neutron flux influences the material properties (raises the nil ductility temperature)	Fast neutron flux changes all material properties and induces dimensional change and creep

It is notable that neutron irradiation changes all graphite properties. Primarily, the irradiation-induced dimensional change is of concern because it affects the core geometry. Internal stresses generated by this phenomenon, if not accommodated or relieved, could result in the initiation and propagation of cracks in the graphite component.

RG 1.232 provides detailed guidance on developing principal design criteria (PDC) for any nonlight-water reactor (LWR) designs for nuclear power plants, as required by the applicable NRC regulations. The RG also describes the NRC's proposed guidance for modifying and supplementing Appendix A, "General Design Criteria" (GDC), to Part 50, "Domestic licensing of production and utilization facilities," of Title 10 of the *Code of Federal Regulations*, to develop PDC that address two specific non-LWR design concepts: sodium-cooled fast reactors (SFRs) and modular high-temperature gas-cooled reactors (MHTGRs). The RG includes the U.S. Department of Energy's (DOE's)-proposed set of advanced reactor design criteria (ARDC), which could serve the same purpose for non-LWRs as the GDC serve for LWRs. The DOE proposed two sets of technology-specific, non-LWR design criteria. These criteria are intended to apply to SFRs and MHTGRs and are referred to as the SFR design criteria (SFR-DC) and the MHTGR design criteria (MHTGR-DC), respectively.

An analysis of RG 1.232 reveals that the ability to meet several design-functional expectations is governed by functionality requirements controlled by graphite properties. Table 1-2 and Table 1-3 show a cross-linking of the general component functional DC that may be affected by graphite properties.

Table 1-2 GDC and MHTGR-DC considerations and potentially affected GCCs related to graphite properties

ARDC	GDC title	Potentially affected GCC	Graphite property
1	Quality standards and records; same as GDC	All	All
2	Design bases for protection against natural phenomena; same as GDC	All (seismic)	Strength, fatigue strength, Young's modulus
3	Fire protection (adaptations)	All ("chimney effect")	Oxidation resistance
4	Environmental and dynamic effects design bases (adaptations)	All (fatigue loading)	Fatigue
10	Reactor design; same as GDC	All	All
11	Reactor inherent protection (adaptation)	Mainly moderator	Neutron absorption, scattering
12	Suppression of reactor power oscillations (adaptation)	Reflector	Neutron absorption, scattering
20	Protection system functions; same as GDC	Fuel blocks containing control rod/channel	Dimensional stability
21	Protection system reliability and testability; same as GDC	Fuel blocks containing control rod/channel	Dimensional stability
23	Protection system failure modes; same as GDC	Fuel blocks containing control rod/channel	Dimensional stability
26	Reactivity control systems (adaptation)… (4) A means for holding the reactor shut down under conditions that allow for interventions such as fuel loading, inspection, and repair shall be provided.	(Replaceable reflectors, fuel blocks)	Strength, dimensional stability

Table 1-3 Applicable regulations/GTMHR GDC for GCCs

MHTGR-DC	GDC title	Potentially affected GCC	Graphite property
1	Quality standards and records; same as GDC	Same as GDC	All
2	Design bases for protection against natural phenomena; same as GDC	Same as GDC (seismic)	Strength, fatigue strength, Young's modulus
3	Fire protection; same as ARDC	All ("chimney effect")	Oxidation resistance
4	Environmental and dynamic effects design bases	All (fatigue loading and potential for "missile" originating from "inside," e.g., spalling, keys loosening)	Fatigue, Hertzian (impact) fracture
10	Reactor design	The concept of specified acceptable system radionuclide release design limits (SARRDL)	Density, permeability
11	Reactor inherent protection (adaptation) Same as ARDC	Mainly moderator	Neutron absorption, scattering
12	Suppression of reactor power oscillations	Reflector (potentially related to SARRDL).	Neutron absorption, scattering, density, permeability
20	Protection system functions; same as GDC	Fuel blocks containing control rod/channel (potentially related to SARRDL)	Dimensional stability

MHTGR-DC	GDC title	Potentially affected GCC	Graphite property
21	Protection system reliability and testability; same as GDC	Fuel blocks containing control rod/channel	Dimensional stability
23	Protection system failure modes; same as GDC	Fuel blocks containing control rod/channel	Dimensional stability
26	Reactivity control systems (adaptation) … (4) A means for holding the reactor shut down under conditions that allow for interventions such as fuel loading, inspection, and repair shall be provided.	(Replaceable reflectors, fuel blocks)	Strength, dimensional stability (damage tolerance)
28	Reactivity limits	Moderator, reflector	Neutron absorption, scattering
34	Residual heat removal	Fuel sleeve	Thermal conductivity

Several types of computer codes are typically used to evaluate the operational reliability of graphite components. The accuracy of these codes is dependent on the availability and quality of measured graphite properties. The various codes provide detailed design and operational information based on the knowledge of special, time-dependent changes to the properties. Figure 1-2 shows a schematic of this.
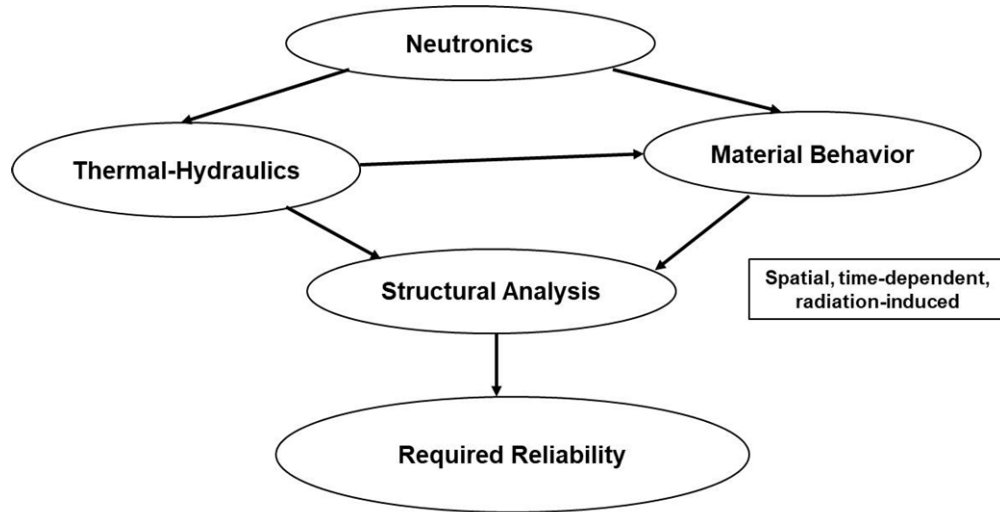
Figure 1-2 Various computer codes requiring graphite properties data for reliability assurance

For current research, the properties deemed to be most significant to graphite component structural integrity and functionality were selected and evaluated from the design code requirements and the design data need (DDN) documents, submitted to the DOE for the Next Generation Nuclear Plant (NGNP) by reactor designer/vendors AREVA (2009), General Atomics (2008), and Westinghouse (2009), as well as an earlier DDN document by GA Technologies, Inc. (1987).

Figure 1-3 shows a collection of these properties.
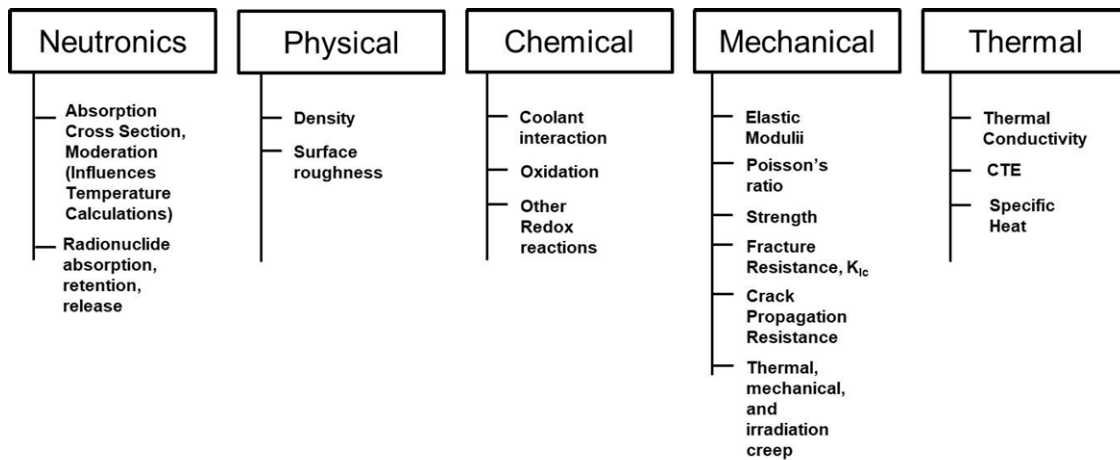
Figure 1-3 A collection of graphite properties affecting graphite performance

Figure 1-4 shows a further analysis of the above properties with respect to their dependence on graphite microstructure, which depends on manufacturing variations, from the objective of assuring adequate structural integrity of the GCC.
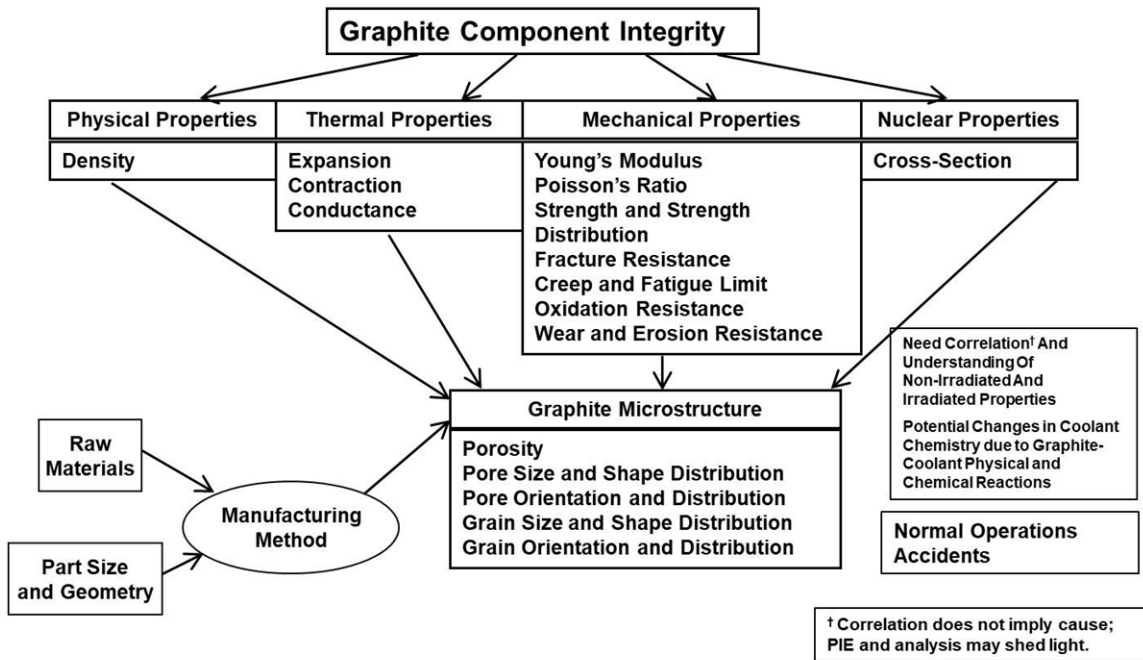
Figure 1-4 Ensuring graphite component integrity with robust database

The governing factor in ensuring graphite integrity is the preservation of the minimum microstructural requirements that influence the graphite properties. The as-manufactured graphite microstructure is dependent on the graphite source, which includes the raw materials, manufacturing method, and size and shape of the component.

Among these dependencies, maintaining the same raw material source has proven to be difficult since the beginning of graphite reactors because of the transient and dynamic nature of the petrochemical industry. The ever-fluctuating demand for specific petrochemicals means that the processes need to be flexible and the products produced in batches, although in continuous batches. Thus, the resulting byproduct coke and pitches can vary in their properties over time. There is no guarantee that the raw materials characteristic of graphite manufacture would be exactly the same from one batch to the next.

In addition to the microstructural variations arising from variability in the graphite source, the microstructure and as-manufactured properties change during irradiation depending on the temperature and time-integrated neutron flux (fluence or dose).

In the past, considerable resources were spent to generate graphite irradiation property data as a function of temperature and fluence. However, much less effort was put into microstructural studies (e.g., microscopy, x-ray diffraction (XRD), porosimetry) aimed at following the changes

important to gaining mechanistic understanding of the processes involved. Therefore, limited success, if any, has been achieved in correlating irradiated properties with unirradiated properties. Many theories are not backed by scientific data and can only be regarded as speculation because correlation does not always imply causation. A detailed postirradiation evaluation is thus necessary to establish a good understanding. Such effort is, of course, very costly and consumes considerable resources and time. Past experience has shown that not pursuing such extensive irradiation programs early has resulted in even greater expense to justify the safety case with degraded graphite components.

Given the above difficulties, it is valuable to have a collection of robust databases that can be analyzed statistically to include uncertainties in the data, analysis model, interpretation, and application to actual reactor operational conditions.

1.3 Graphite in nuclear reactors

Appendix A includes a variety of gas-cooled and liquid-cooled reactors that used graphite in their construction. Beck and Pincock (2011) provided a timeline of the history of HTGR technology, as shown in Figure 1-5. A variety of coolants were used, including carbon dioxide (CO_2) and helium.
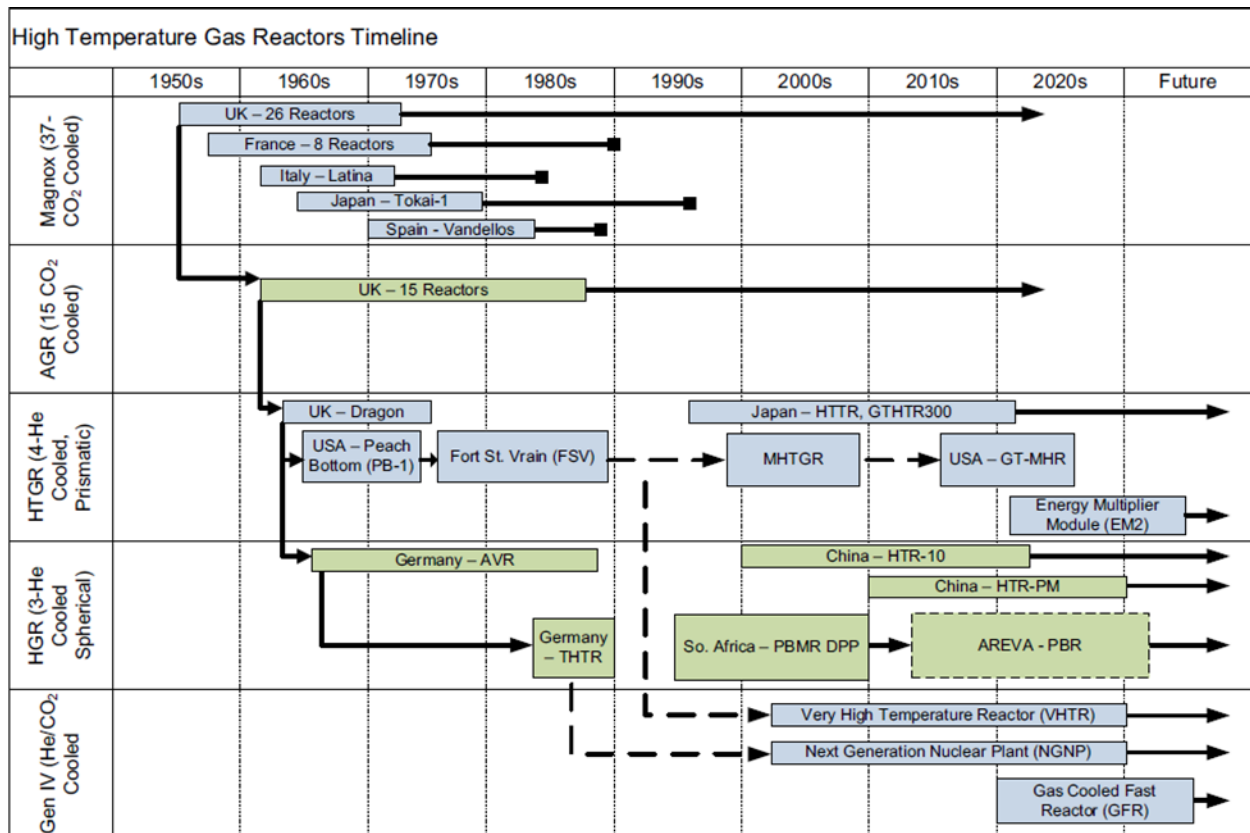
Figure 1-5 A schematic of the evolution of HTGR technology (Beck and Pincock, 2011)

HTGRs have two different principal designs: pebble bed, which is found in AVR and HTR-10, and the prismatic block, which is found at Peach Bottom, the Fort St. Vrain reactor, the High-Temperature Engineering Test Reactor (HTTR), and Dragon reactors.

Graphite has been used in nuclear reactors ever since the first nuclear reactor—Chicago Pile-1 (CP-1), with the first human-made, self-sustaining nuclear chain reaction occurring on December 2, 1942. The reactor used graphite as a neutron moderator. The reactor contained 45,000 graphite blocks weighing 360 short tons (330 t) and was fueled by 5.4 short tons (4.9 t) of uranium metal and 45 short tons (41 t) of uranium oxide.

This was followed by the construction of a series of large-scale reactors for the production of weapons-grade plutonium-239 by neutron activation at the Hanford Engineering Works, northwest of Richland, WA. Three generations of horizontally tubed, water-cooled, graphite-moderated reactors followed. Operation of these reactors revealed that neutron radiation resulted in changes in dimensions and physical properties of the graphite moderator bars (blocks). Considerable knowledge was gained on the effects of neutron radiation on graphite by observing the effects of those changes on the operational characteristics of the reactors, the physical distortions of the graphite moderator blocks, and the physical properties and chemical reactivities of small surveillance samples. This knowledge led to the development of improved nuclear-grade graphites, particularly with respect to using appropriate precursor materials (Morgan, 1996).

However, a systematic correlation between graphite manufacturing variables and the irradiated properties continues to be elusive. At Hanford, each generation of production reactors was constructed (primarily) from a new grade of graphite and was designed to operate under different conditions than was the previous generation; each generation disclosed new radiation-effects phenomena that complicated continued safe operation of the reactors and presented new challenges to the operations (Morgan, 1996).

Nightingale (1966) acknowledged the flexibility offered to the designer by the wide range of graphite properties. He also noted the deficiency in obtaining specified properties within narrow limits with batch-to-batch consistency. He wrote, "For new grades, the properties of interest and their variation may not be known. These are some of the most serious problems with the use of graphite today. Improvements will only come as we are able to better understand and control the fabrication process and provide reliable design information." Unfortunately, Nightingale's observations are as true today as they were then.

The above experience has been repeated for graphite reactors constructed and operated since that time, thereby preventing a firm understanding of the effects of graphite source and manufacture.

During the 1950s, as the gas-cooled reactor concept was developed in Europe and the United States, the requirements for nuclear graphite changed. Materials were required that would perform at intermediate (up to 400–500 degrees C, or 752–932 degrees F) to high temperatures (greater than 700 degrees C, or greater than 1,292 degrees F) and to higher neutron fluences. The gas-cooled reactor projects all had similar requirements for the graphite components,

differing only in degree. The graphite development approaches varied in the United States from those in Europe. In the United Kingdom (U.K.), a needle[1] coke material was first chosen as a moderator for the Magnesium Nonoxidizing (Magnox) reactors, but because of the longer service life required for the advanced gas reactors (AGRs), a denser, near-isotropic graphite manufactured from Gilsocoke was substituted. Graphites manufactured from Gilsocoke had acceptable radiation stability, but the principal limitation was reliance on a single coke source in the United States. U.S. needle coke graphites were selected for HTGRs using large hexagonal fuel blocks, thanks to the existence of a low-cost, easily machinable needle coke product.

An experimental HTGR operated in Peach Bottom, PA, in 1966–1974. The HTGR at Fort Saint Vrain, CO, was a commercial reactor generating electricity and operating in 1979–1989. After these reactors, commercial nuclear production using nonlight-water as a moderator stalled in the United States.

In the U.K., gas (air)-cooled plutonium production reactors were developed at Windscale. This was followed by a significant number of commercial reactors cooled by CO_2, requiring major commercial nuclear graphite production by Anglo Great Lakes (AGL, in Newcastle, U.K.) and British Acheson Electrodes Limited (BAEL, in Sheffield, U.K.). These companies supplied graphite for the 26 Magnox reactors, then 14 AGRs. BAEL later became UCAR and AGL, which later became SGL. Both U.K. graphite plants are now closed, but international offshoots of these companies still exist.

France first developed air-cooled plutonium production reactors at Marcoule, to be followed by a series of commercial carbon-dioxide-cooled Magnox reactors at various other sites in France and Spain. Pechiney, which later became a part of SGL, supplied graphite for these reactors.

In Europe, a high-temperature reactor (HTR) project was developed under the auspices of the Organisation for Economic Co-operation and Development, resulting in an experimental 20 megawatt (MW) Dragon HTGR built at the United Kingdom Atomic Energy Authority, Winfrith. This was followed by an experimental 15-megawatt electric (MWe) HTGR of pebble bed design, AVR, built and operated in Jülich, Germany. The AVR reactor operated for 20 years and was shut down on December 31, 1988, after 123,381 hours (14 years) of operation (Bisplinghoff et al., 2001). This was followed by the construction of the commercial thorium high-temperature reactor (THTR), rated at 300 MWe, built at Hamm-Uentrop, Germany. The THTR started operating in 1983, was synchronized with the grid in 1985, first operated at full power in February 1987, and was shut down September 1, 1989.

Lessons learned from experimental, prototype, and commercial graphite reactors provided guidance for forming opinions on desirable features in nuclear graphite for application to HTGRs. The most detrimental issue was component distortion due to irradiation, which was aggravated by the inherent anisotropic behavior in dimensional change.

---

[1]   Needle coke is the commonly used term for a special type of dense coke with a well-developed lineation that causes it to have a needle-like form. It has a clear ribbon texture with various elongated and parallel anisotropic domains described further in Section 3.3.3.

Operational experience of these reactors has shown graphite to be the preferred material to withstand very high temperatures in HTGRs resulting from nuclear fission. Graphite has also been an excellent moderator, able to sustain controlled fission reactions. Graphite around the core can reflect neutrons back into the core and shield temperature and neutron exposure to surrounding metallic components. Graphite components play the role of heat sink during reactor transients and trips by conducting away the heat. Last but not least, high-purity, large graphite components can be commercially produced for modest cost. The material's relatively easy machinability enables intricate shapes, including the accommodation of various channels for coolant flow and insertions and withdrawal of control rods and fuel rods, or "stringers."

Microstructural damage to graphite during irradiation manifests as macroscopic changes in the distortion of the geometry of the reactor component, which can affect the trueness of fuel and control rod channels and generate internal component stress, which may lead to cracking, thus challenging safe reactor operation. Table 1-4 lists the general forms of graphite damage. For most graphites, a transition exists in the manifested property change at an irradiation threshold temperature of approximately 300 degrees C (572 degrees F).

Table 1-4 List of irradiation damage phenomena for graphite components

Graphite phenomenon	IT[1] < 300 °C (572 °F)	IT > 300 °C (572 °F)
Expansion in the against-grain (AG) orientation[2]	High	Low
Shrinkage in the with-grain (WG) orientation[3]	High	Low
Change in dimensions	Large	Small
Volume change	Increase	Conserved
Irradiation-induced lattice strain	High	Low
Wigner energy	High[4]	Low
[1]IT = Irradiation temperature; [2]AG orientation = Perpendicular to graphite layer orientation; [3]WG orientation = Parallel to graphite layer orientation; [4]Stored energy is an issue only when irradiating graphite well below 100 °C (212 °F), where the rate of release of energy can exceed the graphite-specific heat.		

1.4   Requirements for nuclear graphite

The core graphite functionally supports the fuel, transfers heat from the fuel compact to the coolant, and moderates high-velocity neutrons to thermal energies to sustain the fission reaction. The graphite must have adequate dimensional stability and must retain physical integrity under conditions of high fast neutron fluences and relatively high temperatures. It must also be of high purity to prevent poisoning the nuclear fission reaction.

The requirements for graphite may be established by considering the top-level operational safety needs, such as the following:

- Graphite does not contribute to radionuclide generation by activation.

  It is preferable to avoid elemental impurities that are favorable for neutron activation—activated radionuclides will be a potential issue. Thus, high purity is sought.

- Graphite does not contribute to nuclide transport and entrapment in graphite.

  It is preferable to have graphite with high relative density, with very small pore volume and as much discontinuous distribution as possible.

  It is preferable to have graphite with a very low tendency to generate graphite dust due to mechanical abrasion on contact with moving fuel pebbles (in the case of a pebble bed reactor).

  It is preferable to have graphite with a very low tendency to generate graphite dust due to mechanical abrasion with the coolant flowing at a potentially high-velocity and impacting at random angles to the exposed graphite surface (for both pebble bed and prismatic reactors).

- Graphite does not contribute to fuel heating and degradation of the structural integrity of fuel.

  It is preferable to have graphite with the propensity to retain relatively high thermal conductivity throughout the reactor's life.

- The GCC assembly does not slump into or otherwise impact the graphite fuel rods and thus enables the maintenance of fuel rod integrity.

  The potential for bowing, bulging, buckling, or other potential distortions (dimensional shrinkage and expansion) is kept within limits; it is preferable to have graphite with a relatively high elastic modulus in the reactor operating environment for the duration of the replacement life.

- The GCC assembly does not degrade the ability for control rod movement and the reserve shutdown operation.

  The potential for bowing, bulging, buckling, or other potential distortions (dimensional shrinkage and expansion) is kept within limits; it is preferable to have graphite with a relatively high elastic modulus in the reactor operating environment for the duration of the replacement life.

- The GCC assembly does not degrade its structural integrity and its ability to maintain its coolable geometry throughout the reactor's life.

  Graphite blocks may experience cracking; however, operating experience shows that the load-bearing capabilities are not substantially degraded.

Several independent attempts were made to define the ideal characteristics of raw materials required for optimal graphite performance in nuclear reactors. Engle et al. (1974) provided an excellent summary of demonstrated irradiated dimensional change and desirable characteristics of raw materials for nuclear graphite.

Haag et al. (1990) noted the following key characteristics of graphite used for a reflector for HTRs:

- The density of reflector graphite should be no less than 1.70 grams per cubic centimeter (g/cm^3). This is because the reflecting power depends on the available number of carbon atoms.

- The overall neutron capture cross section is required to be less than 5 millibarn (mb). Thus, the content of neutron-absorbing chemical elements, such as gadolinium (Gd), boron, samarium (Sm), and europium, has to be kept low.

- Iron (Fe), calcium (Ca), strontium, and barium are catalysts promoting corrosion in reactor coolants with impurities such as oxygen, water, and CO_2; thus, the concentration of these elements in graphite should be kept to the very minimum amounts possible.

- The upper limit of ash content in graphite should not exceed about 600 parts per million (ppm).

- Dynamic Young's modulus should not exceed 12 gigapascals (GPa).

- Room temperature thermal conductivity should be greater than 90 watts per degree Kelvin (W/m°K).

- The CTE should be less than 6×10^{-6}/°K from 20 to 500 degrees C.

- Reactor components constructed from isotropic graphites with an anisotropy ratio in CTE of 1– 1.05×10^{-6}/°K are stable enough against fast neutron irradiation damage. The tradeoff in using anisotropic coke that yields low CTE and isotropic coke that yields high CTE poses a challenge.

- Core support columns are exposed to cooling gas streams of varying temperature, which generate thermal stresses as well as contribute to corrosion. Thus, graphite used for support columns should have very high strength and low ash content.

A typical impurity in graphite is boron, which has a large neutron capture cross section and absorbs neutrons, thus giving rise to unacceptably high parasitic neutron losses (Burchell et al., 1991). In nuclear graphite, the boron concentration needs to be kept low. The boron concentration in thermally purified graphite can be less than 0.4 ppm and in chemically purified nuclear graphite, it is less than 0.06 ppm (Nightingale, 1962). For the U.K. AGRs, in terms of waste disposal, carbon-14, hydrogen-3 and chlorine-36 (beta emitters) are the most significant

isotopes likely to be present. Potential ground contamination of these may enter the food chain. Cobalt-60, niobium-94, Eu-152 and Eu-154 are the most significant gamma emitters leading to shielding and handling requirements (IAEA, 2006).

Others also cited property requirements in different ways (see, for example, Burchell et al. (1991), and Marsden (2001)). Generally, they are all similar.

1.5   Properties requirements for recently planned or operated reactors

Table 1-5 shows the properties requirements for the Chinese High-Temperature Reactor, Pebble Bed Module (HTR-PM) reactor summarized by Zhou (2017).

Table 1-5 Typical properties requirements for nuclear graphite for the HTR-PM (Zhou, 2017)

Property	Unit	Extrusion	Vibration molded	Isomolding
Grain size	mm	≤ 1.50	≤ 1.00	≤ 0.04
Density	g/cm^3	≥ 1.75	≥ 1.75	≥ 1.76
Thermal conductivity*	W/m°K	≥ 125	≥ 125	≥ 125
CTE	10^{-6}/°K	≤ 4.5	≤ 4.5	≤ 4.0
Anisotropy factor	-	≤ 1.10	≤ 1.05	≤ 1.04
Tensile strength*	MPa	≥ 20.0	≥ 20.0	≥ 25.0
Compressive strength*	MPa	≥ 65.0	≥ 65.0	≥ 75.0
Boron-equivalent content	ppm	≤ 0.90	≤ 0.90	≤ 0.90
Ash content	ppm	≤ 100	≤ 100	≤ 100
	* Properties in the with-grain and against-grain are to be provided.			

Wright and Windes (2019) cited similar requirements for properties, as shown in Table 1-6. The table also shows the reasons for the desired range for each property and which performance attribute(s) is (are) governed by the specific property. However, it does not indicate the relationship of properties to graphite grain orientation.

Table 1-6 Desired graphite properties for NGNP/HTGR, adapted from Wright and Windes (2019)

Property (room temperature, ambient atmosphere)	Desired range	Reason	Performance attribute
Density	1.7–1.9 g/cm^3	• High density=lower porosity • More effective neutron moderation/reflection per unit volume • Higher strength • Less propensity for radioactive species entrapment • Less propensity to generate dust by mechanical abrasion • Less propensity to generate dust by coolant fluid dynamic abrasion • Higher density=reduced oxidation propensity	Neutron efficiency Structural integrity
Neutron absorption cross section	< 5 mb	• Neutron efficiency of the core • Limiting neutron absorbency is that of pure carbon (~3.5 mbarn)	Neutron efficiency
Thermal conductivity at room temperature	> 100 W/m°K	• High degree of graphitization • Level required for effective heat transfer in HTGR applications • Reduced propensity to fuel heating and degradation	Heat transport
Purity (total ash content)	< 300 ppm	• Required to minimize and reduce susceptibility to catalytic oxidation	Component activity levels during replacement and/or disposal; graphite oxidation

Property (room temperature, ambient atmosphere)	Desired range	Reason	Performance attribute
			under normal and accident conditions
Elastic modulus	8–15 GPa	• Reduced propensity for fuel blocks to slump or otherwise impact fuel integrity • Reduced propensity for dimensional shrinkage or distortion of fuel channel geometry	Structural integrity
Tensile strength	> 15 MPa (tensile)	• Required for structural component integrity • Achievable with isomolding fine-grain graphite, but typically possesses lower fracture toughness • This is a tradeoff that designers take into account	Structural integrity
CTE (20 to 500 °C)	3.5 to 5.5×10^{-6} °K^{-1}	• Higher values indicate coke isotropy and hence isotropy of the graphite • Implies that the graphite may have better dimensional stability when subjected to fast neutron irradiation • However, lower CTE can be beneficial in terms of thermal stress	Structural integrity
CTE isotropy ratio	< 1.10	• Indicative of the bulk graphite isotropy	Structural integrity
Dynamic elastic modulus	8–15 GPa	• Higher modulus typically associated with higher strength material but increased sensitivity to thermal stresses	Structural integrity

Property (room temperature, ambient atmosphere)	Desired range	Reason	Performance attribute
		• Values at the lower end tend to be more beneficial for reduced thermal stress	
Dimensional changes with irradiation	(1) Minimal shrinkage over the applicable fluence range (2) Minimal differences in the with-grain and against-grain directions	• Mainly a function of temperature and fluence but is strongly dependent on the graphite grade • Strongly influence the level of internal stresses generated in core components • Critical in determining their useful life	Structural integrity

PBMR (Pty.) Ltd. discussed the properties of graphite that affect the core structure functions for the earlier South African pebble bed modular reactor (PBMR) design in a technical report to the NRC (2006), as shown in Table 1-7.

Table 1-7 Graphite properties affecting core structure functions of the PBMR, adapted from PBMR (2006)

Affecting property	Core structure function
The graphite reflectors provide neutron reflection (neutrons to the active core).	Maintain a stable geometry of the core fuel.
Permanent deformation of graphite that affects channel geometry	Provide access borings for insertion of the control elements of both the reactivity control system and reserve shutdown system.
Heat transfer ability (thermal conductivity) of graphite	Ensure continued core cooling by the circulating helium in the coolant circuit. When an accident occurs and none of the active cooling systems are available, the residual heat is transferred by natural processes from the core in such a way that the maximum core fuel temperature does not exceed the allowable limit.
Neutron moderation ability by graphite moderator	Limit the temperatures and the fast neutron fluence in the metallic core barrel and the reactor pressure vessel.

Guidelines were also established for Japanese HTGRs with respect to analyzing and providing mitigating means to prevent or manage damage due to distortions arising from irradiation (Sawa et al., 2003; Ueta et al., 2014), as shown in Table 1-8.

Table 1-8 Graphite properties affecting Japanese HTGRs; guidelines for core damage, adapted from Sawa et al. (2003), Ueta et al. (2014)

Affecting property	Guideline
Structural integrity. In the case of an oxidization accident such as depressurization or water ingress, integrity of the bottom plate of the graphite sleeve ensures the fuel stays in the graphite block or sleeve.	Maintain fuel in the graphite block or sleeve. When the fuel is kept in the graphite block or sleeve, the fuel can be cooled by the auxiliary cooling system or vessel cooling system.
Structural integrity. Oxidation resistance/degradation. In the case of an oxidization (air ingress) accident, support post strength may decrease, compromising the needed core configuration.	The graphite core support structures such as support posts carry the core load due to fuel, reflector, and moderator blocks under all operating conditions. Additionally, core stability may be impacted.

The HTGR design considered the impact of irradiation on the properties of graphite to ensure required structural durability. The design life was classified based on the expected duty the graphite components had to endure, with scheduled replacements (Ishihara et al., 2004), as shown in Table 1-9.

Table 1-9 JAEA HTTR component classification (Ishihara et al., 2004)

	Core component	Core support component
Main component	Fuel block Graphite sleeve Control rod guide block Replaceable reflector block Core support post	Hot plenum block Permanent reflector block Core bottom structure Core support post
Replaceability	Routine	Difficult
Irradiation effects	Major	Negligible
Design life	3 years	20 years

For completeness, the literature review included information on many historical grades of nuclear graphites. Many of these grades were produced on a batch scale for exploratory research; commercial-scale production and reactor experience is not available for these graphites. Many of these graphites may not conform to the ASTM nuclear graphite material specifications covered in Section 1.6. Though not relevant for newer HTGRs as these graphites are no longer available, their historical manufacturing issues were considered relevant when examining data on irradiated properties for these graphites and analyzing potential trends. Published comparisons, if any, between ex-reactor irradiated properties—namely, material test reactor data and properties determined by trepanned samples—are expected to be of value. These are available for AGR Gilsocarbon graphite.

1.6   ASTM nuclear graphite specifications

The development of ASTM nuclear graphite specifications for use in reactors considered all of the information contained in Section 0, as well as the operating experience of experimental gas-cooled reactors, such as the AVR, HTTR, HTR-10, and the Dragon project; Hanford reactors; and commercial reactors, such as the U.S. Peach Bottom and Ft. St. Vrain reactors, the German THTR, and the U.K. AGR and Magnox reactors. Consensus is not yet available to reliably assure the necessary functional safety of graphite components without conducting irradiation experiments at the temperature and dose ranges expected for graphite-moderated reactors. This is because of the variabilities expected of (1) newer graphites made from a variety of significantly differing raw materials, processing, and quality assurance, and (2) reactor conditions, which include the range of operating temperatures, fluence ranges, thermal fluid phenomena over the operating life, and the coolant chemistry. Although fundamental studies are ongoing, there are no reliable and benchmarked models that can differentiate the properties and behavior of irradiated graphite from those of unirradiated graphite over the operational life

of the reactor. In this context, the statement by Haag (1990), echoing Engle and Eatherly (1972), is still pertinent: "The mechanisms of irradiation damage and crystallite changes and the relationships between crystallite and bulk dimensional changes have not been developed to the point where dimensional and volumetric changes of reactor graphites can be predicted accurately from pre-irradiation properties or structural features."

ASTM has two specifications for nuclear graphite that are generic in nature and are applicable to different reactor designs, such as the HTGR, either of pebble bed or prismatic core design; molten salt reactors; or liquid metal reactors, based on the graphite's intended use in different regions of a nuclear reactor:

(1)   ASTM D7219, "Standard Specification for Isotropic and Near-isotropic Nuclear Graphites"

(2)   ASTM D7301, "Standard Specification for Nuclear Graphite Suitable for Components Subjected to Low Neutron Irradiation Dose"

These specifications are for the graphites used in different regions of the core subjected to either low-dose neutron irradiation, such as graphite core support posts and reflector blocks, or high-dose neutron irradiation, such as fuel elements and moderator blocks. Generally, irradiation-induced dimensional changes are not a significant design consideration for "low-dose components," while such dimensional changes are significant and need to be considered in the design of "high-dose components." The graphites are further classified according to the method of manufacture and the required purity for use in a reactor. These include "green"[2] forming or the compaction method used and the ultimate purity of the final product.

These ASTM nuclear graphite specifications integrally capture the effects of "source dependency" by requirements defining raw materials, green forming, baking, impregnation, rebake cycles, graphitization, purification, machining, and shipping. The required minimum and maximum values in properties vary for the different graphite classes, based on the expected microstructure resulting from the green forming, carbonization, and graphitization steps. Thus, the ASTM specification innately recognizes the dependence of graphite properties on the "source."

The ASTM specifications allow varying starting grain size distributions in the forming mix within a classification, giving the choice for a suitable green forming method. Such allowance in the starting grain size is notable because a variety of graphites with optimized grain sizes may be manufactured, tailor-made for a specific core component. Generally, finer grain graphites will have higher modulus and strength but lower fracture resistance. Conversely, coarse-grained graphites will have lower modulus and strength but will offer a better resistance to catastrophic fracture.

While the above general relationship between properties and grain size is true for unirradiated graphite, it is pertinent to consider irradiation effects. When graphite is irradiated in an inert environment, initially (within about a year), the modulus and the strength will increase

---

[2] Green forming are the processes used to shape the graphite component prior to graphitization.

significantly. It is important for the designer to consider the modulus, strength, and brittleness of the graphite at this juncture. There may or may not be any significant difference between a fine-grained graphite and a medium-grained graphite at this time. Currently, information is not available for graphites on the dependence of the change in modulus and strength at low dose on grain size. While specific studies have not been conducted on the effects of grain size, data exist for IG-110, NBG-17, NBG-18, and PCEA graphites, which have varying grain sizes and grain size distributions (see Appendix A).

Finer grain graphites are usually made using isostatic molding (isomolding) and simple unidirectional die pressing, either with or without vibration of the contents before molding. Vibrational molding (vibromolding) enhances particle compaction, yielding higher green strength. Green forming mixes with coke particles that have medium-sized grains for maximum dimension can be isomolded, die-compacted, or extruded into shapes. However, extrusion is generally employed for these mixes because of its simplicity and effectiveness in fabricating fairly long articles of a relatively large cross sectional area.

Table 1-10 defines the grain size classifications, based on the approximate maximum coke particle size used in the green mix formulation for any specific graphite class product.

Table 1-10 Definitions for graphite grain size classification

Designation	μm*	mm*
Medium grained	4,000	4
Fine grained	100	0.1
Superfine grained	50	0.05
Ultrafine grained	10	0.01
Microfine grained	2	0.002
*Approximate maximum size for coke particles in the starting mix		

Because shrinkage occurs during graphitization, the maximum graphite grain size in the final product will be less than the maximum coke particle size used in the green mix formulation. Generally, the amount of dimensional shrinkage varies between 5 and 15 percent and depends on the green density; the graphitization temperature; and the rates of heating, hold time, and cool down employed during the graphitization step in manufacturing.

Both ASTM D7219 and ASTM D7301 limit the maximum filler particle size used in the mix formulation to be 1.68 millimeter (mm), corresponding to 1,680 microns (μm), which is in the range of the low end of the medium-grained graphite, as defined in Table 1-10. The low-dose nuclear graphite specification allows the use of anisotropic graphite, with the CTE isotropic ratio (α_{AG}/α_{WG}) greater than 1.15. Both specifications require the bulk density to be greater than 1.70 Mg/m^3.

Coarse-grained anisotropic graphite is unsuitable for use in the reactor core and thus is not included in the specification. Medium-grained anisotropic graphite is only suitable for use in

areas remote from the effects of fluence. Medium-grained and fine-grained isotropic (semi-isotropic) graphites are suitable for use next to fuel, subject to lifetime and design considerations.

ASTM D7219 and ASTM D7301 recognized the need to control harmful impurities in nuclear graphite (Hennig, 1962). Elements such as iron, calcium, and vanadium catalyze the graphite-steam reaction. As mentioned previously, chromium, cobalt, and europium activate and create handling problems after discharge from the reactor. The impurities are classified as (1) neutron-absorbing impurities, (2) oxidation-promoting catalysts, (3) activation-relevant impurities, (4) metallic corrosion-relevant impurities, and (5) fissile/fissionable elements. Table X 1.1, "Impurity Categories for Nuclear Graphites," in ASTM D7219-05 gives the limits for selected major impurities of concern.

ASTM D7219 and ASTM D7301 do not provide requirements for irradiated properties and irradiation behavior. However, the establishment of such a requirement would not be feasible in a consensus process due to the inherent variability in "field" variables, which are dictated by the end use of the reactor output and, thus, the specific design features involved. Such "field" variables include, for example, a reactor's (1) coolant type and its chemistry, (2) operating temperature range, (3) operating pressure and its range, (4) operating neutron fluence range, which dictates graphite temperature, and (5) fluence distribution across and along the length of the core and the resulting temperature distribution of graphite components within the core. As noted, presently, there are no reliable science and engineering models that can estimate the irradiation behavior of core graphite as a function of these "field" variables. Moreover, the vast experience gathered in the U.K. AGRs has shown considerable variation in the dimensional change of reactor core components with irradiation fluence, with increasing scatter and divergence in the data (Gray et al., 2019).

1.7   Summary

This introductory chapter provides a general description of graphite and its unique properties in contrast to conventional metallic materials used in the nuclear industry. Key differences include its inherent inhomogeneity, dependence upon the source material, and brittle mechanical behavior. Graphite component integrity is dependent upon the microstructure of the graphite; in particular, the nature of graphite's porosity and grain size. While this report analyzes data gathered from numerous literature sources taken over the span of decades, there is still a strong need for understanding and correlating the properties of unirradiated and irradiated graphite. One of the key lessons learned from experimental, prototype, and commercial graphite reactors—and the most detrimental issue—is component distortion due to radiation, which is aggravated more by inherent anisotropic behavior and dimensional change. As such, ASTM D7219 and D7301 consider the inherent variability in the source material and limitations of using graphite with more anisotropic behavior. Neither ASTM standard considers material specification requirements for irradiated graphite.

2   DEFINITION OF "SOURCE DEPENDENCE"

In this research, the term "source" encompasses the graphite manufacturer and all the materials and processes used for manufacturing and shipping the final product with predefined quality. Figure 2-1 shows the definition of source dependence schematically.
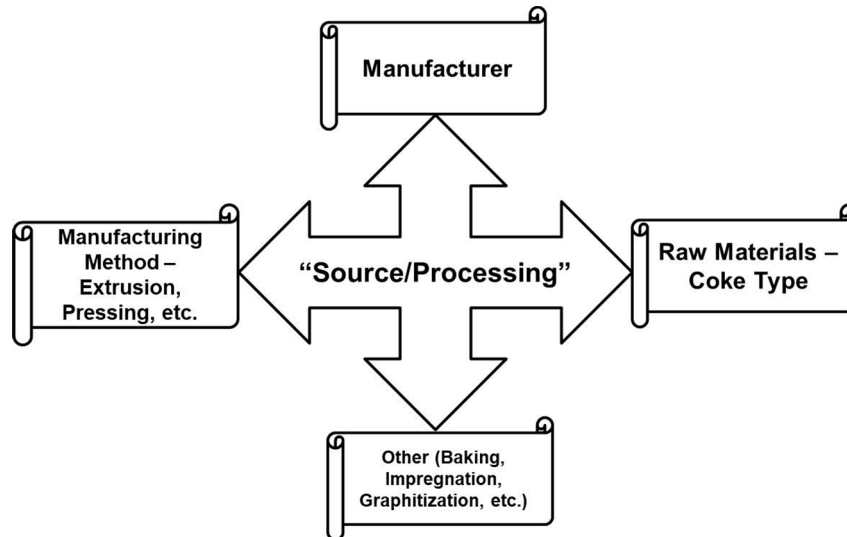
Figure 2-1 Definition of "source/processing" dependence for graphite properties

The source as a variable can be classified in a variety of categories, and entities within these categories have their own set of material and process variables, as discussed below.

2.1   Manufacturer

The manufacturer can be an established organization with extensive experience in manufacturing and supplying nuclear graphite for reactor application. Such experience can include laboratory-scale exploratory research in developing new raw materials, their formulations, green fabrication, and other processes, with appropriate prototype fabrication facilities. These experienced manufacturers typically have good knowledge of the aspects involved in the scale-up and scale-down relationships between the process parameters involved in the fabrication of prototypes and full-scale components as well as other commercial process steps, considering the differences in the size of the machinery and operational parameters. For example, SGL Carbon Company scales down the production process to 1/10th the size in research and development (R&D) (Tahon, B., 2018). In many instances, if market and economic fluctuations cause companies to be sold or merged, for example, it is possible to lose the institutional knowledge of how to scale-up or scale-down technically. Such occurrences play a significant role in the manufacturer being a source of concern for the assurance of nuclear graphite quality. There can also be emerging graphite manufacturers at various stages of expertise in the production technology, with high promise for consistency in product quality. Unfortunately, characterization of their prototype graphites may not always yield usable data for graphite component design, if they are not able to translate their experience of protype development into the fabrication of commercial large components. In fact, such instances are

common, with observations of large variations in properties from billet to billet, when manufactured on a commercial scale.

2.2   Manufacturing practice

Manufacturing practice includes other aspects, shown in Figure 2-1, such as the selection of raw materials; optimizing the raw materials formulation for effective processing, milling, and mixing meeting charge specifications; a green forming method that is suitable for producing the desired shape in large volume; intermediate process steps, such as controlled baking and impregnation; and final heat treatment to obtain a polycrystalline graphite product. The quality assurance and quality control practices using state-of-the art destructive and nondestructive methods and analyses at every step of manufacturing are important to minimize in-process rejects early in the process. Additionally, such prudent practice contributes to the likelihood of producing graphite components of assured quality, saving process time and overall cost of the finished product.

Chapter 3 discusses in detail the various processing steps involved in graphite component manufacturing and quality control tests used by the industry and the effect of the various process variations on the properties of the product.

2.3   Manufacturing experience

A matter of concern in nuclear graphite application is the assurance of consistency in the general quality of graphite over the many years it takes to procure, qualify, and install components in a reactor. A mature graphite manufacturer can produce such quality graphite, as demonstrated for IG-11 graphite by Konishi et al. (2009) in the constancy in several properties over a period of 13 years (Figure 2-2).

In the U.S. NGNP research program, Windes et al. (2013) have characterized several candidate graphites for potential variations in properties within a billet. Figure 2-3 shows the density variation results for IG-110 and historic graphite grade H-451, and Figure 2-4 shows the density variation results for NBG-17, NBG-18, and PCEA grade graphites.
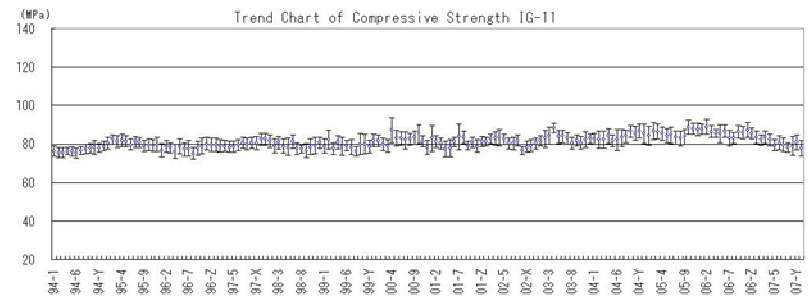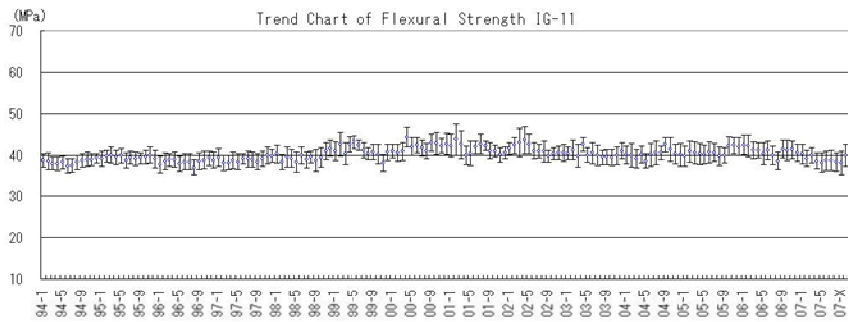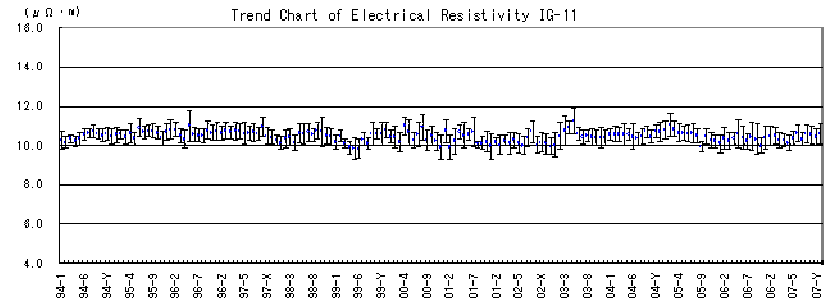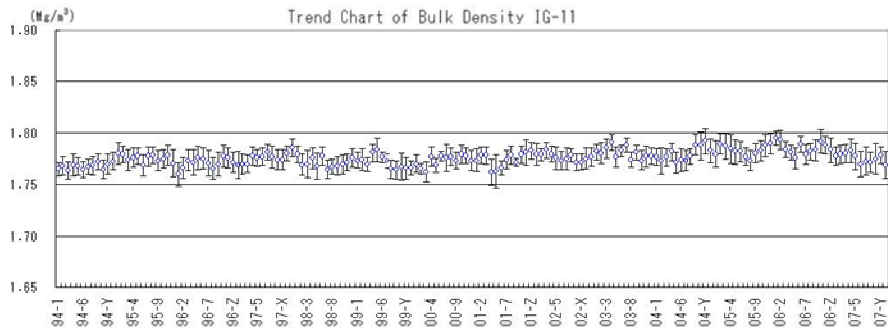
Figure 2-2 Consistency in the properties of IG-11 graphite production over a period of 13 years, from Konishi et al. (2009)
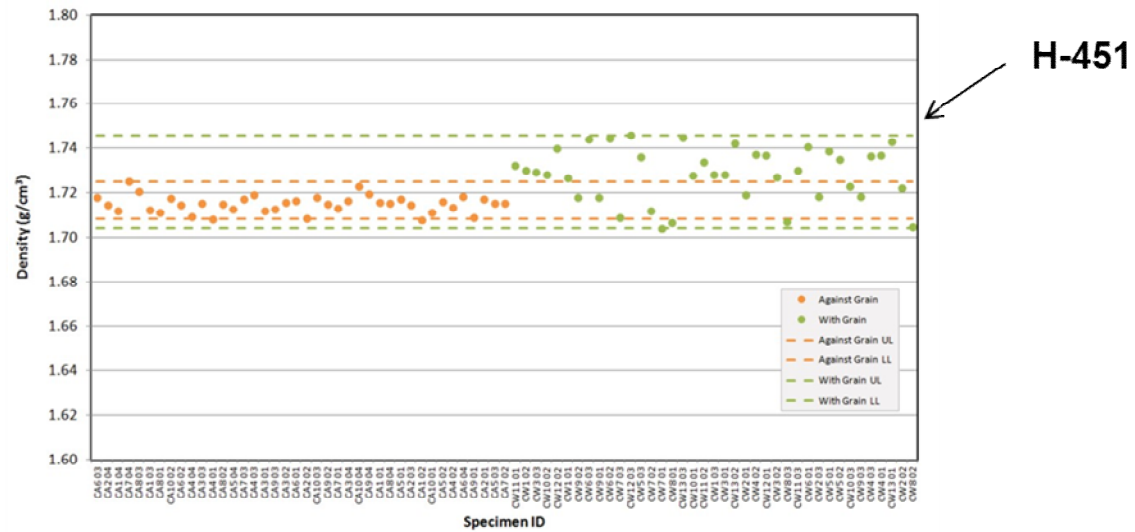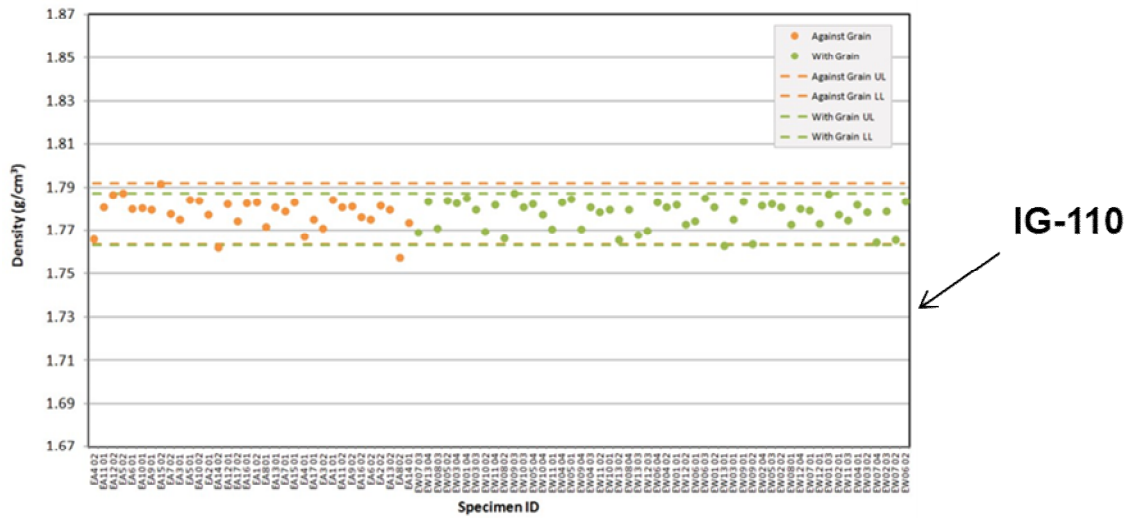
Figure 2-3 Density variation within the billet for IG-110 and H-451 graphites studied under the NGNP research program, from Windes et al. (2013)
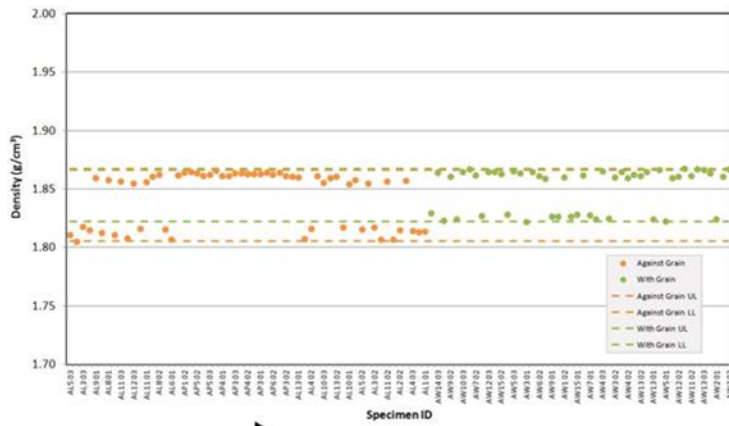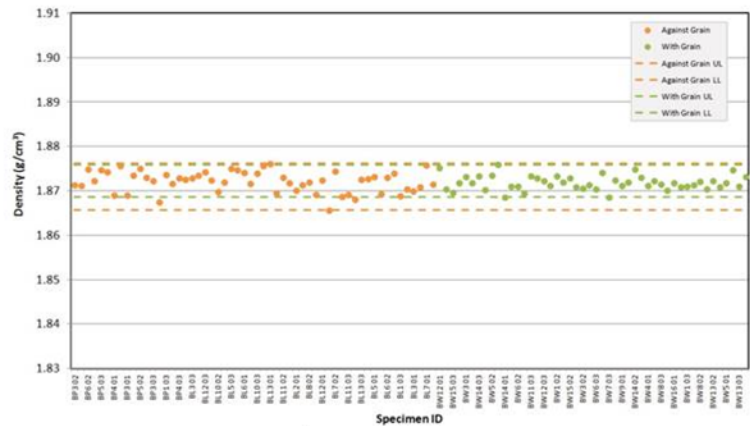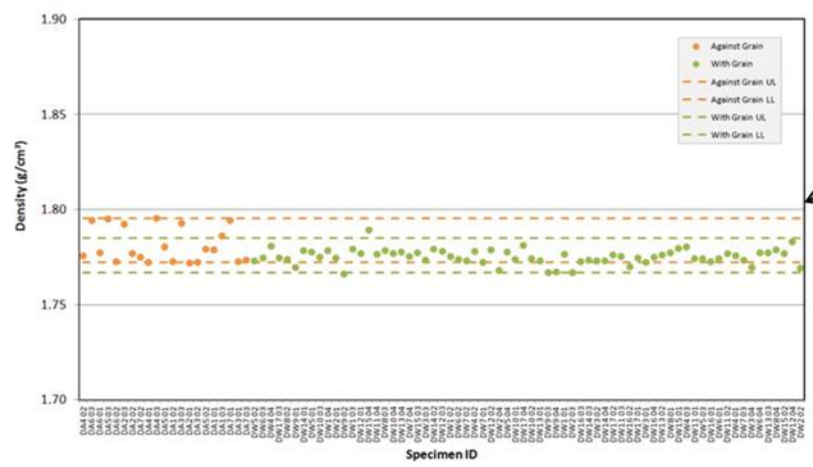
Figure 2-4 Density variation within the billet for NBG-17, NBG-18, and PCEA graphites studied under the NGNP research program, from Windes et al. (2013)

2.4   <u>Summary</u>

This chapter defines the term "source dependency" as the impact of the manufacturer, raw materials, forming method, baking, impregnation, and graphitization upon the final graphite product. The importance of using an established manufacturer cannot be understated as institutional knowledge and experience ensure consistency in the final graphite product over long periods of time. Manufacturers may not be able to produce a prototype graphite on a commercial scale due to the variations in the final graphite product, but experienced manufacturers have demonstrated the ability to maintain consistency in the final graphite product over long time frames (e.g., more than 10 years).

3   GRAPHITE MANUFACTURE

Graphite manufacture consists of several steps, beginning with the selection of raw materials and ending with a very high temperature graphitization furnacing. Figure 3-1 is a schematic of the general graphite manufacturing process.
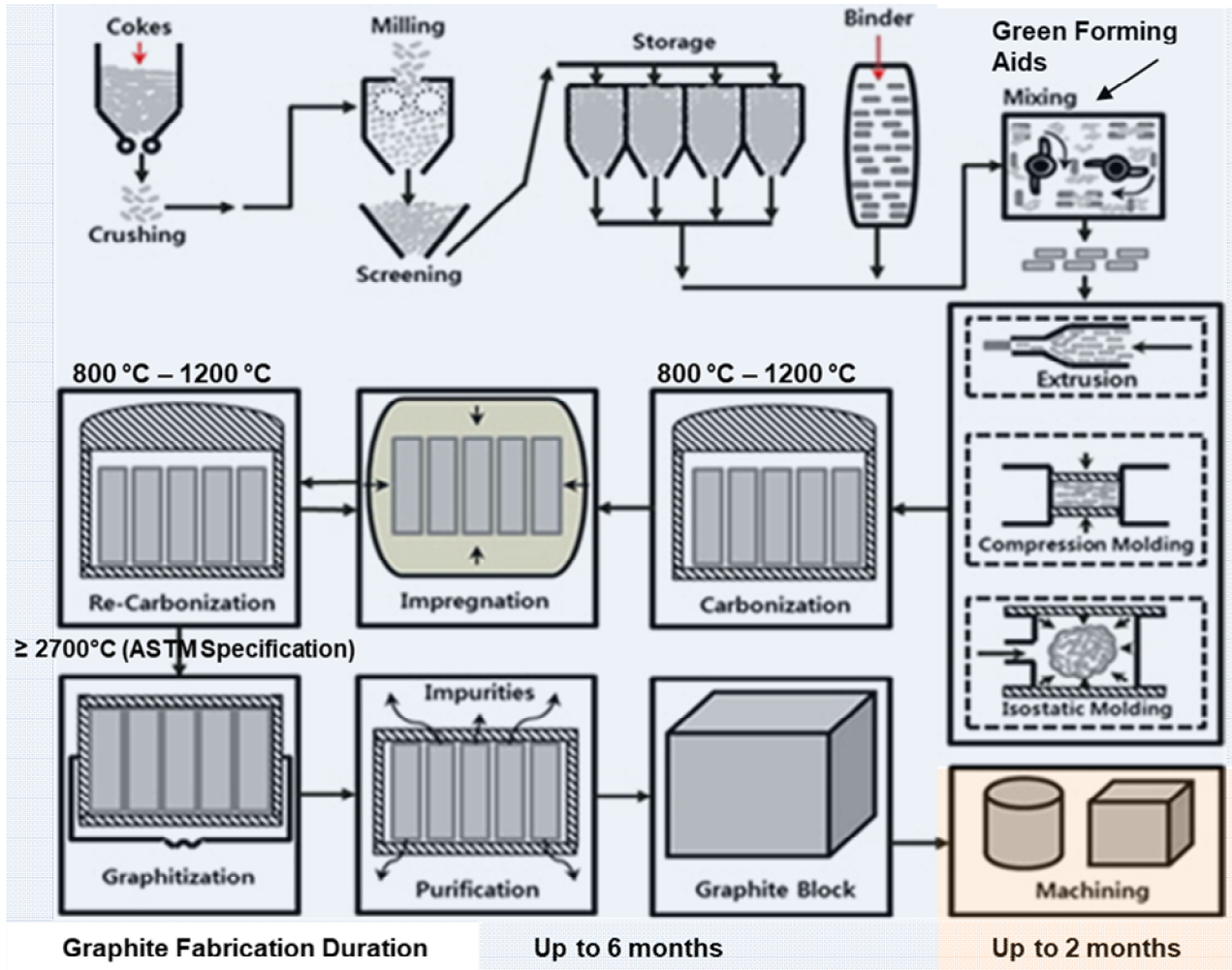
Figure 3-1 A general schematic and process flow involved in nuclear graphite manufacture, adapted from Lee et al. (2015)

3.1   Raw material constituents

The raw materials used for graphite manufacture generally consist of four inorganic and organic materials: (1) fillers, which are the major constituent, (2) binders, (3) impregnant, and (4) additives to aid processing. The proportion of these constituents varies with the end use of the graphite product with specific property requirements and the green forming method used for the product. The filler material is coke, either petroleum coke or coal tar pitch coke. The binder and impregnant are usually coal tar pitch. The additives used for processing include oils and

lubricants to reduce friction between the molding or extrusion compound and the equipment walls in which the molding or extrusion is performed.

3.2   Raw materials selection

Generally, raw materials have a major influence on the properties and cost of the final product. The identification and selection of reliable and continuous sources for appropriate raw (precursor) materials comprise the first and critical step in the manufacturing process. The characteristics of these raw materials, such as the particle size and ash content of cokes and the degree of carbonization of the binder and impregnant, must be taken into account. Nuclear reactors demand a graphite with the lowest possible impurities and the highest possible mechanical properties. This requires the selection of premium-grade precursor materials.

3.3   Coke

The filler matrix is coke as the carbon material, which is known in the industry as a "soft filler" that graphitizes readily; namely, a fully crystalline structure that can be achieved by subjecting the carbonized article to temperatures greater than 2,700 degrees C (4,892 degrees F). Other major fillers are synthetic graphites from recycled electrodes, natural graphite, and carbon black.

3.3.1   Calcined petroleum coke

Calcined petroleum coke is the filler of choice in most applications. It is a porous byproduct of the petroleum refinery industry and an almost-pure solid carbon at room temperature. It is produced by destructive distillation without the addition of hydrogen, almost exclusively by a delayed coking process (DCP), which is a batch process. Heavy crude oil bottom residues are placed into a delayed coking unit or coker, to "drive" off the lighter fractions (jet fuel, gasoline, kerosene) contained in the heavy crude oil. After processing in the delayed coking unit, a solid carbon mass called green petroleum coke remains. The green petroleum coke is removed from the delayed coking unit by high-powered water spray, which leaves it with a high moisture level. The DCP is a mild slow carbonizing procedure that converts crude oil distillation residues. Chen and Walsh (1981) give an example of DCP.

The DCP batch process consists of heating high-boiling petroleum feedstocks under pressure to approximately 430 degrees C (806 degrees F), usually for several days. The variables involved include (1) feedstock reactivity/aromaticity, (2) coking temperature, and (3) flow orientation. The material is then calcined up to 1,200 degrees C (2,192 degrees F) to remove almost all the residual hydrogen and finally ground and sized. The product is commonly referred to as "petcoke." An image of a coke particle and polarized light is shown in Figure 3-2. Regions with the same interference color, optical domains, are regions where partially ordered graphite layers in the coke have the same orientation.
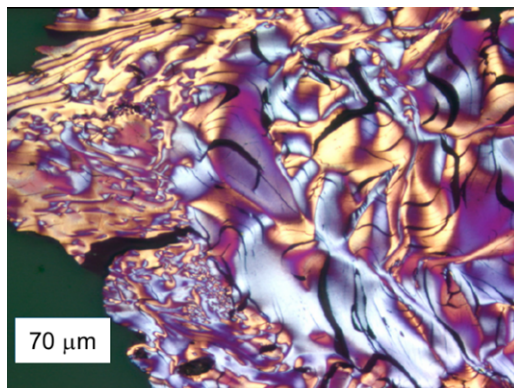
Figure 3-2 Polarized light micrograph of a coke particle. Image courtesy of Stein Rørvik, SINTEF

By varying the source of oil and the process parameters, it is possible to obtain various grades of petroleum coke filler with different properties. For example, source materials with high oxygen and sulfur tend to produce cokes with small-sized optical domains, while those rich in hydrogen tend to produce cokes with large-sized optical domains related to needle coke formation (needle cokes are characterized by optical domains with a large length-to-width aspect ratio). Several patents describe examples of typical manufacturing methods for producing calcined petroleum coke, such as Adee (1963), Smith (1965), Li (1978), Kölling et al. (1981), Hayashi (1982), Hsu et al. (1982), and Becraft (1992).

3.3.2   Calcined coal tar pitch coke

Calcined coal tar pitch coke is also used as a filler constituent in manufacturing graphite. It is made from thermally treated coal tar pitch either by using the DCP or by means of conventional coking procedures. Its structure is less ordered than petroleum coke, but its strength and hardness are higher. Coal tar pitch coke is derived from bituminous coal and is calcined to remove volatiles and moisture. This product is commonly referred to as "pitch coke" and has similar fixed carbon and volatile levels as calcined petroleum coke but has a lower sulfur content (less than 0.5 percent). Several patents describe examples of typical manufacturing methods for producing coal tar pitch, such as Ragoss et al. (1962) and Bhatia et al. (2008).

3.3.3   Calcined needle-shaped coke

Calcined needle-shaped coke, known as needle coke, is produced exclusively from either fluid catalytic cracking decant oil or coal tar pitch. Needle coke is the commonly used term for a special type of dense coke with a well-developed lineation that causes it to have a needle-like form. It has a clear ribbon texture with various elongated and parallel anisotropic domains. Because of its highly ordered structure, it has very high graphitizability, resulting from the strong preferred parallel orientation of its turbostratic carbon[3] structure and the physical shape of the grains. Needle coke has a low CTE and high electrical conductivity. Cokes of this type were used in the Pile Grade A (PGA) and Pile Grade B (PGB) graphites employed in the U.K. and the

---

[3] Turbostratic carbon is characterized by a semi-ordered graphite structure.

KC and CF graphites developed in the United States. If the ground coke is not too fine, it provides isotropic properties containing spherical particles with an onion ring structure, with the graphene planes lying perpendicular to the radius of the particle. Graphitization tends to randomly orient material surrounding each particle, with a characteristic central pore.

The petroleum-based feedstock for producing needle coke has very low ash, as ash constituents will preclude the formation of needle coke during the coking process. Several patents describe examples of typical manufacturing methods for producing needle cokes, such as Suetsugu and Miyazaki (1974), Murakami (1977), Dickinson (1986), Murakami et al. (1989), Hauser et al. (1992), Goval et al. (1994), Eguchi et al. (1997), and Bhattacharya et al. (2004). Some graphite manufacturers may also own the needle coke supplier (e.g., GrafTech International through its Seadrift subsidiary (GrafTech International, 2015), which it acquired in 2010). In 2014, needle coke represented only about 2 percent of the calcined petroleum coke (Frohs and Roeßnera, 2015).

Generally, low levels of impurities within the starting feedstock are necessary for the proper mesophase formation during the coking process, which results in the production of high-purity raw needle coke. Miller and Ball (2009) have produced high-purity graphite, not requiring a postgraphitization purification step, using such high-purity needle coke as raw material in graphite production. Such graphite had an ash content of less than 300 ppm and a boron equivalence of less than about 2 ppm. Such purity meets the specifications in ASTM D7219 for high-purity nuclear graphites.

3.3.4   Gilsocoke

Gilsocoke coke or Gilsonite coke is less than 1 mm in diameter and is a special coke, with near-isotropic properties. It is made from a coke derived from Gilsonite (a naturally occurring bitumen coal) presently mined in Utah. In this coke, graphite-like carbon layers roughly align concentrically. Figure 3-3 shows such a structure. The literature commonly refers to graphite manufactured from Gilsocoke as Gilsocarbon graphite. Typically, this coke has a number of concentric thin cracks and large pores around the center of the particles (Figure 3-3).
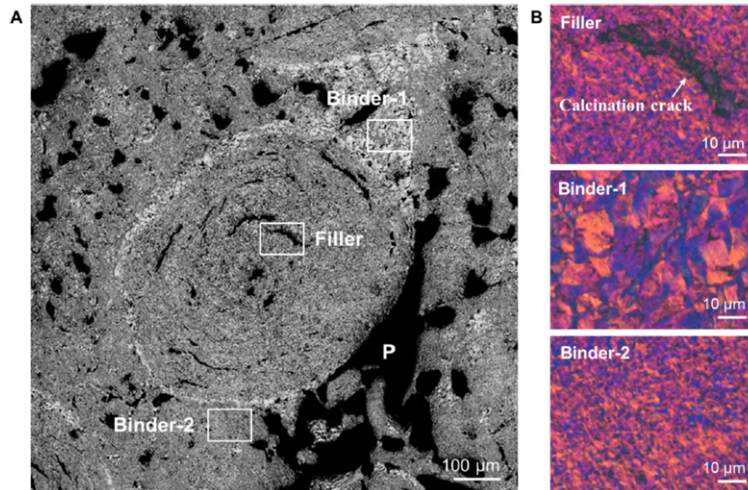
Figure 3-3 (A) The microstructure of Gilsocarbon graphite under a conventional optical microscope; (B) high-magnitude polarized light microscope images of the filler and binder phases, from Shen et al. (2019)

3.3.5 Calcination

The calcination of coke is necessary as a raw material for graphite manufacture. Calcination serves a variety of purposes such as (1) removal of water, (2) removal of volatile carbon matter, (3) lowering of nitrogen and sulfur, (4) reducing the CTE, and (5) reducing electrical resistivity. The latter two are related to the densification of the graphene layer, resulting in improved ordering of the layers within coke due to heat treatment. As the volatile carbon matter departs during calcination, it leaves blank areas that form the basic pore structure within the coke particle that is carried on further through the graphite manufacturing process, up to and including graphitization.

Calcining of cokes is generally performed in rotary kilns, akin to the manufacture of Portland cement. Cold green (raw) coke is added at one end of the direct fired, horizontally mounted rotating kiln and is heated as it moves through the kiln. The calcining residence time for a batch of material may be
30–60 minutes. A typical calcining temperature range is 1,250–1,350 degrees C
 (2,282–2,462 degrees F).

Kennedy (1980) has claimed a novel technique of multiple cycles of coke-binder aggregate powders that are coked, reground, remixed, and coked again. Initial maximum filler coke particle size was less than 90 μm, with an average particle diameter (equivalent area diameter) of 20–40 μm. The fine-ground coke was mixed with pitch and heated in an inert atmosphere such as nitrogen or argon to a temperature of about 505–525 degrees C (941–977 degrees F) to cause fusion. The fused mass was cooled, ground, combined with additional pitch, and again heated to fusion temperature. At every cycle, the coke became more isotropic, with a marked decrease in against-grain CTE, as shown in Figure 3-4. The final coke yielded a higher CTE anisotropy ratio of 1.225, which is higher than the limit in 1.11 in ASTM specification D7219.
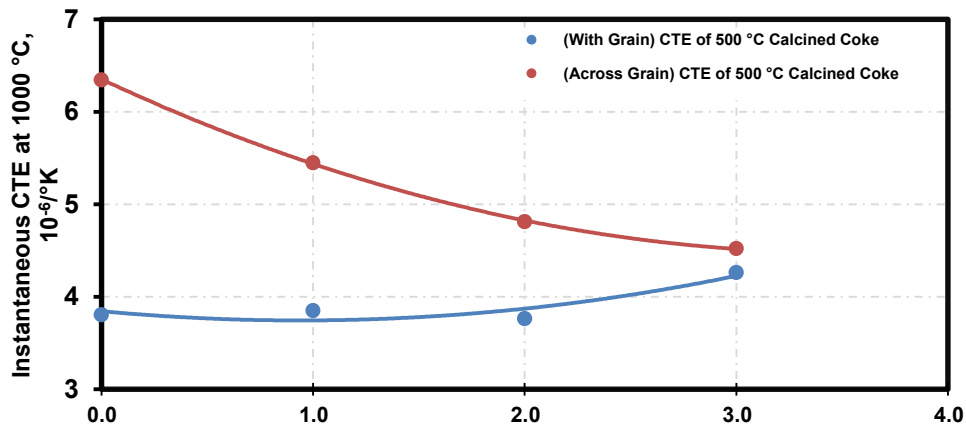
Figure 3-4 Effect of multiple recoking in decreasing anisotropy, adapted from Kennedy (1980)

In selecting coke for nuclear graphite, the most significant properties are the anisotropy in the CTE and the sulfur content. Ash content is also a consideration because it contains information on the overall impurity content in the coke. The coke anisotropy is carried in the processing of the green carbon article and during graphitization. The sulfur content influences "puffing"[4] during the multiple baking, binder, and impregnation cycles of the green-formed body; carbonization of the green body; and the graphitization process. Thus, low sulfur content is desirable.

Table 3-1 generalizes some of the characteristics of coke. Graphite manufacturers have studied puffing during graphitization and can control it by a variety of process innovations (e.g., the addition of iron oxide).

---

[4] Puffing, covered in detail in Section 3.12.4, is related to the primary release of hydrogen sulfide gas.

Table 3-1 Generalized properties of various cokes, adapted from EGCA (2018)

Coke property	Petroleum coke	Coal tar pitch coke	Needle coke	Gilsocoke[†]
Density, Mg/m^3	2.11–2.14	2.07–2.11	2.12–2.15	1.62–1.79 (Inagaki et al., 1973)
Ash, wt.%	0.1–0.3	0.2–0.4	< 0.2 (Solvent refined coal, Hoover, 1984)	7.6 (Bu et al., 2017)
Sulfur, wt.%	0.2–1.8	0.2–0.6	< 0.55	< 0.5 (Al-Haj-Ibrahim and Morsi, 1992); 0.54 (Mochida et al., 1985).
CTE (10^{-6}/°K)	4.5–10.5 (Unknown temp. range)	8.0–10.5 (Unknown temp. range)	4-6 (Kölling et al., 1981) 20–200 °C (68–392 °F)	5.3 (Mercuri and Criscione, 1985) 20–120 °C (68–248 °F)

[†] Gilsocoke has not been available for graphite production since 1971.

As shown in Figure 3-5, puffing generally starts at around 1,700 degrees C (3,092 degrees F) due to nitrogen release. This primary puffing is the most critical for maintaining the integrity of the graphitizing article. During this stage, the material is brittle and sensitive to induced mechanical stress. Secondary puffing occurs around 2,200 degrees C (3,992 degrees F), caused by the release of sulfur encapsulated in closed pores. In the secondary puffing regime, the material structure begins meaningful transition from disorder to order and can accommodate internal stresses much better. The releases of nitrogen and sulfur overlap in the temperature regime up to approximately 2,500 degrees C (4,532 degrees F).
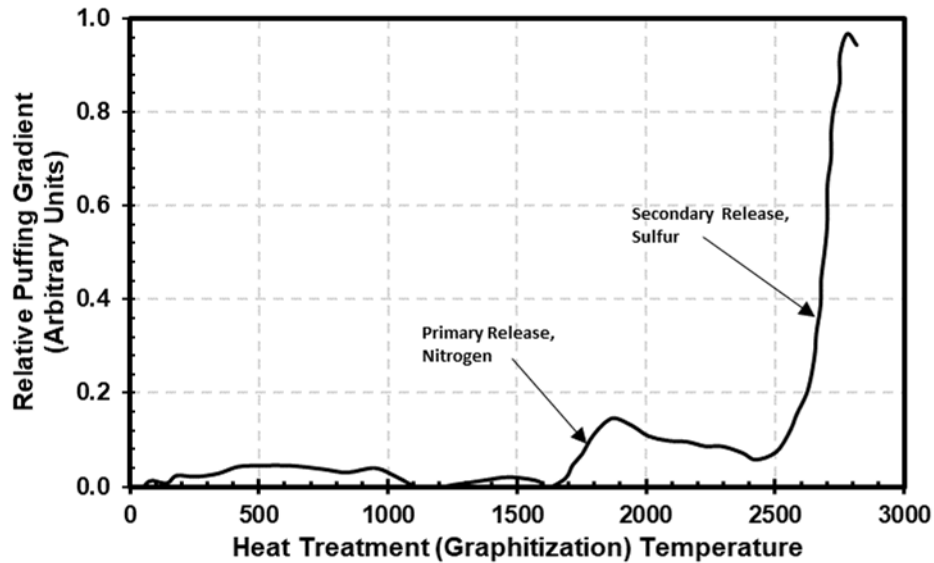
Figure 3-5 Puffing effect on article volume change during graphitization, adapted from Frohs and Roeßnera (1985)

Novel treatments to calcined coke to improve its properties and ultimately obtain a better graphite have been reported. For example, Kennedy (1980) understood the separate, and yet synergistic, contributions of the different types of voids, cracks, and crack-like defects to the graphite failure mechanism. The presence of microcracks provides a stress relief system that differentiates graphite from classic ceramics. However, selective multiple pitch impregnation/bake cycles may seal larger crack-like defects in coke grains ("recoking") to produce a "secondary" coke, which can then be used as the raw material for graphite manufacture, as discussed previously. The density of the recoked secondary coke can be as high as 75–85 percent theoretical.

Kennedy's (1980) process has been further investigated by Haag et al. (1990), who irradiated an experimental graphite produced by the German graphite company SIGRI. SIGRI ground graphite grains made from needle coke grains to finer particles to produce a near-isometric green formulation mix, which was then used to produce near-isotropic graphite. The preferred orientation of the grains was circumvented using a preproduction intermediate step of making a secondary coke from needle coke. Haag et al. (1990) mixed the ground needle coke with standard coal tar pitch binder using a fast mixer and produced large blocks by vibration compression molding of the hot mix. These blocks were then baked at temperatures above 1,100 degrees C and then ground to the size distribution of typical filler constituent. Thus, a nearly spherical grain isotropic coke aggregate was obtained. This secondary coke was used exactly like conventional filler.

ASTM D7219 and ASTM D7301 allow the use of both near-isotropic or isotropic coke derived from a petroleum or coal tar as a filler constituent in the mix. In accordance with paragraph 5.2.1.6 of the specification, the filler particle size used in the mix formulation should be less than or equal to 1.68 mm (approximately 1,700 µm); however, the filler particle sizes can be distributed over a wide range, as indicated in Table 1-10. In accordance with

paragraph 5.2.1.2 of the specification, the coke should have a CTE between 3.5×10^{-6} and 5.5×10^{-6} degrees C measured at 125–500 degrees C (257–932 degrees F).

3.3.6 Grinding of calcined coke

As the first step of artificial graphite production, the calcined coke is crushed, sized, and milled to prepare it for the subsequent processing steps. The application requirements generally set the size of the largest particle. For nuclear graphite, five different maximum coke filler sizes are allowed (Table 1-12). Grinding may be performed in stages to gradually obtain the required coke filler particle-size distribution (PSD), which is an optimized composition of fine and coarse fractions.

Generally, the product application and the green forming method used govern the optimum PSD. The coarsest fraction in extruded graphites may be greater than 25 mm. The finest fraction, termed "flour," in extruded and molded grades typically has a maximum particle size of 210 μm. The flour is usually produced in a mill with a built-in classifier. In normal manufacture, the selected size fractions are recombined with coke flour to produce a dry aggregate (UCAR Carbon Co., Inc., 2001). Isomolded grades are usually all-flour compositions. Flours are milled to controlled maximum and median sizes using built-in or standalone classifiers. Typical maximum particle size varies from about 75 μm to about 5 μm, depending on the grade produced (UCAR Carbon Co., Inc., 2001). The proportion of fractions and the fraction size are varied, within limits, to control the properties of the end product.

The grinding process may involve the use of several types of grinding mills and processing variables, depending upon the required PSD. Figure 3-6 (Morton, 1971) shows an example of the control of the charge feed rate to obtain a desired proportion of a particular size fraction using a hammer mill and the feed rate in an experimental investigation. The coke was Santa Maria LV calcined coke, with a maximum particle size of 9.525 mm. The screen mesh size of 325 means the particle sizes passing through the screen is 44 μm. In graphite manufacture, empirical scale-up and scale-down relationships will usually be established between the machinery and process variables used in laboratory-scale, prototype production and commercial equipment and processes. For a mature and reliable graphite supplier, such controls are essential to reproduce and maintain the quality characteristics observed in the experimental and prototype products on the commercial scale.
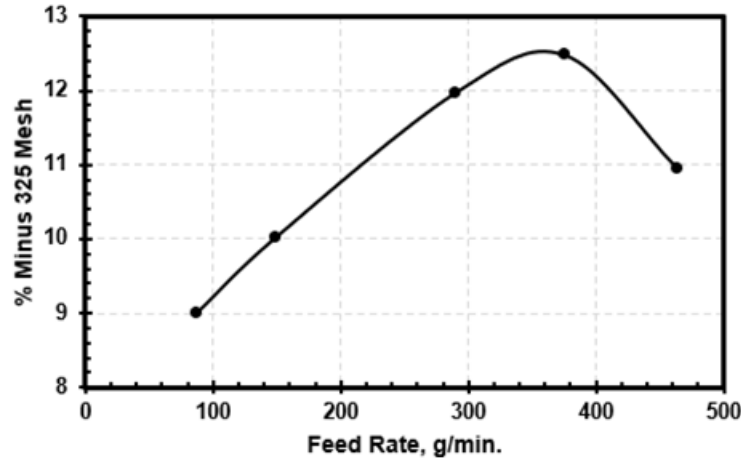
Figure 3-6 Particle size control in coke grinding using feed rate dependence in a hammer mill, adapted from Morton (1971)

An important aspect of PSD relates to the particle shape. Particles with an elongated shape (e.g., rectangular shape) can have a narrow cross section but a length much greater than the cross section of a sieve. Thus, it is not unusual, although still rare, to find rather elongated graphitized coke grains in the graphite article.

An example is optimizing PSD for optimum thermal shock resistance in electrodes used in electric arc furnace steel melting (Sato et al., 1985). Selective PSD has also been used to manufacture graphite with improved mechanical properties by controlling porosity (Nishiwaki et al., 2013). Depending upon the size, various grinding techniques can be used, including ultrafine crushers. Manufacturers may also perform secondary crushing of the cooled kneaded mix using a vertical roller mill or a ball mill to obtain particle sizes ranging from tens of micrometers to several hundreds of micrometers. The resulting powders may be sieved and then mixed in a calculated manner to achieve the required PSD for the green forming process.

An important comminution technique for obtaining the best possible compact density for graphite is attrition milling or autogenous grinding, in which the particles impact one another at an appropriate speed and for a sufficient length of time to produce the required PSD (Spahr et al., 2006). The advantage of attrition milling is that, unlike ball milling, hammer milling, or roll milling, contamination from the grinding media is avoided (Frolov and Dyskina, 2011).

The compact density of the green-formed article depends on the packing density of the coke aggregates. The packing density of the filler is defined by the sizes of the largest and smallest particles, with higher packing density achieved with wider differences. Figure 3-7 shows the dependence of the maximum volume fraction of the filler on the ratio of particle size limits $\delta_{min}/\delta_{max}$ in a filler aggregate with different PSD.
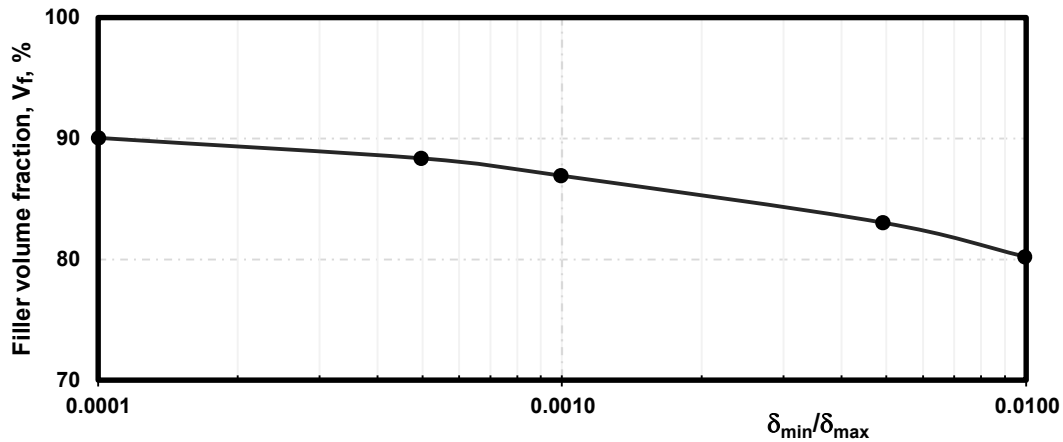
Figure 3-7 Dependence of the maximum volume particle of the filler on particle size on $\delta_{min}/\delta_{max}$ in multisize fraction fillers, adapted from Karvatskii et al. (2017)

Anisometry of the particles in the mix is a negative factor that reduces packing density. Figure 3-8 shows the results of theoretical calculations of the optimum filler size distribution for $\delta_{max} = 100$ μm.
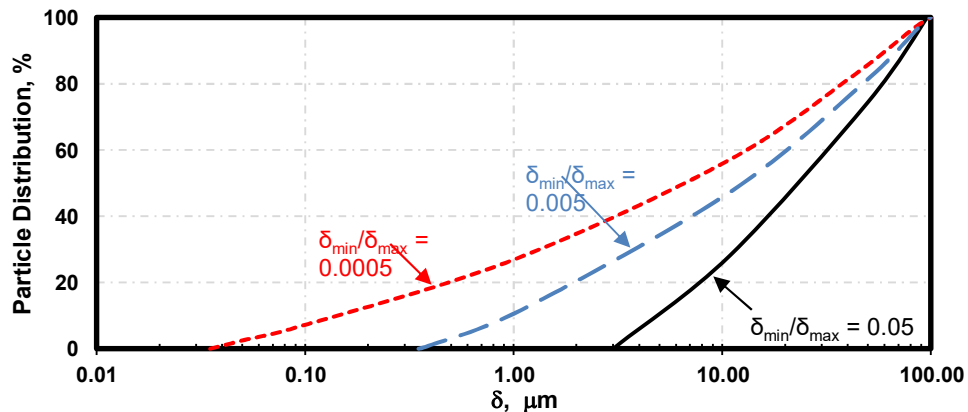
Figure 3-8 Theoretical function value of particle segregation by size, which provides maximum packing density in a mix, adapted from Karvatskii et al. (2017)

While data on the PSD used by the nuclear graphite manufacturers are unavailable, studies have been conducted under the U.S. NGNP research program to obtain the filler size distribution using microscopy, digital imaging, and quantitative analysis techniques on the recent nuclear graphite grades shown in Table 3-2 (Ubic, 2014a). Experiments were conducted with IG-110, PGX, NBG-18, and PCEA graphites. IG-110 graphite is a fine-grained graphite currently being used in the HTTR and HTR-PM. It is in many ways similar to IG-430, also a high-dose candidate for the very high-temperature reactor. PGX graphite is a candidate grade for low dosage regions of this reactor.

Table 3-2 Measurements of observed filler aterial, adapted from Ubic (2014a)

Grade	Coke	Major axis length mean[a] (µm)	Major axis length standard deviation (µm)	Aspect ratio mean[a]	Aspect ratio standard deviation	Porosity (%)
PGX	Petroleum	92 ± 7	85	3.1 ± 0.1	1.6	21.48
PCEA	Petroleum	126 ± 10	94	2.6 ± 0.2	1.6	15.98
NBG-18	Coal tar pitch	360 ± 25	217	~1	–	13.97
IG-110	Petroleum	27 ± 2	22	3.9 ± 0.2	2.4	14.73

[a] Means are two-sided confidence intervals, α = 0.05.

These graphites had an overall porosity ranging from about 14 percent to about 21 percent. The majority of the overall porosity was due to a few large pores. A logarithmic distribution of the pore area was applicable for all grades, with an aspect ratio of about 2, with a preferred orientation.

3.3.7 Coke testing

Graphite manufacturers conduct tests to qualify the raw material coke to provide data that will enable optimizing the process variables, particularly for the fabrication of the green article. Vibrated bulk density is measured as a surrogate pointer of calcined petroleum coke porosity, which affects its suitability for use in pitch-bonded carbon applications. Vibrated bulk density is strongly dependent upon average particle size and particle size range and provides information to determine the maximum achievable packing efficiency during green compaction. Vibrated bulk density tends to increase with decreasing coke size. The industry generally uses ASTM D4292, "Standard Test Method for Determination of Vibrated Bulk Density of Calcined Petroleum Coke," as the standard.

Coke friability determination is needed to establish the extent of the propensity of coke to crumble or to break into smaller pieces during the grinding process. Friability is a physical rather than chemical characteristic of coke. It implies size deterioration or degradation due to breakage along fracture lines, or due to inherent weakness in the coke raw material, big and small. The propensity to be crushed into a large percentage of coke fines is not a desired feature in graphite manufacture. Block et al. (1991) described a method for producing needle coke to reduce the friability of the green coke. Coke friability is related to the Hardgrove grindability index. This index ranks raw petroleum cokes or calcined petroleum cokes in industrial-size mills used for crushing operations. The rankings are based on energy required or feed rate, or both. The industry generally uses ASTM D5003, "Standard Test Method for Hardgrove Grindability Index (HGI) of Petroleum Coke," as the standard.

The graphite manufacturer performs particle size analysis of coke as a part of process variable optimization in green forming an article. Particle size analysis determines the green compaction pressure needed to obtain maximum green density while maintaining the ability to infiltrate pitch during the impregnation process step. The particle size analysis depends on the green forming process used (i.e., pressing or extrusion). The industry generally uses ASTM D293, "Standard Test Method for the Sieve Analysis of Coke," as the standard.

The CTE of coke is performed by fabricating a rod with the coke and measuring its CTE. For example, Hauser et al. (1992) explains a method and the industry generally uses ASTM E228, "Standard Test Method for Linear Thermal Expansion of Solid Materials with a Vitreous Silica Dilatometer," as the standard.

Chemical analysis of coke is also performed, typically to establish the purity before green forming. Typical impurities of interest at this stage are ash, sulfur, and metals. Several ASTM methods are used, as appropriate and as established by the manufacturer and the purchaser, such as (1) ASTM D4326, "Standard Test Method for Major and Minor Elements in Coal and Coke Ash By X-Ray Fluorescence," (2) ASTM D4422, "Standard Test Method for Ash in Analysis of Petroleum Coke," (3) ASTM D7582, "Standard Test Methods for Proximate Analysis of Coal and Coke by Macro Thermogravimetric Analysis" (for determining moisture, ash yield, volatile matter yield, and fixed carbon), noting that fixed carbon is a calculated value that is the difference between 100 and the sum of the percent moisture, ash, and volatile matter, (4) ASTM D4239, "Standard Test Method for Sulfur in the Analysis Sample of Coal and Coke Using High-Temperature Tube Furnace Combustion," and (5) ASTM D6349, "Standard Test Method for Determination of Major and Minor Elements in Coal, Coke, and Solid Residues from Combustion of Coal and Coke by Inductively Coupled Plasma—Atomic Emission Spectrometry."

Some graphite manufacturers determine the crystallite size (L_c) of coke to find the mean crystallite thickness of a representative, pulverized sample of calcined petroleum coke. This is not common, however. The industry generally uses ASTM D5187, "Standard Test Method for Determination of Crystallite Size (L_c) of Calcined Petroleum Coke by X-Ray Diffraction," as the standard.

3.3.8   Effect of coke filler size on strength and elastic modulus

The grain size of the coke used influences the mechanical, thermal, and electrical properties of the graphitized product. Karvatskii et al. (2017) assembled the properties data for high-performance graphites from various manufacturers and published them as shown in Figure 3-9 and Figure 3-10, for the dependence of strength and Young's modulus on grain size. Finer average grain size results in an increase in the average elastic modulus of graphite, with a concomitant increase in the average strength. Arregui-Mena et al. (2019) provided a similar, qualitative relationship between grain size (which also correlates to the mean pore size) and graphite strength.
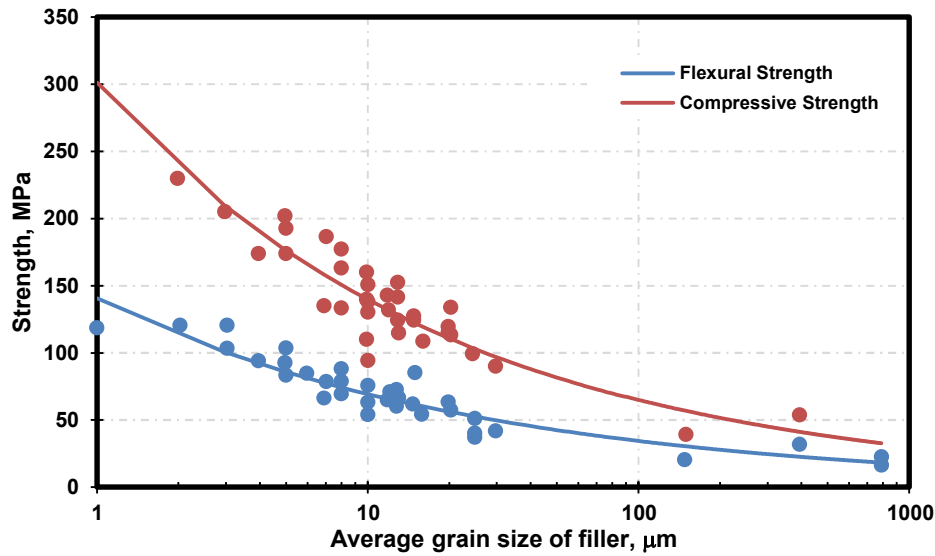
Figure 3-9 Dependence of strength on the average coke filler particle size; data compiled from different graphites and different manufactuers, adapted from Karvatskii et al. (2017)
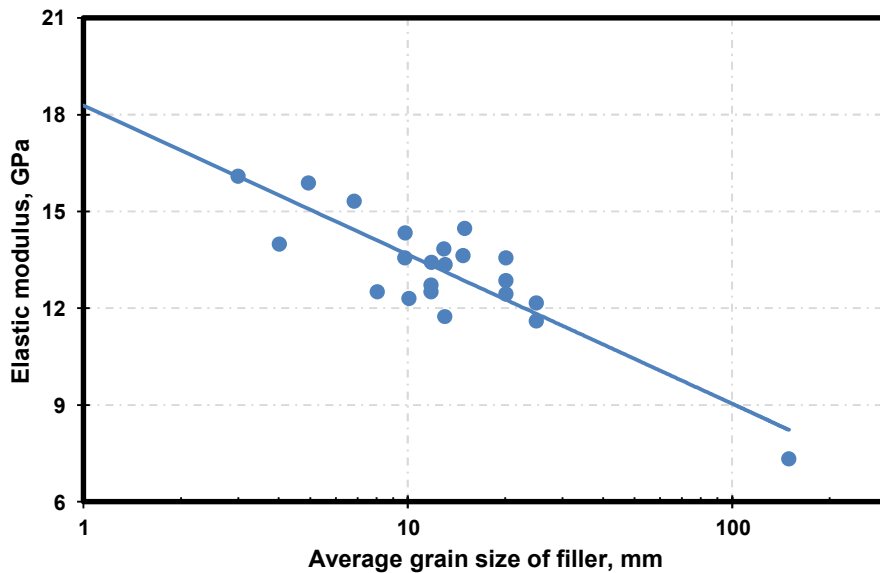
Figure 3-10 Dependence of elastic modulus on the average coke filler particle size; data compiled from different graphites and different manufactuers, adapted from Karvatskii et al. (2017)

3.3.9 The effect of coke filler size on the critical stress intensity factor, K_{IC}

Fracture toughness measurements of nuclear graphite can vary significantly with specimen geometry, measurement method, and specimen size. As pointed out by Burchell et al. (2016), the critical stress intensity factor for IG-110 can vary by approximately 50 percent when measured on six different specimen geometries. Burchell et al. (2016) conducted a systematic study to compare the fracture toughness on several nuclear graphite grades using the ASTM-

specified geometry for a centrally slotted single edge notched beam with dimensions of length 200 x 20 x width 15-mm nominal to ensure the variations in the K_{Ic} data reported could only be attributed to microstructural differences among the graphite grades. Burchell found the critical stress intensity factor, K_{IC} increases with increasing graphite filler particle size, as shown in Figure 3-11. The coarser textured graphite grades undergo more microcracking than the fine-textured graphite grades resulting in a higher K_{IC}.
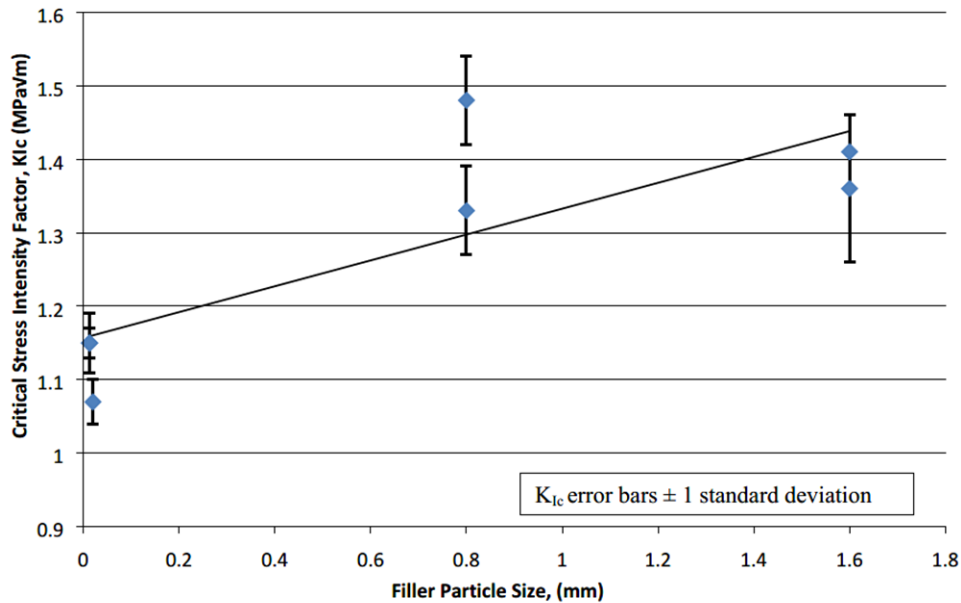
Figure 3-11 The critical stress intensity factor, K_{IC}, as a function of filler particle size in various grades of nuclear graphite. Burchell et al. (2016)

3.4   The pitch binder

Two types of pitch binders are used in manufacturing graphite; namely, coal tar pitch and petroleum pitch, although for nuclear graphite, ASTM D7219 allows only the use of coal tar pitch as the binder in paragraph 5.3. Coal tar pitch is the product of the thermal or destructive distillation of coal. Coal tar pitch consists of a complex mixture of numerous predominantly aromatic hydrocarbons and heterocyclics, which are cyclic compounds that have atoms of at least two different elements as members of its ring(s). It is solid at room temperature and exhibits a broad softening point range. Petroleum pitch is a residue from heat treatment and distillation of petroleum fractions that consists of a complex mixture of numerous predominantly aromatic and alkyl-substituted aromatic hydrocarbons. It is also solid at room temperature and exhibits a broad softening point range instead of a defined melting point.

Table 3-3 gives typical properties of pitches that are important for graphite manufacture. The coking value represents, to a large degree, the percentage of carbon remaining after heating to 1,000 degrees C (1,832 degrees F). Ash content is generally used to establish hard particle contamination (Sawran et al., 1987). Table 3-4 shows typical elements and their amounts for these pitches.

Table 3-3 Typical properties of coal tar and petroleum derived pitches, adapted from Karika (1985), Sawran et al. (1987), and Doolin et al. (2002)

Property	Coal tar pitch (Karika, 1985)	Ashland A-240 Petroleum pitch (Doolin et al., 2002)
Coking value, %	≥ 35	49
Density, Mg/m^3	1.26–1.32	1.22
Softening point, °C	90–95	118–124
Benzene insoluble %	18–29	5 (Karika, 1985)
Quinoline insoluble (QI) %	5–10	0.5
Toluene insoluble %	-	2.10
Ash, %	≤ 0.25	0.7 (Karika, 1985) 0.16 (Sawran et al., 1987)
Sulfur, %	≤ 0.75	3.0

Table 3-4 Typical chemical analysis (wt.%) of raw material pitches used in graphite manufacture, adapted from Karika (1985)

Element	Petroleum pitch	Coal tar pitch
Carbon	92.4	92.1
Hydrogen	5.4	4.8
Oxygen	< 0.1	1.5
Nitrogen	0.1	1.3
Sulfur	1.8	0.5

Two factors can noticeably influence the quality and graphitization characteristics of the pitch: (1) its softening point and (2) the content of insoluble complexes of quinoline (C_9H_7N) (QI). The QI content may vary widely from one pitch to another. Carbon derived from QI is usually heavily cross linked or otherwise composed of "pinned" structures that cannot move or flow. The lack of internal mobility inherent in these materials results in the inability for carbon atoms to align themselves in the pregraphitic "lattice" structure required to be present before the final graphitization heat treatment. The presence of QI results in localized hard carbons. Hard carbons will not readily graphitize or will graphitize only slightly. The industry uses filtration, centrifugation, and aliphatic/aromatic solvent precipitation methods to remove QI.

Assuming the maximum value of QI as 10 weight percent (wt.%) in the pitch (from Table 3-3) and a maximum value of 30 wt.% graphitized binder in the graphitized article, with a char yield of approximately 50 percent, the final microstructure may contain a maximum of about 0.15 wt.% of nongraphitized carbon arising from the QI in the binder pitch. Thus, in terms of its influence in the resulting properties, the effect of QI in graphite can be considered to be negligible, not of concern, and likely included in the typical analysis of scatter in property values.

3.4.1   Pitch testing and qualification

Graphite manufacturers typically perform a number of quality assurance tests on the pitch before production to measure a number of specific properties, such as those described below.

Flash point is determined to assess the tendency of the test specimen to form a flammable mixture with air under controlled laboratory conditions to assess the flammability hazard. The industry generally uses ASTM D92, "Standard Test Method for Flash and Fire Points by Cleveland Open Cup Tester," as the standard.

Insoluble toluene and quinoline are determined using (1) ASTM D4746, "Standard Test Method for Determination of Quinoline Insolubles (QI) in Tar and Pitch by Pressure Filtration," and (2) ASTM D2318, "Standard Test Method for Quinoline-Insoluble (QI) Content of Tar and Pitch."

The softening point for pitch establishes an index for ensuring the consistency of pitches from supply sources. Pitch does not go through a well-defined, single-temperature, solid-liquid phase change when heated and therefore does not have a true melting point. Pitch softens gradually or becomes less viscous with an increase in temperature. Therefore, the softening point is determined by an arbitrary, but closely defined method to produce reproducible test values. The industry generally uses ASTM D3104-14a, "Standard Test Method for Softening Point of Pitches (Mettler Softening Point Method)," as the standard.

Besides the above quality assurance tests, graphite manufacturers also conduct specific tests using custom-developed procedures commensurate with their process control parameters for qualifying the pitches for the particular type or grade of graphite manufactured. These include, for example, filtration testing (Orac et al., 1998), which is used as a measure for effectiveness of separation of solids in the binder pitch; penetration testing (Stiller et al., 1998), which is used for determining the potential of the green-formed article for pitch impregnation; and lubricity. Lubricity of pitch is defined as the ability of a fluid to minimize the degree of friction between surfaces in relative motion under load conditions. Thus, lubricity of pitch is important for optimizing process parameters for the extrusion and molding of green articles. For pitch lubricity determination, the graphite manufacturer likely develops and uses some modified version of ASTM D4866, "Standard Performance Specification for Coal Tar Pitch Emulsion Pavement Sealer Mix Formulations Containing Mineral Aggregates and Optional Polymeric Admixtures."

3.5   Effect of binder content on graphite properties

Engle (1971a) conducted binder-specific irradiation experiments on laboratory-formulated and graphitized articles using a needle coke filler (50 percent less than 75 µm, 50 percent less than 300 µm) and a coal tar pitch binder, graphitized at 2,800 degrees C (5,072 degrees F). Engle (1971a) accounted for both weight losses from graphitization and loss of some binder-coke during the baking process. To account for these weight losses, there are two variables to consider. One is the coke residue, which is the final heat treated compact. This is defined as:

$$\beta \ (wt.\%) = \frac{W_c}{W_f + W_c} \ X \ 100,$$

where W_c is the weight of the binder-coke in the heat treated compact and W_f is the corrected weight of the filler coke in the final compact due to losses during heating to graphitization temperatures. The second entity to consider is the coke yield, C_y, which is defined as:

$$C_y = \frac{W_c}{W_b} \; X \; 100,$$

where W_b is the weight of the binder in the original green mix.

The coking value, defined as the ratio of the weight of the filler coke to the weight of the binder, of the pitch used in these experiments was about 50 percent. The binder-coke fraction β is a linear function of binder content in the green mix, as shown in Figure 3-12. However, as seen, the binder-coke yield decreases when the binder content is increased in the green mix— although the coking value probably remained at about 50 percent in all compacts and the decrease in coke yield was attributed to a systematic loss of pitch during pressing before solidification of the binder. This is an important consideration in both green forming and baking in calculating the final coke yield.

In typical large-size graphite manufacture, such as electrodes for use in an electric arc furnace or moderator and reflector blocks for use in nuclear reactors, practical initial binder content in the green mix can vary from about 18 to about 22 wt.%. The exact amount would be dictated by the coke filler particle size distribution and the green forming method used to fabricate the shape. In such case, the graphitizable coke residue from the binder after carbonization, and available for graphitization, would be in the range of 28 to 32 wt.%, as shown in Figure 3-12.
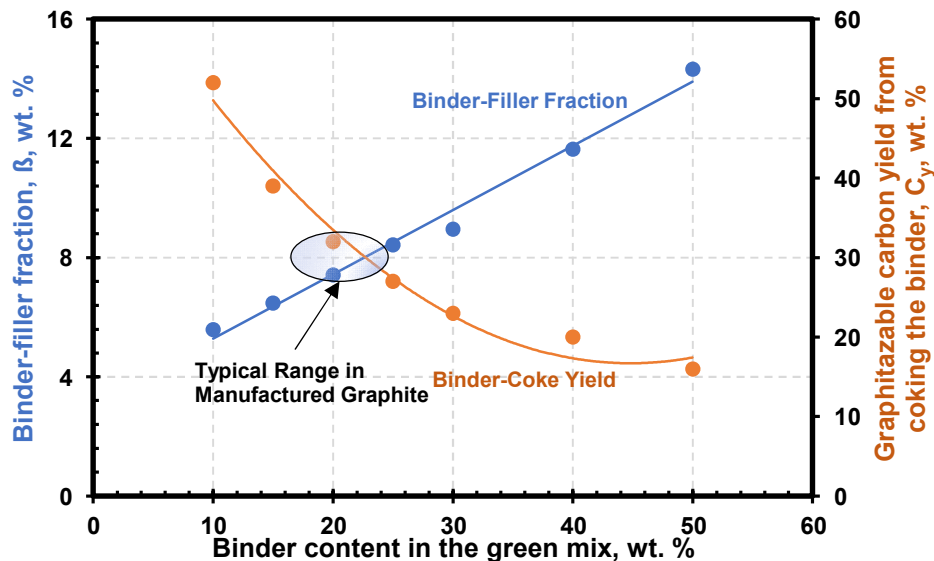
Figure 3-12 Binder-filler fraction vs. pitch content in the green mix, adapted from Engle (1971)

In the research reported in Engle (1971), the binder-filler fraction was in the range of 5.5–14.2 wt.%. Apparent bulk density and apparent crystallite size L_c were dependent on the binder-coke content, as shown in Figure 3-13.
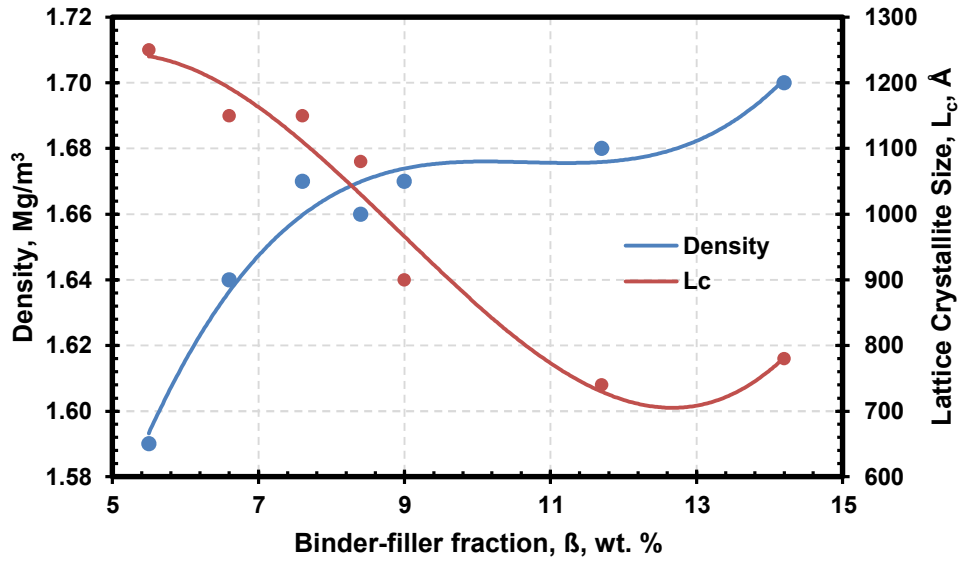
Figure 3-13 Dependence of density and lattice crystalline size on the binder content, adapted from Engle (1971a)

The ASTM nuclear graphite density specification of 1.70 Mg/m³ was achieved between 14 and 15 wt.% of the binder in the green mix for these experimental samples, suggesting a minimum of such binder amount in the green mix. Typical binder content in the green mix is usually between 18 and 22 wt.% for manufactured products, with the variation due to the green forming method used and the geometry of the article.

The binder content seemed to have minor effect on both the WG and AG CTEs of the resultant graphite, as shown in Figure 3-14. This experimental graphite is highly anisotropic and would not qualify as a nuclear graphite today.
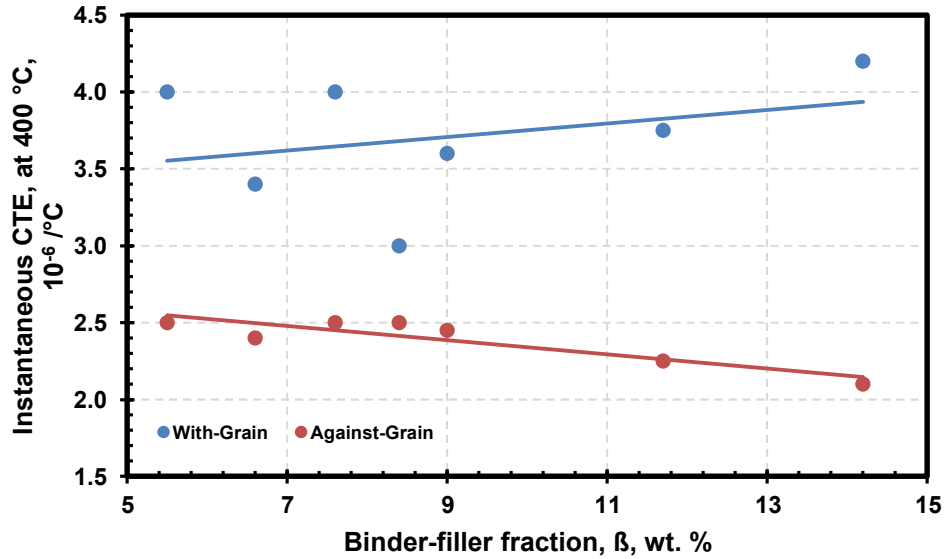
Figure 3-14 Effect of binder content in the green mix on the resultant graphite CTE, adapted from Engle (1971a)

3.6   Other ingredients

Besides coke particles of varied size distribution (fillers) and pitch binder, minor amounts of other ingredients are used in the green mix formulation at various steps in the carbon and graphite manufacturing process. Paragraph 5.5 of ASTM D7219 allows the use of such materials. They can play an important role in determining the quality of the final product. For nuclear graphite, light oils and lubricants are often added to the mix to improve the extrusion rates and the integrity of the extruded products. Chemical inhibitors are introduced to reduce the detrimental effects of sulfur in high-sulfur cokes.

3.7   Mixing and kneading

The coke filler particles are mixed with a binder to cover the surfaces of the filler particles. Figure 3-15 shows a schematic of the blended mix.
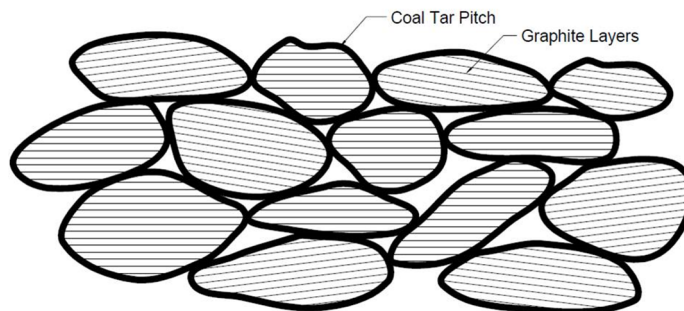
Figure 3-15 Pitch-coated coke grains from mixing and kneading. Image courtesy of Metallized Carbon Corporation

The intergranular bond that can be established between the binder-coated filler coke ultimately determines the properties and structural integrity of the graphite. The more uniformly the binder is distributed throughout the filler components, the greater the likelihood for good compaction during green forming due to the adhesion of touching particles enabled by the binder, which is eventually carbonized and graphitized along with the filler particles.

Using a kneader, the milled aggregate powder, binder, and additives are hot-kneaded thoroughly to uniformly attach a layer of coal tar pitch to the surface of the aggregate particles. Blending is usually carried out at 160–170 degrees C (320–338 degrees F), although temperatures may reach as high as 315 degrees C (599 degrees F). The kneading temperature is dictated by the type of binder, its softening point, and its rheological characteristics, primarily viscosity. After the kneading is completed, the resulting paste-like malleable product is cooled for subsequent secondary grinding. The mixing and kneading step is critical because the final properties of the molded product are controlled to a great degree by the characteristics of the filler-binder paste, such as (1) the temperature dependence of the viscosity, (2) the general rheological behavior, which is also influenced by the filler PSD, and (3) the hydrodynamic interaction between filler particles.

3.8   Final preparation of the green charge

The final preparation of the green forming charge depends on the green forming process chosen. The objective will be to use as light a pressure as possible while still achieving the best compaction possible for the size and shape of the article to obtain the maximum green density as a result of the compaction method.

The degree of compaction is dictated by the compacting ability of the particles. Besides the maximum size of the coke filler particles, allowed by ASTM D7219 and ASTM D7301, particle sizes of graded distribution are used that fill in the gaps obtained in compaction according to the size of the gap between filler particles. The chosen PSD will depend upon the compaction method used and the capabilities of the manufacturer's processing equipment.

3.9   Green compact forming

Paragraph 5.6.2 of ASTM D7219 allows the compaction of the green mix by extrusion, molding (including vibrational molding), or isomolding. The green compaction method is selected based on part size and geometry and manufacturability to near net shape, considering the efficacy of baking and impregnation to achieve the desired green densities before graphitization. The size, shape, and geometry of the graphitized part could also influence the efficacy of the subsequent purification steps.

Table 3-5 shows some of the basic characteristics of the commonly used green forming processes. All these basic processes have been used in the manufacture of graphite components in nuclear reactors. Besides meeting the ASTM specifications, the process selected will largely depend upon the reliability of the vendor source for coke and binder constituents and the consistency in raw material properties requirements by the graphite manufacturer over the duration of GCC manufacture. The cost is always a prime consideration,

and extrusion offers the lowest cost route, while being able to maintain the required properties specifications.

Table 3-5 Characteristics of graphite body green-formed articles, adapted from Pierson (1993)

Green forming method	Product features
Isomolding	Isotropic properties Uniformity No flow lines or laminations High cost
Uniaxial pressing, vibrational molding (vibromolding)	Anisotropic properties Nonuniformity Edge effect Presence of flow lines and laminations Medium cost
Extrusion	Anisotropic properties Nonuniformity of cross section Presence of flow lines and laminations Limited to parts of constant cross section Production of large parts possible Low cost

3.9.1   *Isomolding*

Isomolding (also called isostatic molding, isostatic pressing, or iso-pressing) is typically at ambient temperature. In this process, the green mix is compacted within a flexible rubber membrane and pressure is applied in a liquid-filled chamber evenly in all directions around the part being made. This differs from uniaxial pressing, where pressure is applied in only one direction. Isostatic pressure can vary between 100 and 200 MPa, depending on the size of the part. An isomolded part can be made to near net shape requiring minimal final machining, thus saving both material and process time. Figure 3-16 shows a schematic of molding.

The mix preparation for isomolding is typically the same as or very similar to that for uniaxial pressing. The basic requirements are the same for the mix properties, such as viscosity and thixotropy for easy mix flow into the mold and easier compaction for high green density.
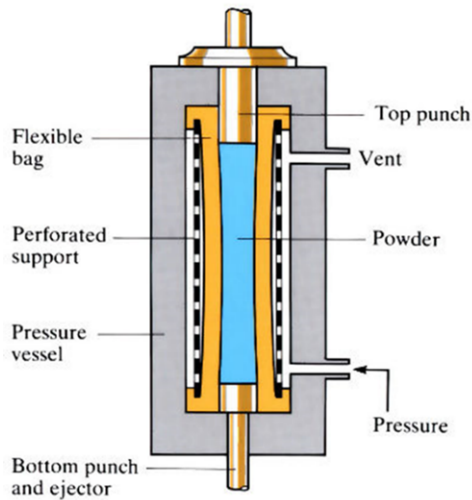
Figure 3-16 A representation of isomolding in which equal pressure is applied in all directions. (The Open University, 2017).

The isomolded product has good uniformity, isotropic properties, and generally few defects. Isomolding produces near-isotropic properties, regardless of the starting coke type. However, the WG and AG designations are carried over from initial molding processes; the minor axis, usually horizontal, is referred to as WG, and the major axis (usually in the vertical) is referred to as AG. While isomolding provides more isotropic behavior than with any other forming method (see, for example, Figure 3-21, the cost is higher than other molding processes.

3.9.2   Uniaxial pressing

In uniaxial pressing (also called uniaxial molding or die compaction), the green mixture is loaded into a die, frequently made of tungsten carbide, and pressed into shape. The molding pressure depends on the size of the part. Die-wall friction and die edge effect may cause nonuniformity in the density of the compacted product.

Figure 3-17 shows a schematic of the process, which is simple and proven to produce graphite compacts of high density. Slight changes in the compacted density might occur during the punch withdrawal and part ejection process, due to elastic spring back, but they are well controlled.
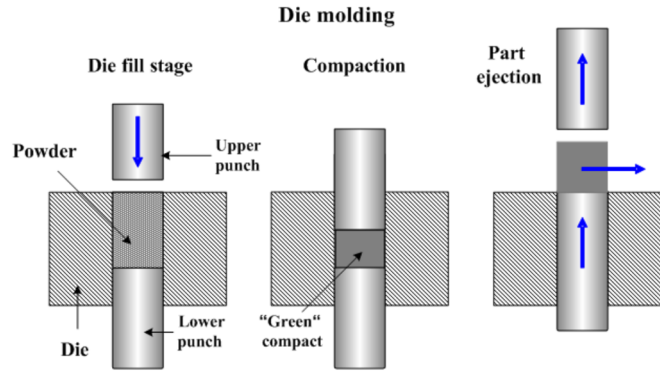
Figure 3-17. Schematic of molding a graphite compact mix. Image courtesy of Substance & Technologies Inc

The die-design for uniaxial pressing involves the application of applied mechanics principles and the flow mechanics of the mix under pressure. The primary consideration is the height to cross section diameter relationship (Barrera, 2009). Generally, the larger this ratio, the more inhomogeneous and more expensive the compact will be. The necessary punch travel distance will depend upon the minimum cold compact density requirements. In a larger mold, which would typically be used for producing green compacts for nuclear reactor components, a fairly large amount of forming mix can flow in any direction during compaction. The resulting shearing forces, and this flow, tend to align the particles along the flow direction, as is observed with extruded bodies. Bradstreet (1958) postulated that, in a large molded specimen, the outermost portions of the structure are suitably oriented normal to the pressing direction; this tendency is lessened toward the center and top of the die, where flow through longitudinal shear occurs more easily.

Wang et al. (2020) analyzed the stresses resulting from compaction using a metal powder. Such analysis is also applicable to mix compaction to form the green body of a graphite component. All the stresses (except for shear stress) are in compression during the compaction stage. Therefore, crack initiation caused by tensile stresses is not possible during this stage; the crack can only be initiated by shear stress. Tensile cracks develop during the ejection stage; the driving force for crack initiation comes from the maximum tensile principal compared with other direction stresses. Shear stress can be a driving force for shear crack initiation, both in the compaction and ejection stages. It is notable that these cracks formed during compaction will be filled by the impregnant pitch during the impregnation process step in graphite manufacture.

Smith (1970) reported experimental results on the effect of compaction pressure used on the density of the green body and the graphitized article. The coal tar pitch binder content was 30 wt.% of the total mix used for compaction. Smith (1970) did not report any impregnation after baking, and graphitization was performed at 2,800 degrees C (5,072 degrees F) in a flowing helium atmosphere. Figure 3-18 shows the results for the general purpose of recognizing process variables in graphite manufacture; the control parameters for these

variables may be expected to vary for graphite grades and the particular process used to make the required shape and quality requirements.
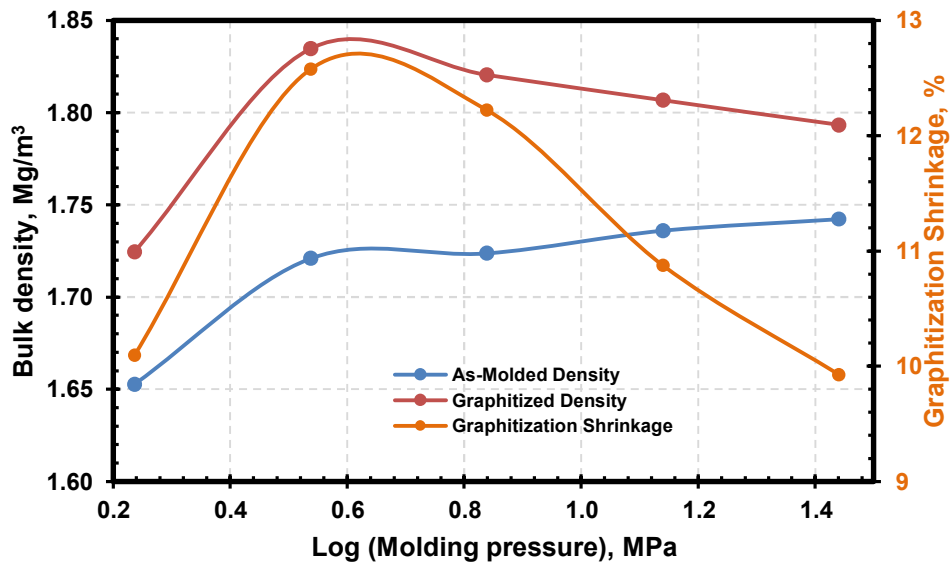
Figure 3-18 Effect of molding pressure on bulk densities and graphitization volume shrinkage, adapted from Smith (1970)

3.9.3 Vibration molding

During vibration molding (also called vibromolding), compaction of the mix during uniaxial pressing is assisted by vibration. During vibration, smaller particles move into the interstices between larger particles, densifying the green body. While mechanical vibration is the easier process, additional enhancements are possible using ultrasonics, especially for micron-sized particles. The resulting structural integrity of the green product can be higher than that of a material processed by uniaxial molding alone. In all instances, proper venting to facilitate the removal of entrapped air is important.

3.9.4 Extrusion

Extrusion is preferred for the production of large parts having a constant cross section, such as electrodes. The electrode manufacturing process has been largely adapted for the production of large blocks of nuclear graphite. The process uses a mix at a temperature just above the softening point of the pitch. Typically, steel dies are used for extrusion. The extrusion pressure and the rate are controlled and depend upon the size of the product and the grain size distribution of the extrudate. The part leaving the extrusion roll is cut to length and rapidly cooled to solidify the pitch before distortion occurs. Figure 3-19 shows an extruded billet leaving the extrusion die.

Figure 3-19 Graphite extrusion exiting from the die. Image courtesy of NAC carbon, NAC Carbon Products, in Punxsutawney, PA

The coke filler particles align preferentially in the direction of shear as it moves within a flow (i.e., along the axis of the product), imparting anisotropy to the properties of the finished product. This anisotropy can be controlled to some extent by changing the mix formulation (e.g., using grains of near-spherical shape) and the extrusion geometry. The center of the extruded material is usually of lower quality than the material near the outside edge, and defects such as flow lines and laminations are difficult to avoid. Extrusion represents the largest tonnage of synthetic graphite and is the lowest cost technique. As shown in Figure 3-20, graphite grains align along the extrusion axis when anisotropic coke grains are used in the extrusion mix.
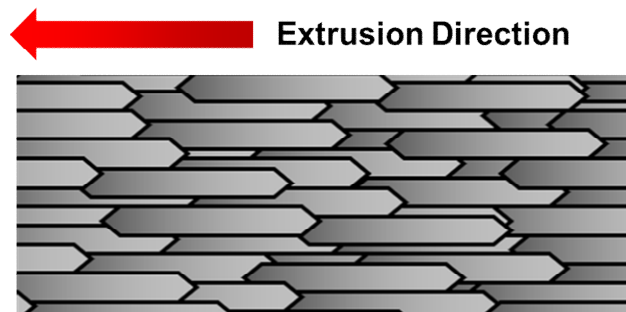
Figure 3-20 Oriented graphite grains due to coke particle alignment during extrusion green forming

It is generally considered that the properties of the extruded product exhibit transversely isotropic behavior. That is, the properties measured on specimens oriented in the direction perpendicular to extrusion are the same and exhibit radial isotropy. Figure 3-21 shows the effect of the maximum coke grain size on typical anisotropic behavior exhibited in some properties.
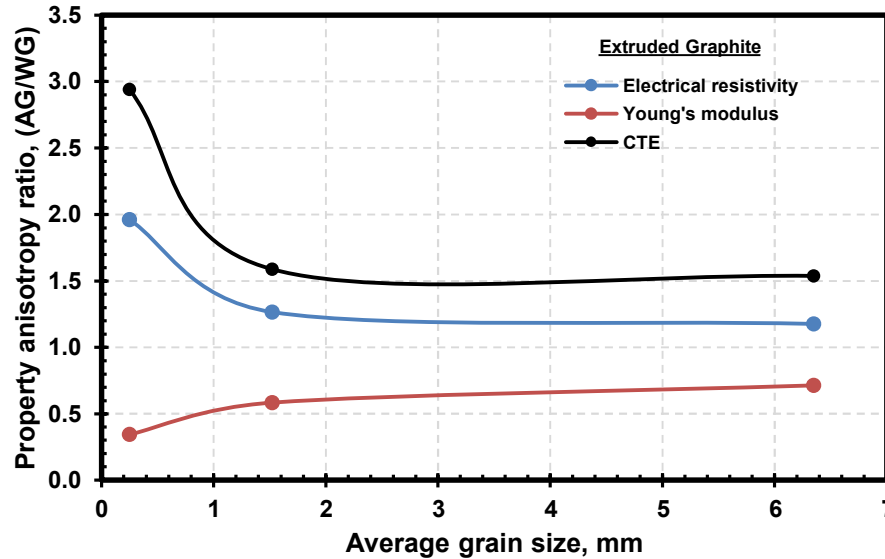
Figure 3-21 Typical anisotropy ratio of some properties of extruded graphite, adapted from UCAR Carbon Co., Inc. (2001)

The common quality assurance tests for green-formed articles are green density and visual observation of defects. The process control parameters optimized using such tests are firing schedule, off-fire temperature schedule, and time.

3.10   Baking

The green-formed article is then baked generally at temperatures less than 1,250 degrees C (2,282 degrees F). However, higher temperatures, even up to 1,400–1,600 degrees C (2,552–2,912 degrees F) may be used in special cases. Baking, or carbonization, is performed in an inert or reducing atmosphere, which takes a few days to several weeks, depending on the constituents and the size and geometry of the part. The temperature is raised slowly to 600 degrees C (1,112 degrees F), at which stage the binder softens, volatiles are released, and the material begins to shrink and harden. Typical shrinkage is 6 percent. The parts must be supported by a packing material to prevent sagging.

During baking, complex chemical reactions occur, and the binder decomposes and releases a large quantity of volatiles, but polycondensation reaction results in residual carbon. During the low-temperature preheating phase, the green body expands due to the heat, and in the subsequent heating that increases the temperature, the volume shrinks due to the polycondensation reaction. The larger the volume of the green body, the more difficult it is to release the volatiles from the interior of the body to the surface. At the same time, the surface and the interior of the green body are more prone to temperature differences and nonuniform shrinkage, which may cause cracks in the green body. The manufacturer optimizes the staged baking rates and the temperature holds, depending on the size of the green compacted article. Since the load is large and has poor thermal conductivity, slow baking rates are necessary to

keep temperature differences at a minimum. Baking cycles from 20 to 72 days, depending on furnace size and product mix, are not unusual (UCAR Carbon Co., Inc., 2001).

Figure 3-22 is an example of an optimized baking schedule for a large isomolded green graphite block.
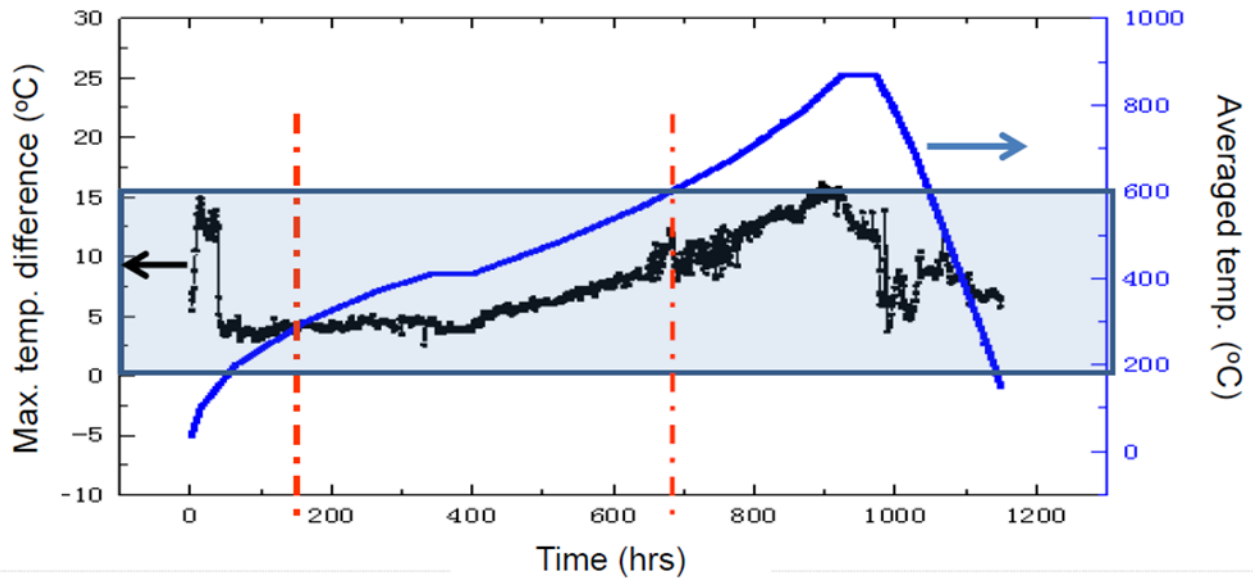
Figure 3-22. Temperature control in baking furnaces, from Yang et al. (2014)

The common quality assurance tests after first bake are bulk density, specific electrical resistivity, and observation of visual defects. After the second bake, visual observations are made for any defects and are then used to optimize the firing temperature, off-temperature schedule, and time. However, more extensive tests are also performed, if agreed upon by the purchaser and the graphite supplier. Perruchoud et al. (2011) have presented data that show the importance of maintaining proper quality assurance procedures for the prototype product that can be translated into producing graphite electrodes on a commercial scale. Additional tests for the baked article include measurements of flexural strength, compressive strength, dynamic Young's modulus, air permeability, thermal conductivity, and CTE. X-ray fluorescence (XRF) elemental analysis is also performed. Table 3-6 shows the test protocols, using International Standards Organization (ISO) standards.

Table 3-6. Baked electrode core testing, adapted from Perruchoud et al. (2011)

No	Test property	ISO standard
1	Baked apparent density	12981-1
2	Specific electrical resistivity	11713
3	Dynamic Young's modulus	51915
4	Flexural strength	12986-1
5	Compressive strength, modulus	18515
6	Air permeability	15906
7	Thermal conductivity	12987
8	CTE	14420
9	XRF elements	12980

3.11   Impregnation and rebaking

During baking, volatile components of the binder escape, and fine pores are left in the product. These are mostly open pores. Figure 3-23 is a schematic of the baked article structure.
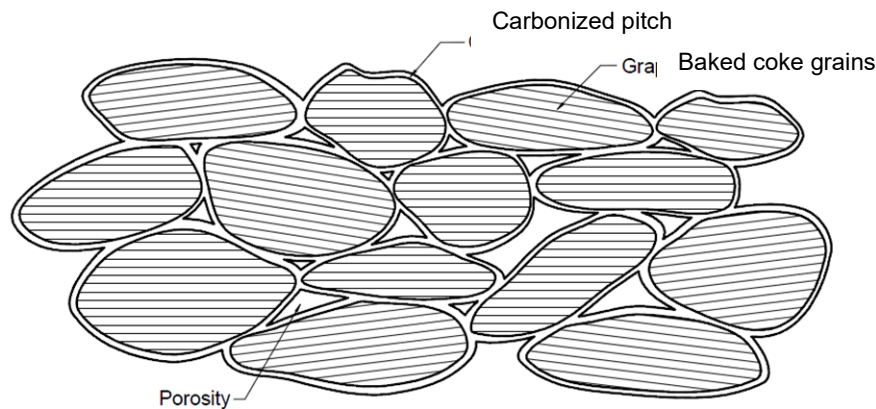
Figure 3-23 Schematic of the compacted article structure after baking. Image courtesy of Metallized Carbon Corporation

The presence of these pores can impair the bulk density, mechanical strength, electrical conductivity, thermal conductivity, and chemical resistance of the product. In production, the porosity is mainly reduced by the asphalt impregnation method (i.e., coal tar pitch is impregnated into the interior of the product through the open pores), and then a rebake carbonizes the impregnated asphalt that filled the initial pores.

The impregnation process consists of first preheating the product in impregnated saggers with good tightness (e.g., Anderson et al., 2002). The preheating temperature depends on the type of pitch impregnant selected, usually around 100 degrees C (212 degrees F); then the impregnation tank is evacuated and the degree of vacuum is controlled. The product is degassed; then the molten pitch is poured into the impregnation tank until the product is

completely immersed. The temperature of the impregnation tank is raised, generally up to about 300 degrees C (572 degrees F). Finally, the tank is pressurized to facilitate impregnation. The applied pressure depends on the size and the green compaction method used. Figure 3-24 is a schematic of a sagger.
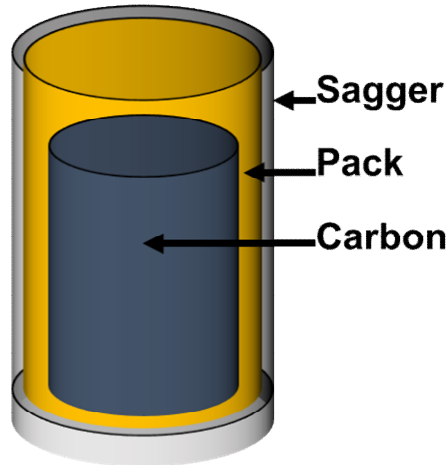
Figure 3-24 Sagger for baking a carbon article

The density of the green compact can be increased gradually using multiple impregnation-bake cycles. Figure 3-25 shows the results of an experimental study. For the mix formulations cited by Nightingale et al. (1962), which likely represent mixes for electrodes as products, the extent of density increase seems to diminish after two impregnations, regardless of the green forming process used; namely, extrusion or molding.
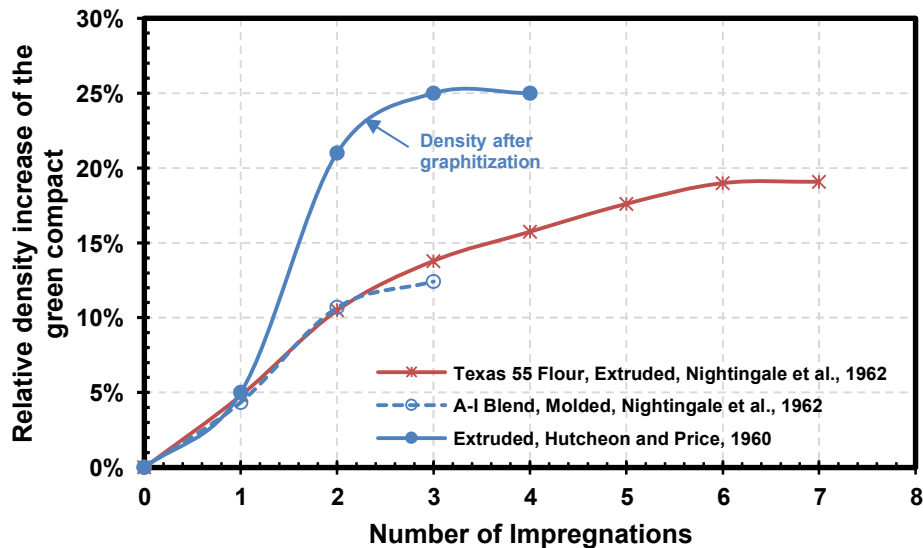
Figure 3-25 Increasing the density of the green compacted body through multiple impregnations, adapted from Nightingale et al. (1962), or increasing the final graphitized density through multiple impregnations, adapted from Hutcheon and Price (1960)

The Hutcheon and Price (1960) data represent an unknown commercial green mix formulation. The relative density increase represents densities measured on graphitized articles. The largest amount of increase in graphitized density was achieved with just two impregnations. Improvements in other properties were also observed, as shown in Table 3-7, on the product graphitized at a temperature of 2,700 degrees C (4,892 degrees F) in an argon atmosphere. In this investigation, properties improvement seems to be generally optimized at three impregnations. The orientation of the specimens tested for bend strength was not reported by Hutcheon and Price (1960).

Table 3-7 Effect of the number of impregnations on the graphitized product, modified from Hutcheon and Price (1960)

Property	Orientation	Number of impregnations				
		0	1	2	3	4
Density, Mg/m^3		1.62	1.77	1.83	1.87	1.87
Air permeability, (10^{-8} m^2)	WG	409	144	50	24	23
	AG	956	194	92	33	11
Electrical resistivity, (10^{-5} Ω/m)	WG	1.06	0.8	0.71	0.67	0.61
	AG	1.82	1.34	1.17	1.11	1.00
Thermal conductivity (W/m°K)	AG	79.5	113	121	134	-
CTE (10^{-6}/°C)	WG	0.8	0.93	0.92	0.94	0.94
	AG	2.44	2.82	2.92	2.99	2.81
CTE (AG/WG) anisotropy		3.05	3.03	3.17	3.18	2.99
Young's mod, MPa	AG	1.99	3.38	4.27	4.55	4.27
Bend strength, MPa		5.24	7.93	17.58	15.86	-

The maximum green density of the carbonized compact can also be substantially increased with just two impregnations, beyond which there is only marginal improvement in green density, based on the data in Nightingale et al. (1962). Improvement in properties can also be observed even with one impregnation, as shown in Table 3-8, from the investigation by Lee et al. (2015).

Table 3-8 Properties of green article after a single impregnation, adapted from Lee et al. (2015)

Property	Before impregnation		After impregnation	
	With grain	Against grain	With grain	Against grain
Bulk density, Mg/m^3	1.6		1.7	
Young's modulus, GPa	7.4	4.4	11.0	6.3
Flexural strength, GPa	10.0	7.1	17.0	13.0
Tensile strength, GPa	5.0	4.4	8.1	7.3
Compressive strength, GPa	21.0	21.0	34.0	33.0
Permeability, μm^2	0.4	0.4	0.2	0.2
CTE, 10^{-6}/°K	1.3	2.7	1.5	3.1
Specific resistivity, μΩm	8.8	13.0	7.6	11.0

Rebaking after impregnation is typically accomplished in large furnaces similar in size and design to those used for the initial baking. However, rebaking is significantly faster because the artifact is already rigid, and it is a minor carbonaceous component within the porosity that is converted to carbon. Generally, the impregnated bulk artifact does not require support during the rebaking. However, protection from oxidation is essential. The cycle of impregnation and rebaking is repeated until the desired properties are achieved.

3.12 **Graphitization**

The basic process for molded synthetic graphite was invented and produced by E.G. Acheson (1896). It is a product manufactured by a compaction process from a mixture of carbon filler and organic binder that is subsequently carbonized and graphitized. Parts of considerable size, weighing several hundred kilograms, such as the electrodes for electric arc furnaces, are manufactured in large quantities. Figure 3-26 shows the original patent drawing.

BB = Carbon rods or electrodes
C = granular carbon core
M = Mixture of coke, sand, salt, and saw dust
A = Acheson graphitization furnace
D = Electric energy source
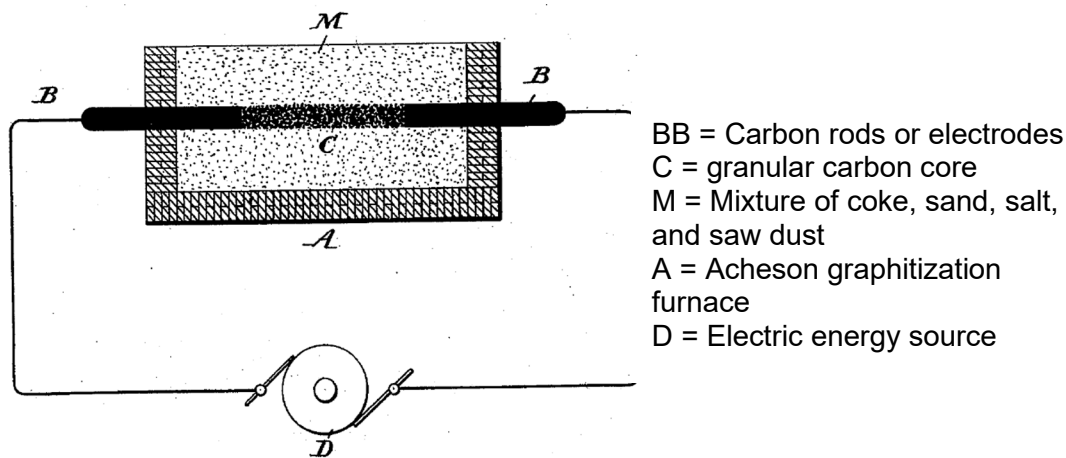
Figure 3-26 Cross sectional representation of the graphitizing furnace in Acheson's patent, adapted from Acheson (1896)

Generally, details of a specific process cannot be uncovered by suitable analyses of the finished product. Graphite manufacturers maintain secrecy of the sources of raw material and processing used to produce graphites, due to the high cost of developing new grades of graphite for specific applications in a highly competitive business. As an example, the reader is directed to a graphite manufacturer's annual Form 10-K disclosure to the U.S. Securities and Exchange Commission (GrafTech International, 2015). Nevertheless, a great deal of information on the basic materials and processes is disclosed in patents, product literature, and other publicly available technical journal articles.

Carbonization after the final bake involves a complex process in which several reactions may take place at the same time, such as dehydrogenation, condensation, and isomerization. The carbon content of the residue is a function of the nature of the precursor and the pyrolysis

temperature. The baking step takes considerably longer to allow the release of pyrolysis gaseous products, minimize thermal gradients, and minimize cracking. It usually exceeds 90 wt.% at 900 degrees C (1,652 degrees F) and 99 wt.% at 1,300 degrees C (2,372 degrees F). The diffusion of the volatile compounds to the atmosphere is a critical step and must occur slowly to avoid disruption and rupture of the carbon network. As a result, carbonization is usually a slow process. Its duration may vary considerably, depending on the composition of the end product, the type of precursor, the thickness of the material, and other factors.

The carbonized structure, known as baked carbon, has little graphitic order and consists of an aggregate of small crystallites, each formed of a few graphite layers with some degree of parallelism and usually with many imperfections. Baked carbon is hard, abrasion resistant, brittle, and has low thermal and electrical conductivities. Therefore, it is used in gas-cooled nuclear reactors as a thermally insulating material.

Graphitization is generally performed by heating the calcined interim product to greater than 2,700 degrees C (4,892 degrees F). The lattice of carbon atoms is arranged in an orderly manner, and the process of converting from carbon to graphite is called graphitization. The graphitization methods include the Acheson method, the internal heat series method, the high-frequency induction method, and the like. The usual Acheson method takes about 1 to 1.5 months from the time the product is installed to the furnace.

3.12.1 Acheson furnacing graphitization

Typically, in the Acheson furnace, the baked carbon product is arranged rectangularly, stacked over one another, and covered with granular refractory resistance material to prevent oxygen intrusion into the furnace. The packing cover mix will scavenge oxygen. Petroleum coke, metallurgical coke, or other carbon-containing oxygen getter is typically used for this function. This packing must also be somewhat conductive to electricity since it will form part of the electrical pathway through the furnace. In addition to restricting oxygen from the articles being graphitized, the packing cover mix serves as a thermal insulator and keeps the heat within the furnace so that the extreme process temperature required for graphitization can be reached.
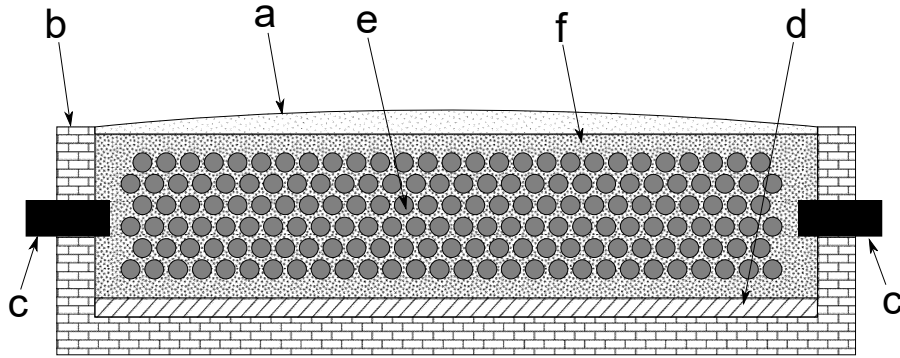
Figure 3-27 A schematic of an Acheson furnace for commercial graphitization, (a) mixture of coke and sand, (b) bricks, (c) carbon electrodes, (d) refractory material, (e) rods to graphitized, (f) granulated coke

Resistance heating to graphitization temperatures occurs with electric current being applied to graphite electrodes through bus bars (Figure 3-27). The cover mix accommodates any increase in volume of the graphitizing product due to sulfur oxidation. With an increasing degree of ordering of crystals or graphitizing, the volume of the graphitizing charge decreases. The major disadvantage of this method is the low energy efficiency and the low productivity per unit area. Such an Acheson process is also known as the "transverse graphitization" process.

3.12.2   Lengthwise graphitization

An improvement over the Acheson method is the Castner process, which involves lengthwise graphitization. Its advantage is the significantly lower cost due to almost one-third in energy consumption and operation time, compared with the Acheson process (Frohs and Roeßnera, 1985). In Castner graphitization, the baked carbon articles, arranged lengthwise, are clamped between the carbon electrodes of a port and are heated directly in contact with the carbon electrodes so that current flows through them, and the surrounding granulated carbon acts as a thermal insulator; otherwise, the furnace is similar to the Acheson design. Figure 3-28 is an example of longitudinal graphitization furnacing.

Figure 3-28 Longitudinal furnace graphitization operation, from Burchell (2018). Image courtesy of Richard W. Barnes, President, ANRIC

The manufacturer controls several process variables in graphitization, depending upon the end use and the properties required. Generally, the manufacturer controls whether or not the interim product has been preheated to 1,400–1,800 degrees C (2,552–3,272 degrees F) for a period of time, the load and the loading arrangement, the heating rate, and the hold time. Graphitization is usually performed by conventional heating rates of about 3 degrees C (37 degrees F) per minute. However, Kennedy (1980) found that the thermal stress resistance of the graphite could be enhanced still further by increasing the heating rate to about 10 degrees C (20 degrees F) per minute over the range from about 1,400 degrees C (2,552 degrees F) to a temperature above the puffing temperature. Heating slowly to 1,400 degrees C (2,552 degrees F) minimized the differential of shrinkage from thermal gradients and pyrolysis. After near-complete dehydrogenation at 1,400 degrees C (2,552 degrees F), the heating rate could be increased without the detrimental sulfur puffing effect.

Figure 3-29 is a schematic of typical temperature-time durations for baking and graphitization steps, which involve slow heating and cooling.
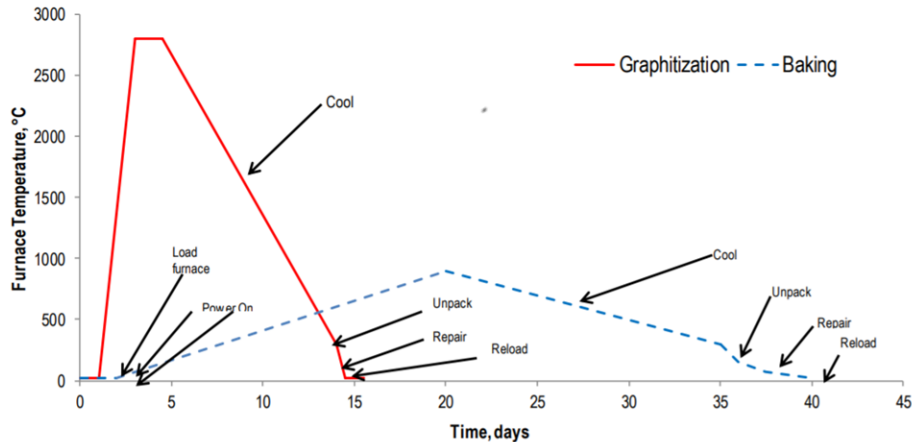
Figure 3-29 A schematic of temperature-time schedule for typical baking and graphitization steps involved in graphite manufacture, from Burchell (2018). Image courtesy of Richard W. Barnes, President, ANRIC

3.12.3   Induction heating graphitization

Induction heating can also be used for graphitization for parts requiring a very well controlled temperature profile—a vertical or horizontal graphite tube of rectangular or cylindrical cross section, with the outside being insulated with carbon black surrounded by a carbon felt jacket. The carbonized material is passed through the furnace either continuously or in batches. Graphitization is performed with the exclusion of oxidation by using water-cooled seals at the ends of the furnace and by applying a stream of inert gas. The main advantage of such furnaces is very close temperature control. Usually, induction heating is useful for relatively small-sized parts requiring substantial product uniformity.

3.12.4   Changes occurring during graphitization

Some fundamental changes in the form of structural rearrangement in the atomic scale to the material occurs in the graphitization process. Such rearrangement is dictated by past processing history, including the ingredients used in the process steps. Ordinary hexagonal graphite is the thermodynamically stable crystalline form of carbon at ordinary pressures. All other forms of solid carbon are metastable and tend to transform to graphite at elevated temperatures. This transformation is called graphitization.

The term graphitization is often misused to designate high-temperature (equal to or greater than 2,500 degrees C (4,532 degrees F)) treatment of carbons without regard for the structure developed. This is incorrect. Graphitization, the development of the hexagonal graphite structure with a regular ABABAB layer stacking sequence, differs from any of the other metastable forms of carbon. These metastable carbons include both crystalline forms (cubic and hexagonal diamond rhombohedral graphite) and forms with poorly developed, disordered

structures (e.g., cokes, pyrolytic carbons, carbon blacks, glassy carbons). There are, then, two general types of graphitization:

(1)   An order-order type involves the transformation of other crystalline forms of carbon to graphite. Graphitizable petroleum coke and coal tar pitch coke, for example, would fall under this category.

(2)   The more common disorder-order type is one in which crystalline graphite is formed from an initially disordered carbon. Pitch used as the binder and impregnant would fall under this category.

As shown in Figure 3-30, graphite crystals have parallel layers (d-spacing of 0.3354 nanometers) of planar C6 rings, in which each layer with one-atom thickness has van der Waals bonding with other neighboring layers. This relative weak bonding (compared to covalent bonding) may allow two-dimensional layers mutually to slip.
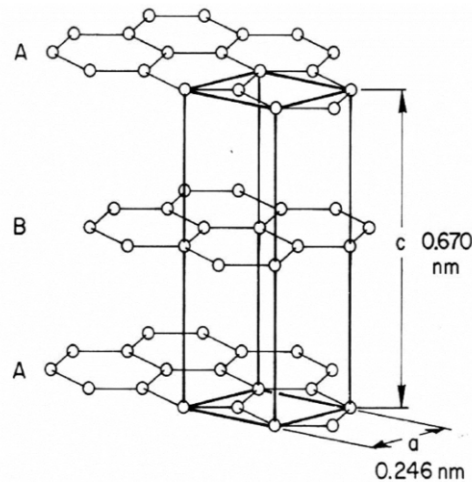
Figure 3-30 Crystalline structure of graphite, from Burchell (2018). Image courtesy of Richard W. Barnes, President, ANRIC

The mean interlayer spacing is a linear function of the mean shear displacement of the layers, so the interplanar spacing, đ, is a good measure of the degree of graphitization. However, there is a broad distribution of interlayer spacing values around đ that contributes importantly to the breadth of the (001) diffraction peaks. Therefore, L_c is more a measure of distortion than of layer stack height in very disordered carbons (Fischbach, 1970). Graphite crystallite sizes are measured along the c-axis, L_c, and the a-axis, L_a, respectively.

Graphitizing carbons have large but very imperfect layers with substantial near-parallel stacking. High-temperature heat treatment improves and perfects this intrinsic graphitic structure toward that of perfect graphite by removing the defects. Graphitization is, therefore, a sort of

generalized disorder-order transformation[5] that proceeds by a process of annealing. During the graphitizing process, the turbostratic carbon is converted into a three-dimensionally ordered graphite structure. Graphitization is a time- and temperature-dependent thermally activated rate process (Figure 3-31).
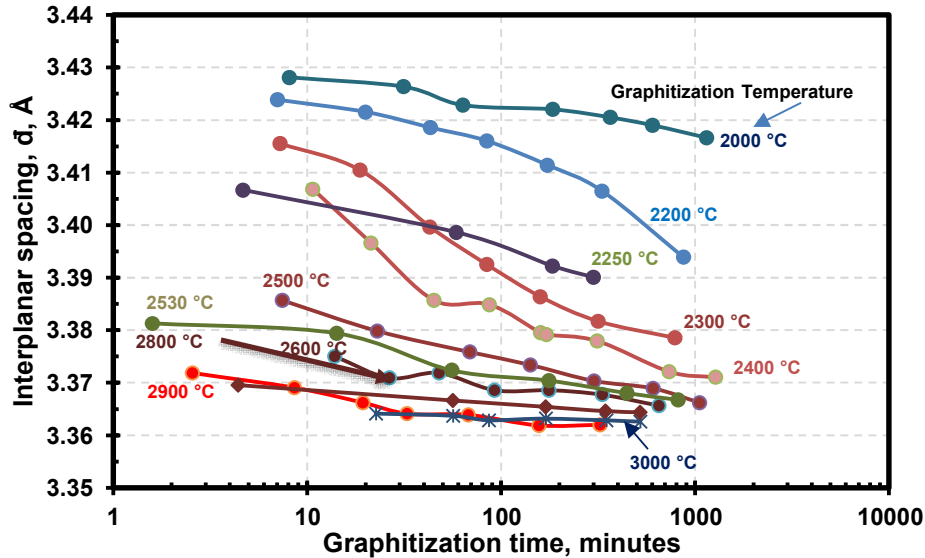
Figure 3-31 Typical isothermal graphitization curves for a petroleum coke, data adapted from Fischbach (1970) and Pierson (1993)

In Figure 3-31, the data for 2,000, 2,250, 2,530, 2,800, and 3,000 degrees C (3,632, 4,082, 4,586, 5,072, and 5,432 degrees F, respectively) are due to Pierson (1993). The data for 2,200, 2,300, 2,400, 2,500, 2,600, and 2,900 degrees C (3,632, 4,082, 4,586 and 5,072 degrees F, respectively) were extracted from Fischbach (1970). Information on the constituents of the initial mix formulation, milling, mixing and kneading, green forming, impregnation cycles, and baking are not available for these data. The general trends dictated by the thermally activated process are maintained in both data sets. The data coincide at graphitization temperatures greater than about 2,900 degrees C (5,252 degrees F), confirming that the disorder-order transformation mechanism to form crystalline graphite is solely defined by the graphitization temperature, once the initial pseudo-ordering has taken place for the graphitizable carbons, constituting the graphitizable product resulting from the baking and carbonization process.

The data shown in Figure 3-31 can be used to estimate the degree of disorder (DOD) of the graphitized article. The theoretical value of d_{002} has usually been stated as 3.354 Å for graphite with "completely or perfectly" ordered structure (Marsden, 2001; Zhang and Wang, 2017). Using this value, Figure 3-32 gives the estimates for DOD.

---

[5]   This term is used here in the general sense relating to lattice perfection. It is dissimilar to the configurational short- or long-range order-disorder phenomena observed in many metal alloy systems and in some graphite interlaminar compounds (Fischbach, 1970).
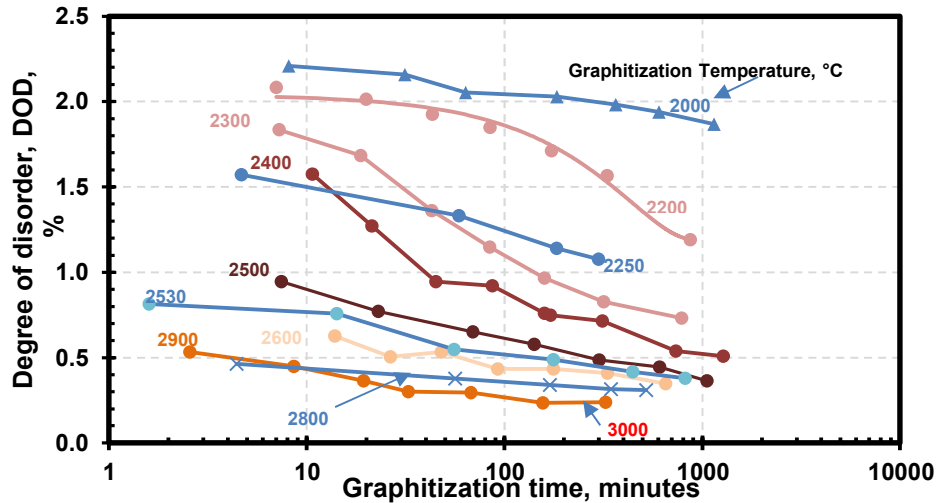
Figure 3-32 Ordering of the structure as a result of graphitization,
data adapted from Fischbach (1970)

The graphitization of carbons is a thermally activated disorder-order process in which the existing structure is improved toward the ideal graphite structure over time. Appreciable ordering of the graphitic structure seems to occur only at temperatures greater than 2,800 degrees C (5,072 degrees F). Paragraph 5.6.3 of ASTM D7209 requires a graphitization temperature of at least 2,700 degrees C (4,892 degrees F).

The data shown in Figure 3-31 and Figure 3-32 confirm the kinetics of graphitization of cokes to be a growth process and not a nucleation-based process. Usually, a single-valued activation energy is reported at 962 ± 60 kilojoule per mole (230 ±15 kilocalorie per calorie) in the range of 2,300–2,900 degrees C (4,172–5,252 degrees F) for typical industrial cokes (Pierson, 1993).

Gallego et al. (2018) studied the structure of unirradiated and irradiated NGNP research samples of NBG-18, IG-110, and PCEA graphites using XRD. Figure 3-33 shows their baseline average estimated degree of crystalline disorder for these three graphite grades. No specific manufacturing details are available for the graphitization steps for these graphites, although it is surmised they were all graphitized at temperatures greater than 2,800 degrees C (5,072 degrees F). The data indicate that more than 99 percent of the structure is ordered. Similarly, Huang et al. (2014) characterized IG-110, IG-430, NBG-17, and NBG-18 by XRD and found more than 99 percent of the structure of these graphites was ordered, as well.
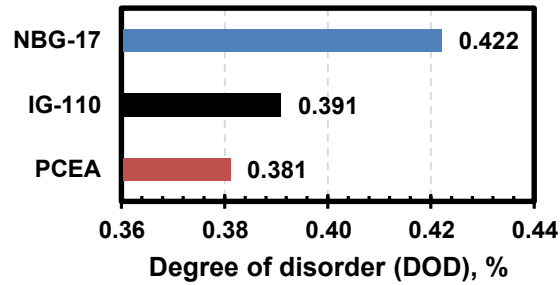
Figure 3-33 Degree of crystalline disorder for three grades of graphites examined in the NGNP research, data adapted from Gallego et al. (2018)

Another factor impacting the crystalline order of final graphite is the crystalline preorder of the solid used, as cokes with a higher degree of crystalline preorder show a tendency toward better graphitization.

The reduced lattice layer distances during graphitization are macroscopically noted as a contraction in volume. This graphitization shrinkage is generally approximately 3–5 percent but can be up to
8–10 percent. The density of the graphite increases due to this shrinkage. Figure 3-34 shows an example of the shrinkage observed during graphitization for a needle coke graphite.
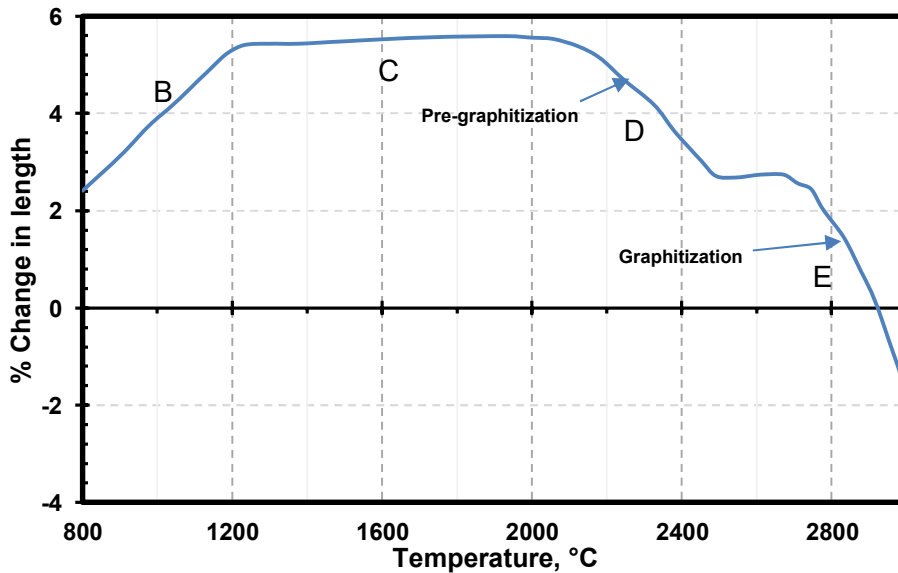
Figure 3-34 Graphitization dilatometric curve for graphite with petroleum needle coke, from Perruchoud et al. (2011) (see Table 3-9 for changes occurring in B to E regions)

During graphitization, the heteroatoms (nitrogen, oxygen, sulfur), which are always present to some degree in coal tar pitch coke and petroleum coke, become unstable as heat treatment progresses, and their evolution can have significant microstructural effects. At temperatures up

to 1,400 degrees C (2,552 degrees F), oxygen and nitrogen are released during shrinkage cracking. Accordingly, their evolution is likely innocuous in coke calcining processes. However, sulfur-evolution from petroleum coke only just begins as calcining is completed and can continue to temperatures as high as 2,500 degrees C (4,532 degrees F). The sudden evolution of sulfurous gases (primarily hydrogen sulfide) develops submicron-size porosity in the coke particle and can produce destructive dimensional changes ($\Delta l/l_0 \sim 3\%$) in a binder-filler artifact. These swelling effects, generally termed "puffing," are dependent on the microstructure as well as the sulfur content of the coke. The fine fibrous morphology of needle coke is very susceptible to puffing despite the presence of shrinkage cracks; on the other hand, the stronger particles of isotropic cokes, which are commonly high in sulfur content, are resistant to puffing. Although only limited micrographic evidence of the puffing phenomenon is available, diffraction studies indicate that puffing induces graphitization (White, 1975). Table 3-9 summarizes the structural changes that accompany graphitization.

Table 3-9 Structural change and phenomena occurring during graphitization

Step	Temperature range	Governing phenomenon/property
A	Room temp. up to final baking temperature	Normal thermal expansion
B	900–1,200 °C (1,652–2,192 °F)	Calcination of the filler component is completed; graphitic structure formation begins slowly
C	1,500–2,000 °C (2,732–3,632 °F)	Evolution of hydrogen and sulfur from the binder (puffing) and an irreversible volume expansion occurs
D	> 2,000 °C (4,352 °F)	Conversion to the graphitic structure proceeds more rapidly and increases at > 2,200 °C (3,992 °F)
E	2,600–2,900 °C (4,712–5,252°F)	Crystallite growth predominates with simultaneous contraction in volume
F	3,000 °C (5,432 °F)	Thermal and electrical conductivity reach the optimum

The various phenomena stated in Table 3-9 lead to intergraphitic grain accommodation of thermal expansion and contraction, resulting in the formation of microcracks within the graphite grains. The graphitization shrinkage cracks are found in a variety of sizes and spacings. A major fraction of the high thermal expansion in the c-direction can be accommodated by the graphitized coke grain, which is aligned parallel to the layers. The accommodation efficacy depends on the spacing relative to the size of the filler coke particles employed in fabrication.

The shrinkage cracks also provide mechanisms to decrease the effective elastic modulus and the cleavage strength of a graphitized coke grain. Additionally, when cracking occurs, the progress of a fracture across the convoluted folded structure will be tortuous, and many blind fractures will initiate before the main fracture path is developed. This effect will absorb energy and contribute to the enhancement of the fracture toughness of the graphitized coke grain.

3.12.5   Property changes occurring during graphitization

Table 3-10 summarizes the changes to the artifact property from the baked stage to the graphitized state.

Table 3-10 Property changes due to graphitization

Property	Change
Apparent density	Decreases, ↓
Porosity	Increases, ↑
Weight	Decreases, ↓
Elastic modulus	Decreases, ↓
Strength	Decreases, ↓
CTE	Decreases, ↓
Electrical resistivity	Decreases, ↓
Thermal conductivity	Increases, ↑

Figure 3-35 shows the decrease in specific electrical resistivity as a function of graphitization temperature for a fine-grained isomolded graphite (UCAR Carbon Co., Inc., 2001).
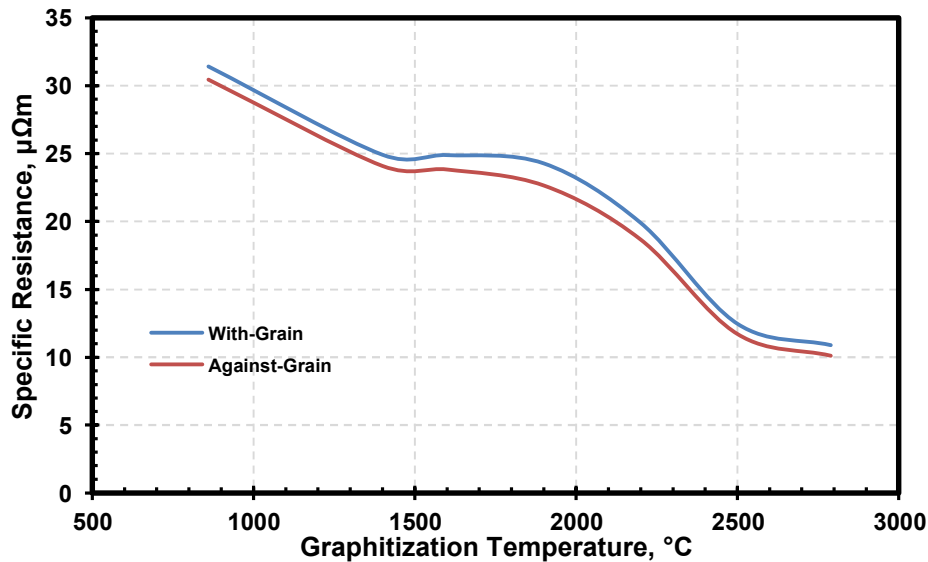
Figure 3-35 Electrical resistivity as a function of final graphitization temperature, adapted from UCAR Carbon Co., Inc. (2001)

Figure 3-36 shows the decrease in flexural strength as a function of graphitization temperature for a fine-grained isomolded graphite. Figure 3-37 shows the decrease in tensile strength as a function of the graphitization temperature for a fine-grained POCO graphic.
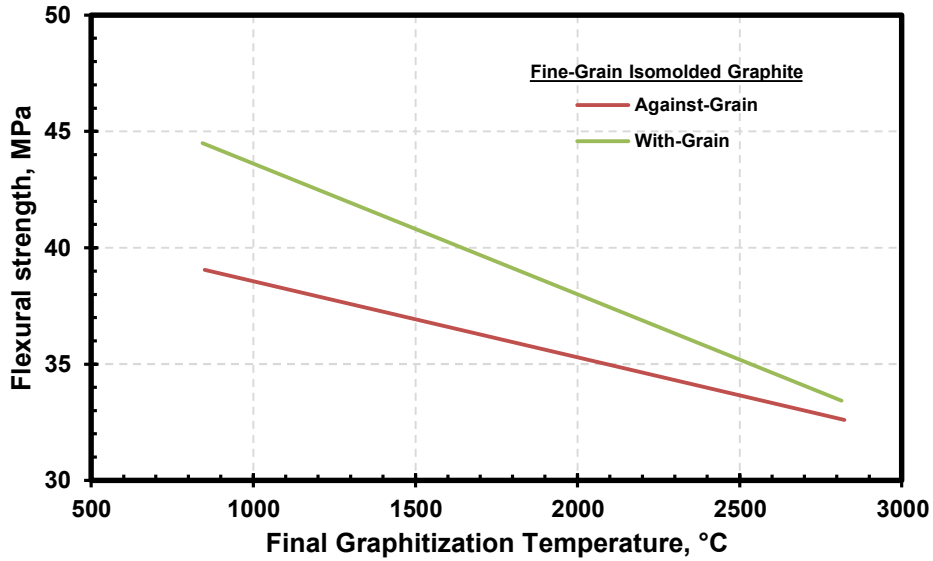
Figure 3-36 Flexural strength as a function of final graphitization temperature,
adapted from UCAR Carbon Co., Inc. (2001)
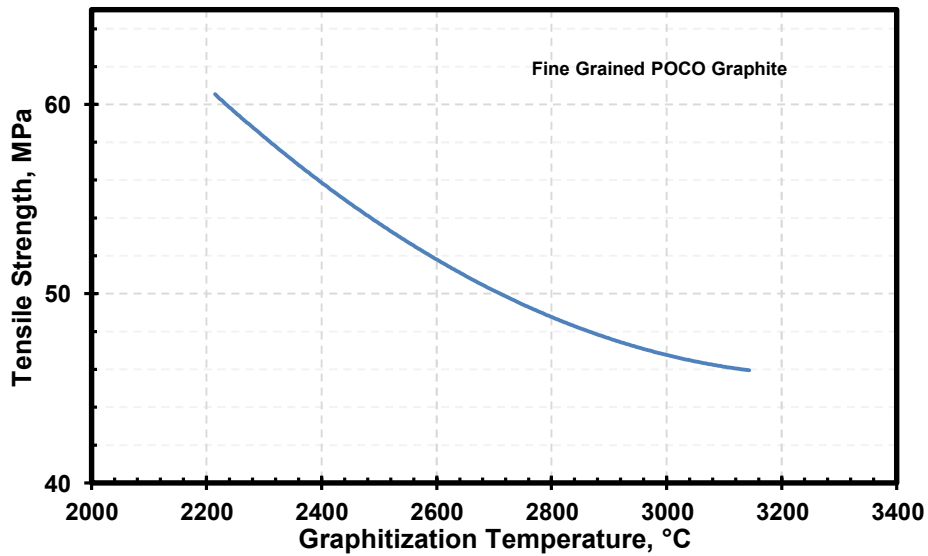
Figure 3-37. Tensile strength as a function of final graphitization temperature,
adapted from POCO Graphite, Inc. (2015)

Figure 3-38 shows the decrease in CTE as a function of the graphitization temperature for a fine-grained isomolded graphite.
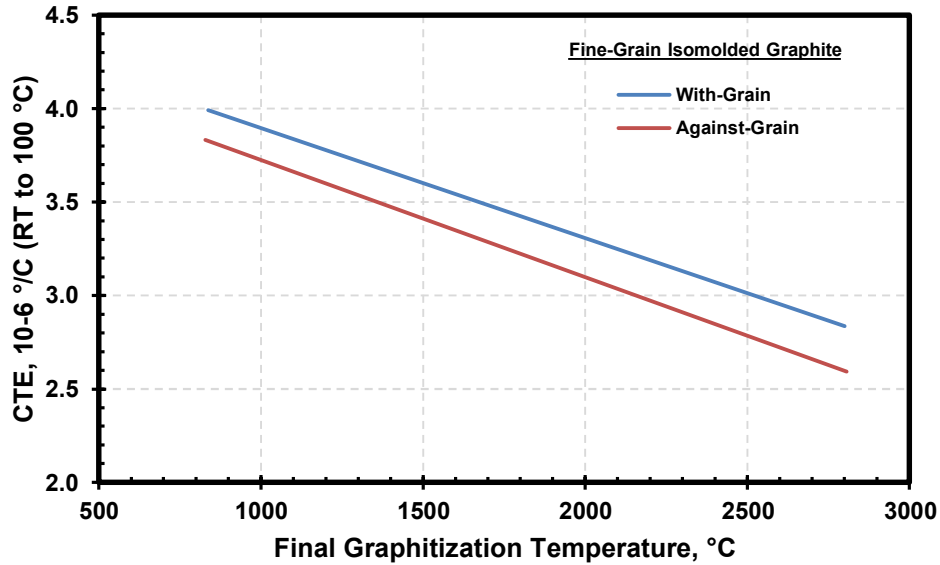
Figure 3-38 CTE as a function of final graphitization temperature, adapted from UCAR Carbon Co., Inc. (2001)

3.12.6   Purification for nuclear use

The graphitizing process is also accompanied by a purification of the product due to thermal reaction, vaporization, and elimination of impurities that would have migrated to the outer surface. Normally, the overall impurities content is reduced to less than 1,000 ppm. Graphitization is a sort of zone-refining process, in which impurities migrate gradually by diffusion to lower temperature regions, mostly from the interior of the body outwards.

Additional reduction can be achieved by thermal treatment. For example, Marek et al. (1968) heat treated graphite to contain ash content to less than 16 ppm. They thermally purified the filler to an ash level of less than 16 ppm. However, when the filler was mixed with pitch and processed normally, the ash level of the graphitized samples increased to more than 500 ppm. Postgraphitization thermal treatment at 2,350 degrees C (4,262 degrees F) decreased the ash content to 32 ppm; at 2,900 degrees C (5,252 degrees F), the ash content was less than 5 ppm (Figure 3-39).
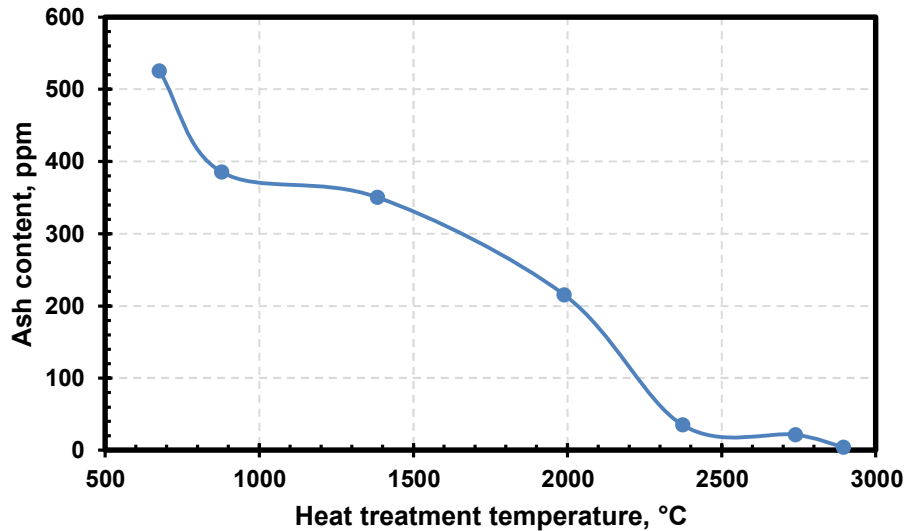
Figure 3-39 Purification by thermal treatment of graphite, adapted from Marek et al. (1968)

The above result was achieved on a laboratory-made small sample. Purification to a higher degree on a commercial scale usually does not reproduce the efficacy observed by the thermal treatment of laboratory-made samples.

To meet nuclear graphite specifications, graphite purity resulting from graphitization may be insufficient. In such cases, a thermal purification at higher temperatures, up to 3,100 degrees C (5,612 degrees F) with longer residence time can reduce the overall impurities concentration to less than 200 ppm. If still lower ash values are required, a thermo-chemical purification is necessary.

Because the impurities migrate to the exterior of the graphitized article, they can be removed by a halogenation treatment to about 2,000 degrees C (3,632 degrees F). By adding halogens (typically chlorine[6]) or halogen gaseous compounds that decompose at high temperatures to produce gaseous carbon tetrachloride (CCl_4), dichlorodifluoromethane (CCl_2F_2), all heteroatoms forming stable carbides react to form low-boiling volatile halogen compounds and are thus removed. A total impurities content of less than 1 ppm can be achieved by thermo-chemical purification. However, the residual chlorine content after purification should be minimized to avoid disposal issues by the long-lived and soluble chlorine-36 neutron activation product.

For example, Albers et al. (2010) promoted a purified halogen gas treatment from about 2,200 degrees C (3,992 degrees F) to 2,600 degrees C (4,712 degrees F). A general purification efficiency has been provided by Eatherly and Piper (1962), as given in Table 3-11.

---

[6]   The use of chlorine has led to significant decommissioning issues due to the generation of chlorine-36, which has an extremely long half-life. Its half-life is 301,300 ± 1,500 years. ASTM D7219 suggests limiting chlorine to less than 5 ppm.

Table 3-11 Representative impurity reductions after graphitization treatments, adapted from Eatherly and Piper (1962)

Impurity	Impurity content, ppm		
	As-graphitized	Thermally purified	Chemically purified
Total ash	1,600	540	5
Silicon	94	46	<1
Iron	310	10	<2
Vanadium	30	25	<0.2
Titanium	34	11	1
Aluminum	40	2.5	0.1
Calcium	320	147	1.4
Boron	0.5	0.4	0.06
Sulfur	175	19	10

3.13   **Microstructure of graphite**

The microstructure of graphite is characterized primarily by four features: (1) pores, (2) graphitized filler particles, (3) the graphitized binder, and (4) shrinkage cracks. Most commercial graphites have a typical formulation of approximately 25 wt.% binder with a graphitizable[7] char yield of about 50 wt.% so that the final graphite will have approximately 10 wt.% of the graphitized binder and 90 wt.% of the graphitized filler (Thrower, 1983). Once transformed into graphite, it is difficult, if not impossible, to distinguish between the graphitized binder and filler regions using ordinary microscopy techniques. However, it is well known that some poorly graphitized binder regions remain, which have a higher chemical activity. The microstructure of four graphites reported by Ubic (2014a) are described below as examples of the graphite microstructure.

---

[7]   Graphitizability represents the potential for crystallite growth to the theoretical interlayer spacings for graphite. Crystallite growth is very temperature dependent but the limitation for growth is a characteristic of the raw material (Marek et al., 1968).

IG-110 graphite: This graphite is isomolded with a petroleum coke filler. Figure 3-40 shows the optical micrograph of IG-110 graphite.
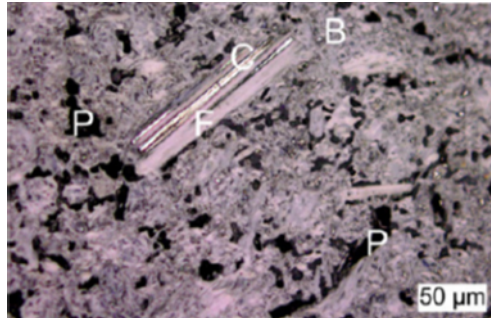
Figure 3-40 An optical micrograph of IG-110 graphite; pore (P) areas, graphitized filler coke (F), graphitized binder (B), and graphitization shrinkage crack within the filler (C), from Ubic (2014a)

The mean length of filler coke was estimated as 27 ± 2 μm with a standard deviation (σ) of 22 μm, as compared to the manufacturer's value of 20 μm. The mean aspect ratio was 3.9 ± 0.2, σ = 2.4. Such an aspect ratio is rather large for an isomolded material. Since many of the basic properties are governed by the porosity, anisotropic behavior may be expected for this graphite.

It is considered normal to sometimes observe long, rectangular coke grains in graphite microstructures. The reason is the way the ground coke is sieved for separating into a range of desired sizes to form a mix. The initial coke size is defined by the mesh size through which the grains pass. It is possible for a long but thin needle, or rectangular shaped particle, to pass through a mesh if the cross section of an elongated particle is smaller than the mesh size.

PGX graphite: This graphite uses petroleum needle coke as a filler. Figure 3-41 shows the optical micrograph of PGX graphite.
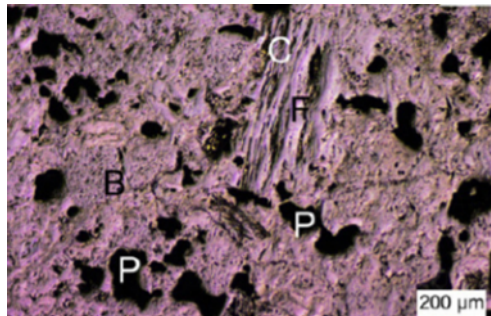
Figure 3-41 An optical micrograph of extruded PGX graphite; pore (P) areas, graphitized filler coke (F), graphitized binder (B), and graphitization shrinkage crack within the filler (C), from Ubic (2014a)

The graphitized filler coke particles in PGX graphite were approximately three times larger than those in IG-110, with a length of 92 ± 7 μm and σ = 85 μm. Remarkably, despite extrusion being the green compaction route, the aspect ratio of PGX filler coke, 3.1 ± 0.1 with σ = 1.6, is

lower than that found for IG-110 graphite. Shrinkage cracks in PGX were more numerous and wider than those observed in IG-110 graphite.

NBG-18 Graphite: NBG-18 graphite uses a coal tar pitch coke as a filler and is vibrationally molded in green forming. Figure 3-42 shows the optical micrograph of NBG-18.
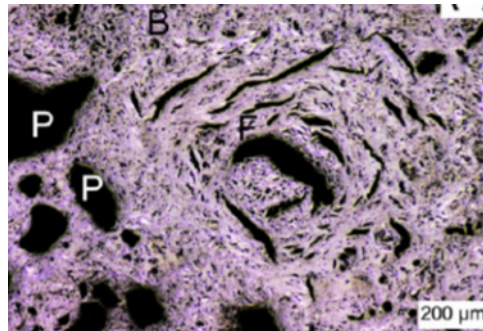
Figure 3-42 An optical micrograph of extruded NBG-18 graphite; pore (P) areas, graphitized filler coke (F), graphitized pitch binder (B), and graphitization shrinkage crack within the filler (C), from Ubic (2014a)

The graphitized filler coke has mostly spherical geometry. The mean particle size was estimated as 360 ± 25 µm with σ = 217 µm. The maximum particle size observed was approximately 1,800 µm, as compared to the manufacturer's stated maximum nongraphitized coke particle size of 1,600 µm in the initial mix. Considering that about 6 to 10 percent shrinkage occurs due to graphitization, this is a surprising result.

The nearly spherical nature of the NBG-18 filler material could contribute to the presence of some disordered crystallites. The crystallites in the center of the particles, in general, appear to be small and randomly oriented. Those toward the particle exterior appear larger, with their long axes aligned with the particle circumference. In conformance, the small shrinkage cracks toward the center of the graphitized filler grains appear to be randomly oriented, while those near the perimeter of the grain appear to be oriented similar to the larger shrinkage cracks.

PCEA graphite: PCEA graphite uses petroleum needle coke as a filler and extrusion in green forming. Figure 3-43 shows the optical micrograph of PCEA graphite. Approximately 70 percent of graphitized filler grains had acicular geometry, with a mean length of 137 ± 12 µm with σ = 88 µm. The mean aspect ratio of the acicular grains was 3.2 ± 0.2 with σ = 1.4. The acicular graphitized filler grains in PCEA are slightly larger than those in PGX but had a nearly identical aspect ratio. The graphitized spherical filler grains in PCEA had a mean diameter of 99 ± 21 µm with σ = 102 µm. PCEA filler grains exhibited varying degrees of crystalline ordering.

The shrinkage cracks in PCEA were relatively narrow compared to cracks observed in NBG-18. Small shrinkage cracks had a random orientation. Large shrinkage cracks had a preferred orientation along long axes for acicular grains. For near-spherical grains, the shrinkage cracks were aligned with one another but not along any particular axis of the graphitized filler grain.
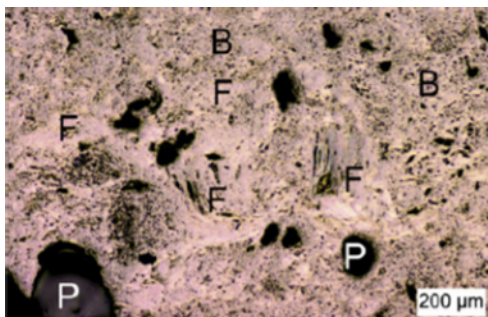
Figure 3-43 An optical micrograph of extruded PCEA graphite; pore (P) areas, graphitized filler coke (F), graphitized binder (B), and graphitization shrinkage crack within the filler (C), from Ubic (2014a)

Ubic (2014a) analyzed the distribution of porosity of these graphites using automated quantitative image analysis, with the results shown in Figure 3-44. They show that each graphite grade had a relatively similar distribution. The largest deviation was for IG-110 graphite. Ubic attributed this observation to isomolding used in green compaction versus extrusion for other graphites. Ubic estimated the continuous probability distribution functions of porosity fit an elliptical shape. The results showed that only about 6 percent of the total pores may be described as approximately spherical while nearly 75 percent of the pores examined have aspect ratios between 1.5 and 5. The average aspect ratio of porosity in nuclear graphite is approximately 1.7 and ranges from a low of 1.66 for IG-110 to a high of 1.75 for PGX graphite. Differentiation in shape distribution between pores and microcracks was not possible by analyzing image data.
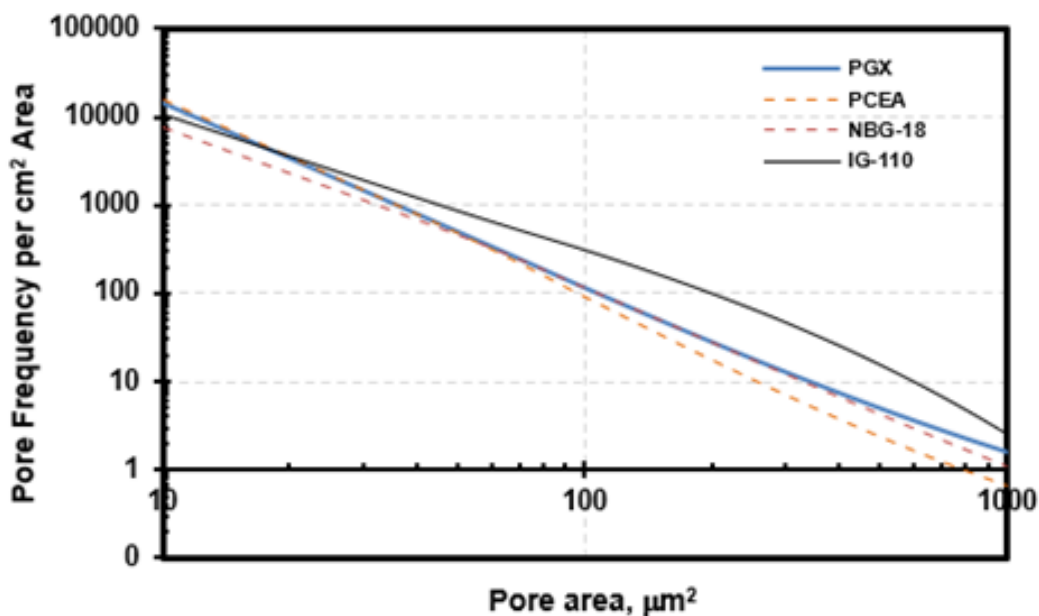
Figure 3-44 Pore size distributions for several recent grade nuclear graphites, adapted from Ubic (2014)

Generally, the distributed porosity and the microcracks within the graphite grains influence many of the graphite properties. The distributed porosity can be traced back to the compacting of the green mix during forming; subsequent impregnation-baking cycles; and the escape of residual volatile organics, nitrogen, and sulfur during heat treatment before graphitization. While prediction of porosity distribution using process parameters can be difficult, to obtain near-isotropic properties, it is good practice to start with near-isotropic powder that has been ground to as near a spherical shape as possible.

3.14   Graphite qualification

Customarily, graphite manufacturers perform the following quality assurance tests on graphitized logs by using predetemined sampling, which depends on the size of the graphitized body. Bulk density is determined using ASTM C559, "Standard Test Method for Bulk Density by Physical Measurements of Manufactured Carbon and Graphite Articles." Specific resistivity is determined using ASTM C611, "Standard Test Method for Electrical Resistivity of Manufactured Carbon and Graphite Articles at Room Temperature." Room temeprature Young's modulus and shear modulus are determined using rectangular bars and establishing their resonance nodal lines, applying the method in ASTM C747, "Standard Test Method for Moduli of Elasticity and Fundamental Frequencies of Carbon and Graphite Materials by Sonic Resonance." The elastic modulii are also determined using ultrasonic excitation and by establishing the sonic velocity through the specimen, applying the method in ASTM C769, "Standard Test Method for Sonic Velocity in Manufactured Carbon and Graphite Materials for Use in Obtaining an Approximate Value of Young's Modulus." The graphitized article is also visually examined for surface blemishes and cracks.

For meeting customers' purchase specifications, graphite manufacturers also conduct qualification tests on parent stock by sampling and machining, such as (1) ash content, (2) total carbon, (3) bulk density, (4) specific electrical resistivity, (5) CTE, (6) Young's modulus, (7) permeability, (8) off-gas rate, (9) flexural strength, and (10) hardness. Table 3-12 shows an example of tests conducted by R&D Carbon, Ltd., in Switzerland, for graphite electrodes. It is likely that nuclear graphite manufacturers follow a similar practice.

Table 3-12 Typical tests for graphitized electrode ores, adapted from Perruchoud et al. (2011)

No	Test property	ISO standard
1	Apparent density	12981-1
2	Xylene density	8004
2	Specific electrical resistivity	11713
3	Dynamic Young's modulus	51915
4	Flexural strength	12986-1
5	Fracture energy	12986-1
6	Compressive strength, modulus	18515
7	Air permeability	15906
8	Thermal conductivity	12987
9	CTE	14420
10	XRF elements	12980
11	XRD, L_c, and c/2	20203

The finished graphite is also inspected for flaws. As an example, the following criteria were set for the Chinese HTR-PM for IG-110 graphite components: "HTR-PM IG-110: <u>External appearance</u>: Surface shall be free from detrimental cracking (> 0.5 mm), chipping, pinhole (> 0.5 mm diameter), or attachment of foreign substance. Slight difference in dimensions and chipping of corners shall be within the allowable range (that will not affect machining of products)" (Yu and Sun, 2010).

ASTM D7219 paragraph 12.1 *requires* all graphite billets be visually inspected for external flaws where the allowable size, type, and number of flaws are agreed upon between the purchaser and the manufacturer as described in the purchase specification.

ASTM D7219, paragraph 12.2, *recommends* all graphite billets be nondestructively tested (NDT) to screen for internal defects where the allowable size, type, and number of flaws are agreed upon between the purchaser and the manufacturer as described in the purchase specification

It is noted that, whereas actions stated in paragraph 12.1 are requirements, the actions stated in paragraph 12.2 are recommendations.

Screening for internal defects in large graphite components will require custom-optimized x-ray analysis and ultrasonics as nondestructive tests, which have been demonstrated in literature. Sato et al. (2007) demonstrated the use of ultrasonics to detect flaws in isomolded graphite intended for aerospace applications. Kunerth and McJunkin (2011) reported on the use of radiography, eddy current and ultrasonic techniques for detecting flaws and graphite. Figure 3-45 below provides an example of ultrasonic nondestructive evaluation of a production grade medium-grain, vibrationally molded billet (Block A) and an experimental grade of fine-grained isomolded graphite (Block B) from Kunerth and McJunkin (2011).
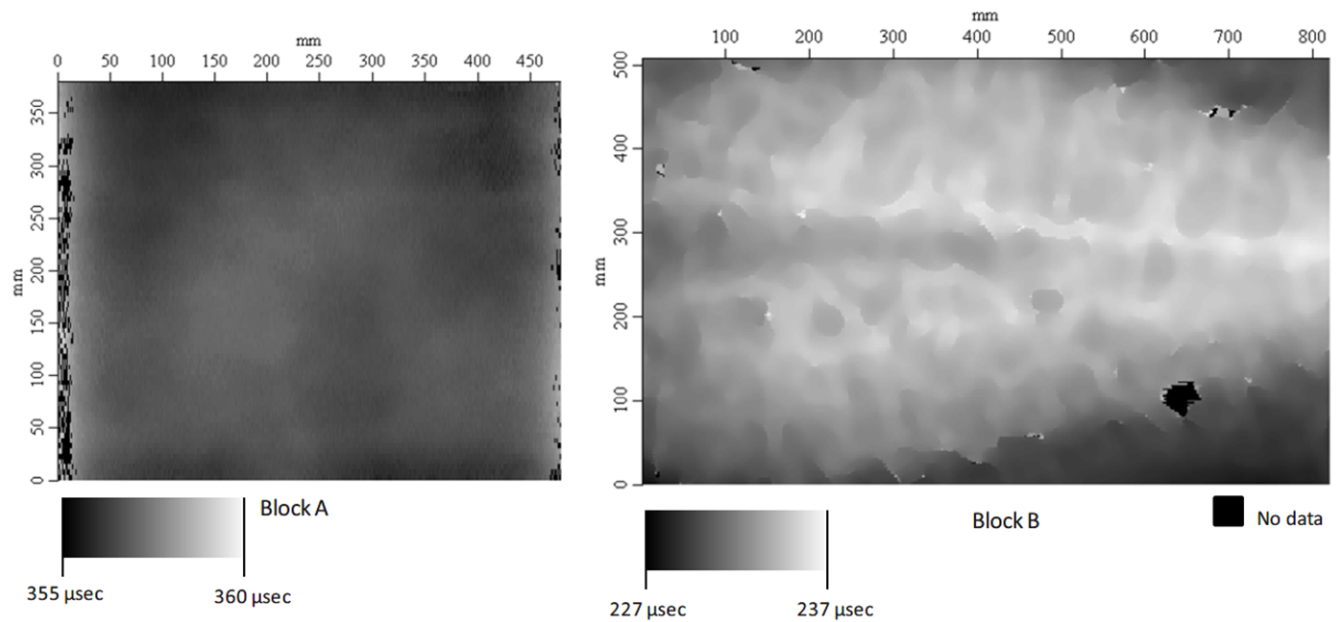
Figure 3-45 Back wall time-of-flight C-scan images of two different machines graphite blocks. Block B has significant variations in acoustic velocity suggesting that there will be similar variations and mechanical properties.

3.15   Summary

The manufacture of graphite generally consists of fillers, binders, and impregnants, as well as additives to aid processing. Fillers are made of either petroleum coke or coal tar pitch coke. Combinations of distillation and/or pyrolysis take the raw source material (heavy crude oil or coal tar pitch) and transform it into a solid coke to be used as the filler material in graphite. It is possible to vary the source of oil and the process parameters and obtain coke with different degrees of crystalline order, strength and CTE values. Once the coke has been prepared and delivered to the graphite manufacturer, the manufacturer will grind the coke filler particles to the required PSD to optimize the particle packing density. Graphite manufacturers test the quality of the coke using several techniques, such as (1) vibrated bulk density, which is used as a surrogate for measuring coke porosity (2) coke friability, to establish the propensity of the coke to crumble or break into fragments during the grinding process (3) particle size distribution (4) chemical analysis to establish the coke purity, including ash content (5) the CTE, and (6) less commonly, the crystallite size of the coke. As the average size of the coke filler particle size decreases, the strength and elastic modulus of graphite increases, and the fracture toughness decreases.

The other main component of graphite is made the pitch binder, typically coal tar pitch. Manufacturers will qualify the pitch intended for use. Of particular consideration are (1) insoluble organic compounds such as quinoline, which produce nongraphitizable carbon, (2) the flashpoint of the pitch to assess its flammability hazard during production, and (3) the softening point of the pitch, which is used as an index for ensuring consistency of pitches from different supply sources. In addition to these standard tests, graphite manufacturers typically

develop custom procedures to measure the effectiveness of the separation of solids in the pitch; the potential of the pitch to penetrate the green-formed article; and lubricity, which is a measure of friction between services for optimizing process parameters for molding. The binder content of the green mixture appears to have a minor influence on the CTE of the resulting graphite, where increasing binder content increases the CTE, although the final binder content in the green mixture for most graphites is typically between 18 and 22 wt.%.

The green body is then formed by isomolding, uniaxial pressing, vibrational molding, or extrusion. The method used to form the green body affect the final isotropy and uniformity throughout the graphite component. In general, superior isotropy and uniformity across the graphite product is provided by isomolding, followed by uniaxial pressing and vibrational molding, and finally, extrusion, where extrusion typically produces the most anisotropic properties and nonuniformity.

After the green body is formed, it is baked, typically below 1,250 degrees C (2,282 degrees F). Following the baking cycle, the baked carbon body is impregnated with additional pitch (typically coal tar pitch) and rebaked. The relative density of the green body increases with the number of impregnations, with diminishing effect as the number of impregnations increases. Following the final baking, the carbon body is graphitized at a minimum of 2,700 degrees C (4,892 degrees F). The actual process of graphitization is a generalized disorder-order transformation where less ordered carbon is converted into the predimensional ordered graphite structure. Perfect graphite crystals have a spacing of 0.3354 nm between the parallel layers of the graphite structure, which can be measured by XRD. Higher graphitization temperatures result in a more ordered (more perfect) graphite structure, or a smaller DOD. Thermal conductivity and irradiation resistance improve with a more ordered graphite structure, while the CTE and strength decrease. Following graphitization, the purity of the graphite can be improved through thermal purification and halogenation. Halogenation can introduce residual chlorine, which has potential implications for long-term storage, as chlorine-36 is a long-lived insoluble activation product. The final graphite microstructure is inherently heterogeneous, consisting of graphitized filler coke, graphitized pitch binder, shrinkage cracks, and pores.

After graphitization and any subsequent purification steps, the graphite is tested and inspected to ensure it meets internal quality controls and customer purchase specifications. Common tests include measuring ash content, bulk density, electrical resistivity, CTE, Young's modulus, and flexural strength. ASTM D7219 requires the visual examination of graphite to detect external flaws and only recommends nondestructive examination to detect internal flaws.

4 THERMAL OXIDATION RESISTANCE

Generally, the extent of the thermal oxidation of graphite by air is determined by a number of different processes depending on the temperature, as shown in Figure 4-1.
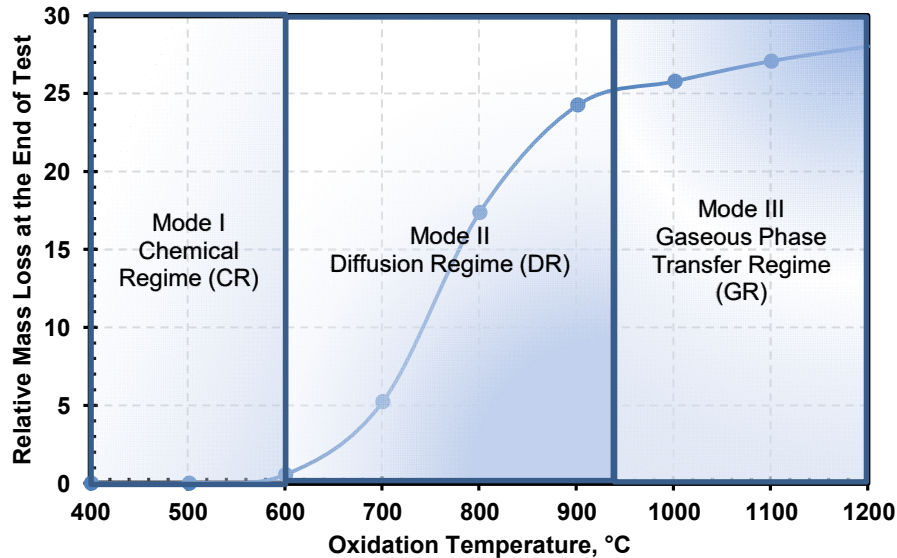
Figure 4-1 A general schematic of the oxidation of a typical nuclear graphite (modified from Commissariat à l'énergie atomique, 2006)

In Mode I, the chemical regime, oxidation is controlled by the kinetics of the chemical oxidation reactions. In this regime, mostly open volume pores, with abundant surface free active sites and complexes, contribute to oxidation. Thus, it may not change the outside dimensions, and as a result, mass may be preserved to a large extent. Oxidation progressively weakens the structural strength of the graphite by increasing the size of the open pores and access to previously closed pores. The resulting decrease in density with weight loss could eventually compromise the structural integrity of the graphite (El-Genk and Tournier, 2012). Growcock et al. (1980) published thermal oxidation data on several graphites showing the weight loss is highest near the surface (volume pores) and decreases almost exponentially with distance into the test specimens. This is because the weight loss within the volume pores is not uniform; the chemical regime exists in combination with the in-pores diffusion-controlled regime, Mode II, or diffusion regime. In Mode II, the mobile oxygen molecules diffuse into the volume pores and gradually deplete with penetration distance (Growcock et al., 1980). As the temperature is increased, the oxygen diffusion into the pores is increasingly blocked by the counter-current diffusion of the carbon monoxide and CO_2 gases within the pores. Thus, the thermal oxidation rate in Mode II increases with increasing temperature but at a progressively lower rate. As the oxidants penetration into the volume pores decreases, the thermal oxidation reaction eventually shifts to the outer surface, marking the transition to a gaseous phase transfer regime. In Mode III, thermal oxidation occurs at the outer surface and is limited by the diffusion of oxidant through the boundary layer.

4.1   The effect of chemical purity on oxidation resistance

Other than the effect on neutronics, purity is important for nuclear graphite because of the adverse effects of impurities on properties, most notably oxidation. Several investigators have conducted oxidation studies on a variety of graphites to understand the effect of impurities.

Chi and Kim (2006) performed oxidation experiments on both IG-11 and IG-110 between 400–1,350 degrees C (752–2,462 degrees F). Both graphites are fine-grained, isomolded petroleum coke graphites produced by Toyo Tanso Ltd. and have similar microstructures and properties; however, IG-11 is not purified, and IG-110 has undergone a thermal purification treatment. Chi and Kim (2006) reported a value for ash content of 479 ppm for IG-11, using the manufacturer's property data, as shown in Table 4-1.

Table 4-1 Typical properties of IG-11 and IG-110 graphites, adapted from Chi and Kim (2006)

Grade	IG-11	IG-110
Coke	Petroleum coke	
Grain size, mm	0.02	0.02
Density, Mg/m^3	1.77	1.77
CTE anisotropy ratio	-	1.1
Ash content, ppm	479	< 10
Impurities, ppm	-	~ 0.1
Young's modulus, GPa	9.04	9.7
Tensile strength, GPa	25.4	27.2
Compressive strength, GPa	86	79
Thermal conductivity, w/m°K	122	129–140

The impurities and their levels in these graphites were reported by Lee et al. (2017), as shown in Table 4-2.

Table 4-2 Typical Impurity levels in IG-11 and IG-110 graphites, wppm, adapted from Lee et al. (2017)

Impurity	IG-11	IG-110	Impurity	IG-11	IG-110
Ash	> 200	< 10	K[†]	-	< 0.1
Al[†]	< 0.4	< 0.05	Li[††]	0.06	< 0.01
B*	2.9	0.03	Mg[†]	0.99	< 0.5
Ca[†]	22.32	< 0.05	Na[†]	-	< 0.05
Cd[††,*]	< 0.05	< 0.1	Ni*	8.31	< 0.1
Co[††]	0.2	< 0.05	Si[†]	0.7	1.6
Cr	< 0.1	< 0.5	Sm*	< 0.05	< 0.05
Fe[†,††,*]	9.59	< 0.01	V*	177.2	< 0.01
Gd[††,*]	< 0.05	< 0.05			
From ASTM D7301, Table X1.1, Impurity category for nuclear graphites: [†]Oxygen-promoting catalyst, [††]Activation-relevant impurity, *Neutron-absorbing impurity					

Figure 4-2 provides the measured oxidation rates for IG-11 and IG-110 in dry air by Chi and Kim (2006), clearly showing the negative effect of impurities on oxidation resistance.
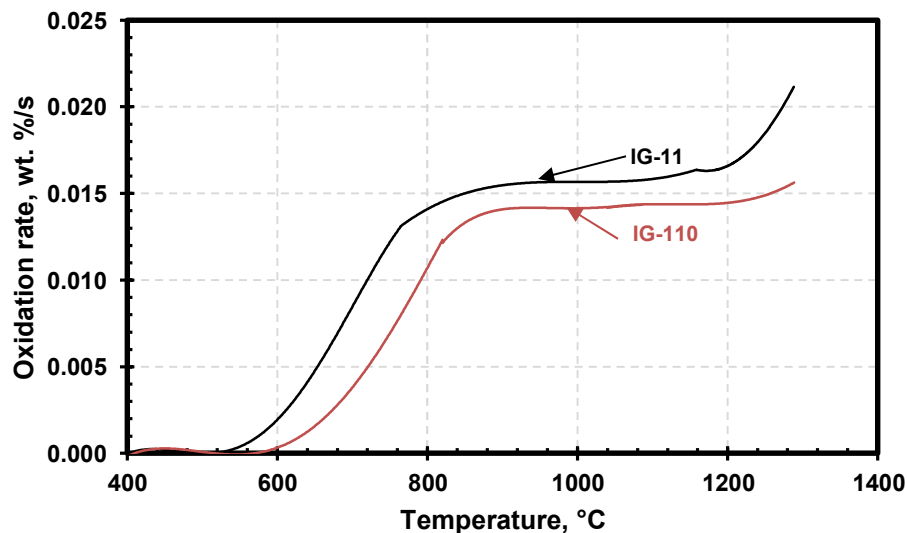
Figure 4-2 Temperature dependence of oxidation rate of IG-11 and IG-110 isotropic, isomolded graphites, adapted from Chi and Kim (2006)

It is worth noting that ASTM D7219-05 listed specific chemical purity requirements and recommendations for individual elements. Many of these elements contribute to catalytic oxidation. These requirements and recommendations were deleted in later editions of ASTM D7219. ASTM D7219 now recommends that the supplier and purchaser agree on chemical impurity limits listed in Table X 1.1.

4.2 *Thermal oxidation resistance studies in different environments*

4.2.1 *Oxidation in dry air*

Chi and Kim (2010) reported thermal oxidation data on four commercially available graphites described in Table 4-3.

Table 4-3 Commercial graphites used in the thermal oxidation studies, adapted from Chi and Kim (2010)

Grade	Manufacturer	Green compaction	Coke type	Average grain size, μm	Density, Mg/m^3
IG-110	Toyo Tanso	Isomolded	Petroleum	~ 20	1.77
IG-430	Toyo Tanso	Isomolded	Coal tar pitch	~ 10	1.82
NBG-18	SGL Carbon	Vibrationally molded	Coal tar pitch	~ 300	1.85
NBG-25	SGL Carbon	Vibrationally molded	Petroleum	~ 300	1.82

Temperature-sensitive oxidation behavior in dry air was observed for the four grades of graphite shown in Figure 4-3. There was approximately a 10-hour difference between NBG-18 and NBG-25 to reach a weight loss of 10 percent.
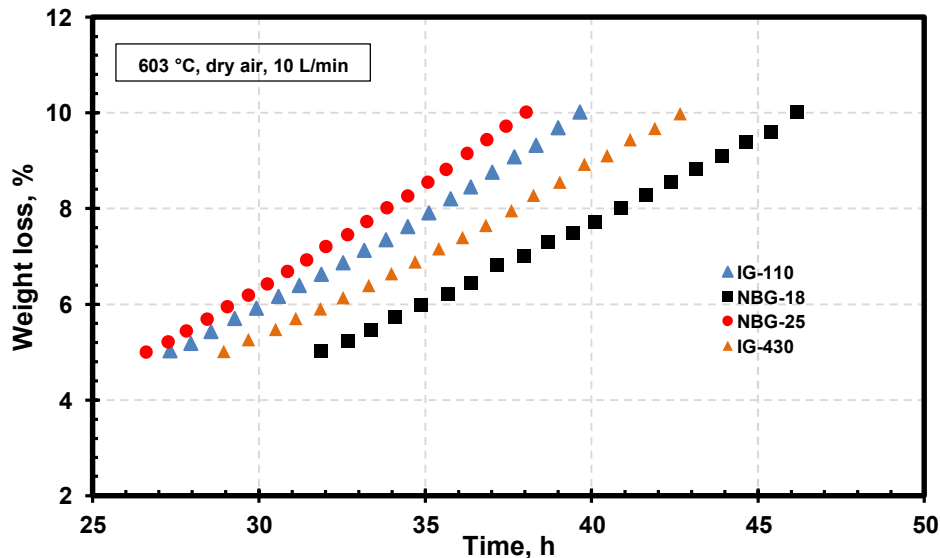
Figure 4-3 Thermal oxidative weight loss for four nuclear-grade graphites, adapted from Chi and Kim (2010)

The thermal oxidation rates were the most dissimilar between 702–854 degrees C (1,296–1,569 degrees F), but these differences became smaller at higher temperatures, as shown in Table 4-4. The convergence of the oxidation rates for different graphites corresponds to the change from the diffusion regime to the gaseous phase transfer regime in Figure 4-1.

Table 4-4 Steady-state thermal oxidation rates observed, adapted from Chi and Kim (2010)

Graphite	Steady-state thermal oxidation rate (5 to 10% weight loss regime) $(g/h.m^2)$					
	603 °C (1,117 °F)	702 °C (1,296 °F)	808 °C (1,486 °F)	854 °C (1,569 °F)	911 °C (1,672 °F)	953 °C (1,747 °F)
NBG-18	27	211	1,634	2,783	2,890	3,209
NBG-25	34	301	2,380	3,150	3,079	3,446
IG-430	28	215	2,215	3,115	3,079	3,340
IG-110	30	323	2,475	3,150	3,126	3,363

Chi and Kim (2010) concluded that graphites made with a coal tar pitch coke filler showed a higher resistance to oxidation than the graphites made using a petroleum coke filler; however, this conclusion should be put into additional context with the study by Huang et al. (2014). Huang et al. (2014) measured the oxidation rate for IG-110, IG-430, NBG-17,[8] and NBG-18 dry air at 700–1,100 degrees C (1,292-2,012 degrees F). In their report, they characterized the graphites by microscopy, XRD, mercury porosimetry, and nitrogen adsorption isotherms using the Brunauer–Emmett–Teller (BET) method. Huang et al. (2014) found IG-110 had the highest oxidation of the graphites that were tested, shown in Table 4-5. The difference in oxidation rates was most noticeable in the diffusion regime.

Table 4-5 Oxidation rates $(g/h.cm^3)$ of for graphites tested in dry air, adapted from Chi and Kim (2010)

Temperature	IG-110	IG-430	NBG-18	NBG-17
700 °C (1,292 °F)	0.037	0.012	0.003	0.005
800 °C (1,472 °F)	0.142	0.064	0.045	0.053
900 °C (1,652 °F)	0.273	0.26	0.224	0.248
1,000 °C (1,832 °F)	0.311	0.302	0.297	0.301
1,100 °C (2,012 °F)	0.418	0.415	0.352	0.367

Similar to Kim and Chi, Huang et al. (2014) found that oxidation resistance increased with larger coke filler particle sizes and less open porosity. They also found that increased coke filler shape anisotropy contributed to porosity and, as a result, less oxidation resistance. IG-110 had the most anisotropic coke filler particles of the graphites tested and was also the only graphite tested by Huang et al. (2014) using a petroleum coke filler. Citing their own work and other literature, including references to historical, petroleum-based needle cokes, Huang et al. reported petroleum coke tends to form anisotropic needle-shaped filler particles, thus increasing porosity, implying that graphite manufactured from petroleum coke is less oxidation resistant than graphite manufactured from coal tar pitch coke. Ubic (2014a) also observed that petroleum coke fillers tend to be more anisotropic than fillers made from coal tar pitch coke. However, a general conclusion that coal tar pitch coke graphite is inherently more oxidation

---

[8]   NBG-17 is similar to NBG-18 but has a finer maximum coke filler size.

resistant than petroleum coke graphite may not be accurate in all cases, since other factors can affect oxidation resistance.

Windes et al. (2019b) reported strength degradation due to thermal oxidation of IG-110 and NBG-18 graphites, with properties shown in Table 4-6. Figure 4-4 shows the observed strength degradation.

Table 4-6 Graphites used for oxidation study by Windes et al. (2019b)

Graphite	Manufacturer	Coke type	Grain size designation	Coke particle size, μm	Green compaction	Density, Mg/m³
IG-110	Toyo Tanso	Petroleum	Superfine	20 (average)	Isomolded	1.774
NBG-18	SGL Carbon	Coal tar pitch	Medium	1,600 (max); 300 (average)[1]	Vibrationally molded	1.852

[1] Data from Chi and Kim (2010)
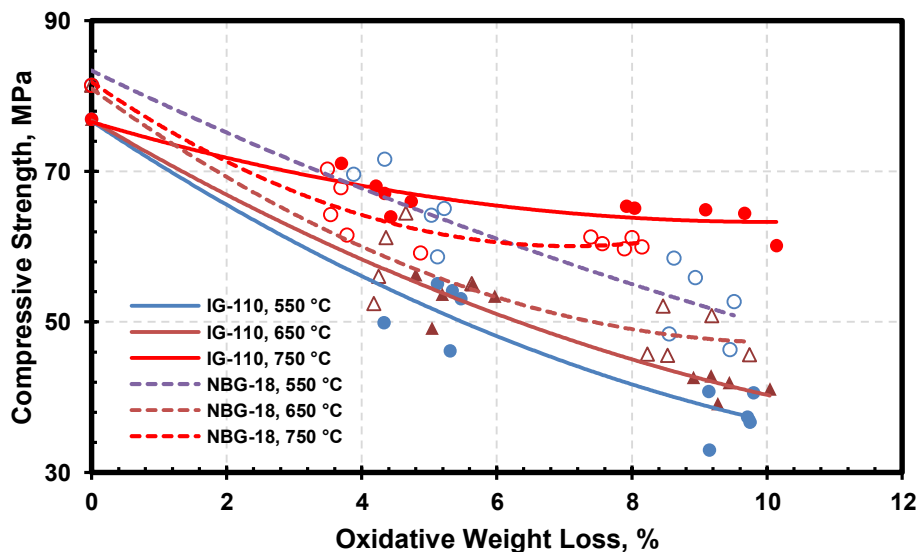
Figure 4-4 Effect of thermal oxidation on the compression strength loss for IG-110 and NBG-18 graphites, data adapted from Windes et al. (2019b)

As shown in Figure 4-4, the compressive strength decreased with thermal oxidation weight loss for graphite at all temperatures. IG-110 specimens oxidized at the aggressive thermal oxidation condition of 750 degrees C (1,382 degrees F) had higher failure-stress values than specimens oxidized to similar mass loss levels at lower temperatures. Oxidation at 650 degrees C (1,202 degrees F) yielded mixed behavior, with the medium-grained grade (NBG-18) showing lower failure-stress values than the NBG-18 specimen at 550 degrees C (1,022 degrees F).

Windes et al. (2019b) also conducted extensive microscopy analysis to better understand the oxidation characteristics of these two grades of graphite. They observed that the two graphite grades exhibit differences in oxidation and strength changes, which was attributed to the difference in oxygen-penetration depth within the unique graphite microstructure. Also, because

IG-110 has a much higher effective diffusion coefficient than NBG-18 (Kane et al., 2018), oxygen penetration is higher for this graphite. NBG-18, with its higher overall density, larger grain size, and lower open-pore density than IG-110, affects the differences between oxidation-penetration depths at a given temperature (Chi and Kim, 2008).

4.2.2   Steam oxidation

The oxidation of graphite within the reactor core due to moisture (steam) ingress has been of concern. Two distinct types of steam ingress can occur in an HTGR: (1) a major steam leak caused by, for example, rupture of a heat exchanger steam tube and (2) continuous low-level in-leakage. The reactor would be shut down if a major steam leak occurs. However, a low-level leak could result in moisture concentrations in the range 1 to 10 pascals (Pa) (10 to 100 microatmospheres) over the 40-year life of the reactor graphite components (Valesquez et al., 1978). Low levels of steam for long periods of time could lead to small but measurable oxidation of the core graphite.

The study of the steam oxidation of graphite has been quite limited. Contescu et al. (2014) explicitly state, "to the authors' knowledge such [an extensive] study has not been done since the detailed analysis of reaction of H-451 graphite with steam (Velasquez, Hightower, Burnette, 1978)."[9] Contescu et al. (2014) tested H-451 and PCEA graphite between 900–1,100 degrees C (1,652–2,012 degrees F), at water pressures 15–715 Pa and hydrogen pressures 30–150 Pa. H-451 is a historical grade of extruded graphite manufactured from petroleum coke for use in the Fort St. Vrain HTGR with a maximum grain size of 1.3 mm. PCEA is an extruded graphite made with a petroleum coke filler with a maximum grain size of 0.8 mm, manufactured by GrafTech. Appendix A to this report gives further documentation on PCEA. Contescu et al. (2014) observed that PCEA appears to be more oxidation resistant by moisture above 850 degrees C (1,562 degrees F) than H-451, but simulations showed faster oxidation rates for PCEA than H-451 below 850 degrees C (1,562 degrees F). After reporting the kinetic rate for both graphites, Contescu et al. (2014) concluded, "kinetic data cannot be transferred from one graphite grade to another." An earlier study by Eto and Growcock (1981) measured the oxidation kinetics of H-451, IG-11, and PGX graphites in dry air, steam, and CO_2. Their measurements showed the activation energies for oxidation H-451 and IG-11 were similar to each other in dry air and steam environments. However, they also observed that the relative reactivities for individual PGX graphite specimens varied by as much as a factor of 50 in steam environments. Eto and Growcock (1981) believed the wide range of reactivities in PGX could be due to impurities, crystallite size and orientation, and the degree of graphitization.

4.3   Summary

This chapter explains that the thermal oxidation resistance of graphite, while influenced by the grade of graphite, is temperature dependent. There are three distinct regimes of oxidation (from lowest temperature to highest)—the chemical regime, the diffusion regime, and the gaseous

---

[9]   The authors of this report were also aware of NRC-sponsored research at Brookhaven National Laboratory on steam-oxidation of H-451, PGX, and IG-11 graphites (Eto and Growcock, 1981), as described later in the paragraph.

phase transfer regime. The steady-state oxidation rates are most sensitive to the grade of graphite within the intermediary regime (the diffusion regime). Within this regime, graphite with larger grain sizes and less open porosity shows the greatest resistance to thermal oxidation. There have been a very limited number of studies on the steam-driven oxidation of graphite. Contescu et al. (2014) concluded the kinetic data for steam-driven oxidation are not interchangeable among different grades of graphite.

5 IRRADIATED BEHAVIOR OF GRAPHITES

5.1 Generalized irradiation behavior of graphites

The following information summarizes the current consensus general understanding of the irradiation phenomenon for synthetic graphites. Swelling in the c-direction is initially accommodated by aligned microcracks formed during graphitization. At low doses, initially, a-axis shrinkage is major and contributes to an overall decrease in net volume. Fast neutron irradiation, above about 0.1 megaelectronvolt, leads to cascades of atomic displacements in the graphite lattice, as shown in Figure 5-1.
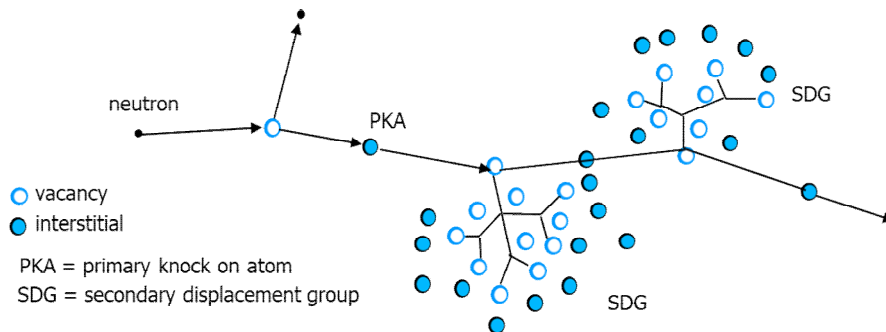
Figure 5-1 Cascade effects due to neutron irradiation in graphite, adapted from IAEA (2000)

Most of the displaced atoms find vacant lattice positions, but many vacant and interstitial point defects are formed. These point defects are mobile and coalesce to form dipoles, clusters, and larger defects, depending on the irradiation temperature. These lead to significant crystallite dimensional changes, where the crystal c-axis increases and the a-axis shrinks; however, the change in lattice spacing remains relatively small. In the polycrystalline graphite, due to the many nanocracks parallel to the basal planes, the c-axis expansion is accommodated and only the influence of the a-axis shrinkage is apparent. With increasing dose, most of the c-axis accommodation is exhausted eventually, and bulk polycrystalline graphite exhibits volume "turnaround" behavior from initial shrinkage to growth. The graphite begins to swell at a greater rate, with increasing damage dose due to c-axis growth, and new porosity is generated. Eventually, the internal crystal strain becomes so great that microcracking leads to a reduction in modulus and strength.

The structural changes occurring due to the mechanism described above lead to changes in many of the bulk physical, mechanical, and thermal characteristics after irradiation.

The structural changes occurring for the above-mentioned general reasons manifest as changes in the physical, mechanical, and thermal characteristics after irradiation. Some of these are mentioned in a generalized manner in Table 5-1. These changes do not all manifest themselves exactly to coincide with volumetric turnaround.

Table 5-1 General tendencies in property changes due to irradiation of graphite

Effect of graphite structure change on graphite property after irradiation	Before turnaround in dimensional change with dose	After turnaround in dimensional change with dose
Density	Increases	Decreases from turnaround value
Volume	Decreases	Increases from turnaround value
Elastic modulus	Increases	Decreases
Strength	Increases	Decreases
CTE	Decreases	Decreases
Thermal conductivity	Decreases rapidly	Secondary decrease

A generalized summary of the irradiation behavior, in a theoretical isotropic graphite grade, of important properties can be made from the observations of Gilsocarbon graphite (Marsden et al., 2020). Figure 5-2 compares the relationship between the irradiation-induced change in dimensions with dose (blue color curve, left vertical axis) and the rate of such change as a function of dose (burgundy-color curve, right vertical axis). After an initial drop in the rate of change in the dimension, and after the achievement of some constancy, the rate increases rapidly beyond a certain dose, which may be well below the turnaround dose for dimensional change.

As observed in Figure 5-3, the Young's modulus rises rapidly within a few tenths of a displacements per atom (dpa) dose, which is then followed by a small plateau, then a gradual increase, and then a final decrease after a maximum level. There does not seem to be a 1:1 direct correlation of the minimum in dimensional shrinkage and the modulus response to irradiation dose.

The transition in CTE, from an initial increase with dose to a rapid decrease, occurs at an irradiation dose that is much less than the dimensional change turnaround dose, as shown in Figure 5-4. The maximum in CTE occurs well before the dimensional turnaround dose.
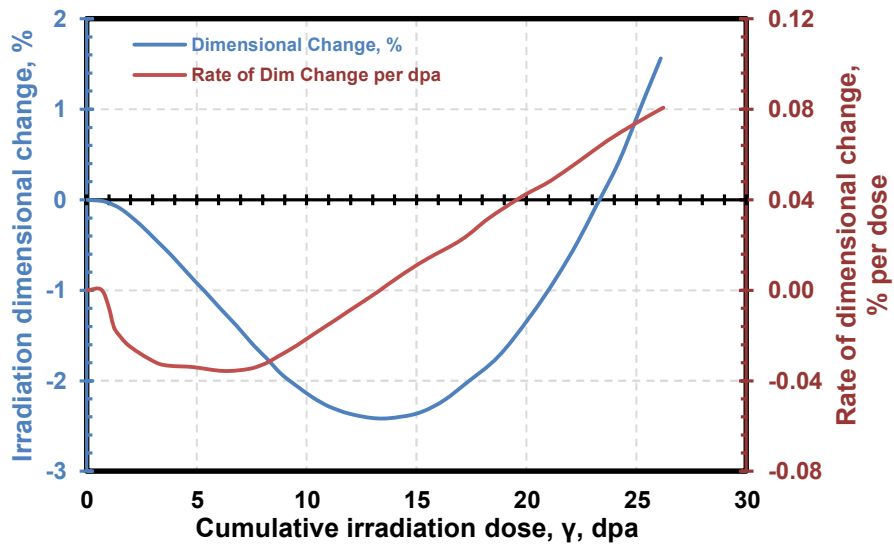
Figure 5-2 Typical schematic of irradiation dimensional change information for Gilsocarbon graphite for an irradiation temperature of 550 degrees C (1,022 degrees F), adapted from Marsden et al. (2020)
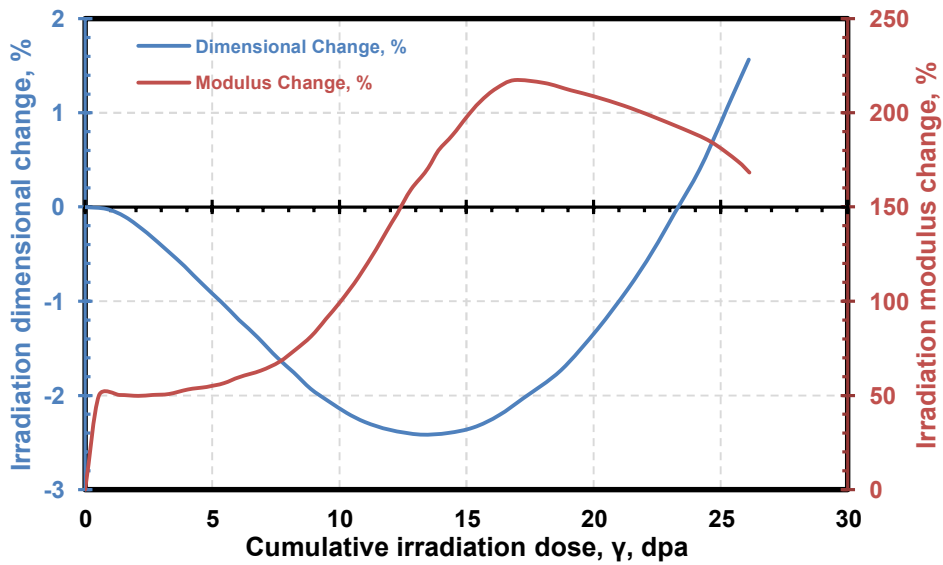
Figure 5-3 Typical schematic of irradiation dimensional change and modulus change information for Gilsocarbon graphite irradiated at 550 degrees C (1,022 degrees F), adapted from Marsden et al. (2020)
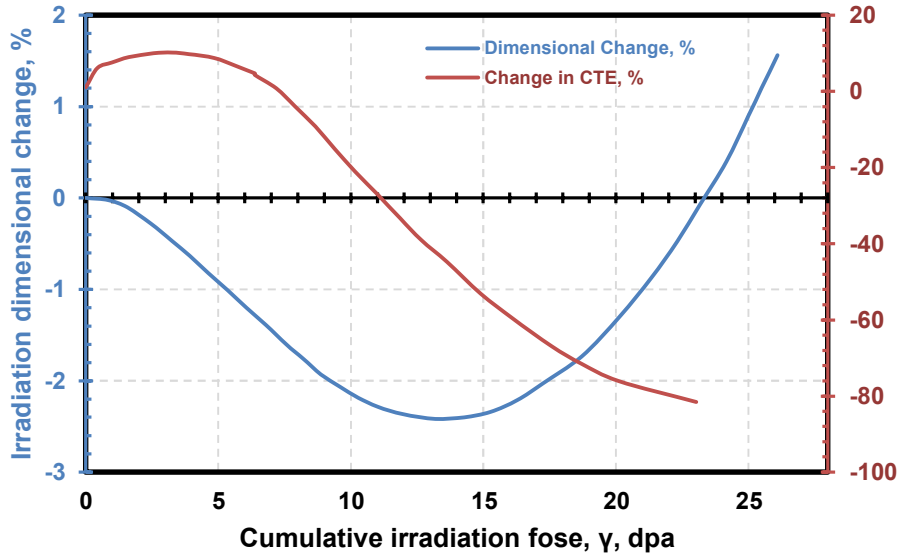
Figure 5-4 Typical schematic of irradiation dimensional and CTE changes for Gilsocarbon graphite irradiated at 550 degrees C (1,022 degrees F), adapted from Marsden et al. (2020)

5.2   Effect of coke type

5.2.1   Effect on relative strength

The strength of irradiated graphite typically increases with the irradiation dose up to the turnaround dose for the shrinkage in volume; after that dose, the strength decreases. However, the type of coke used does not seem to influence the strength behavior of irradiated graphite, at relatively low doses, as shown in Figure 5-5 (Haag, 2001). Here, the ratio of the room temperature irradiated strength to that of the room temperature unirradiated strength is plotted against the irradiation dose.
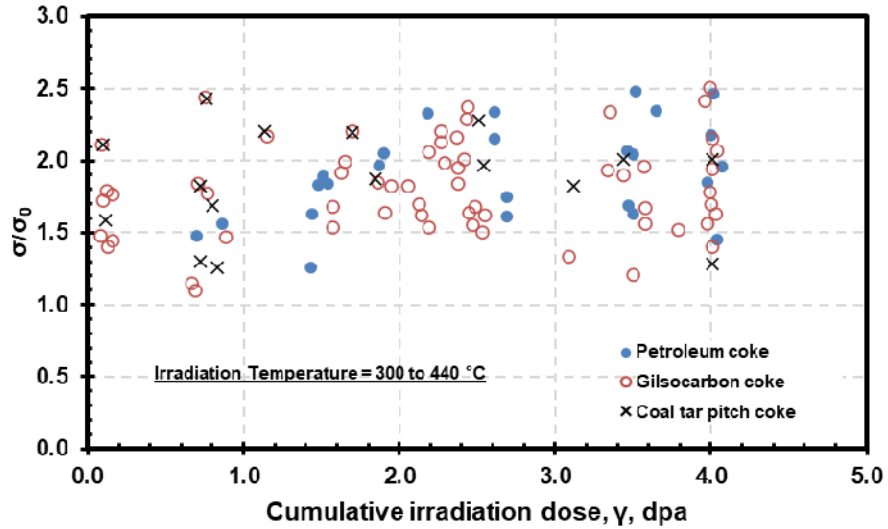
Figure 5-5 Influence of the type of raw coke on irradiated strength of graphite, adapted from Haag (2001)

Details are not available on the green processing, including the mix composition, binder content, number of impregnations, and graphitization temperature, for the data shown in Figure 5-5.

5.3   Effect of binder-coke fraction

Engle (1971a) conducted a series of experiments with varying binder content, as detailed in Section 3.5 of this report. These samples were irradiated at 1,225 degrees C (2,237 degrees F) to approximately 9 dpa. The discussion here is on the effect of binder content on the changes in dimensions and volume after exposure to irradiation. Figure 5-6 shows the length of change due to irradiation versus the binder-coke fraction, β, is defined as:

$$\beta \ (wt.\%) = \frac{W_c}{W_f + W_c} \ X \ 100,$$

where W_c is the weight of the lead in the heat treated compact and W_f is the corrected weight of the filler coke in the final compact due to losses during heating to graphitization temperature.
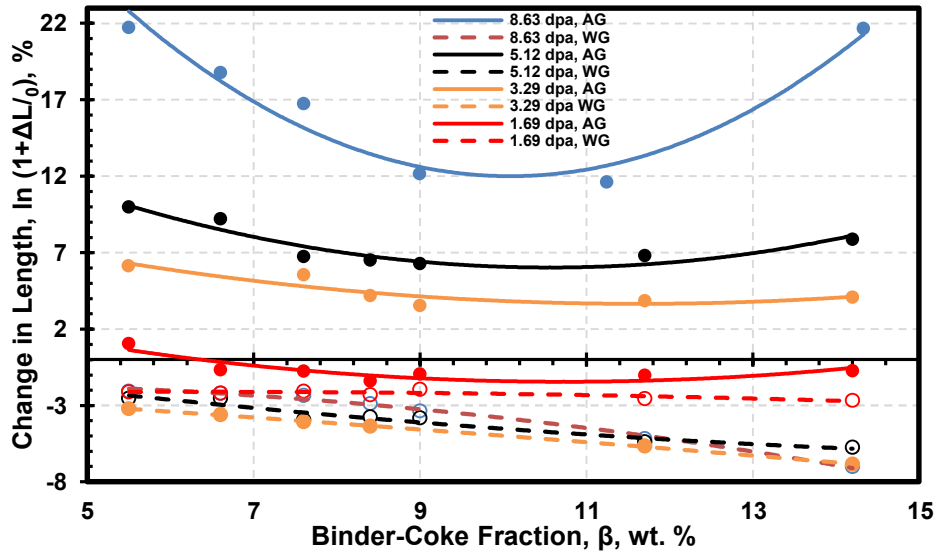
Figure 5-6 The influence of the green mix binder-coke content on dimensional change due to irradiation at 1,225 degrees C (2,237 degrees F) at various dose levels shown on WG and AG orientations, adapted from Engle (1971a)

The dimensional change behavior is similar to that observed in other irradiation studies of needle coke graphites. The contraction in the AG direction at low doses is followed by a rapid expansion at higher doses and contraction in the WG direction. The changes in the AG direction were sensitive to the binder-coke fraction, showing increasing shrinkage with increasing β where the fluence to turnaround is optimized at a binder-coke fraction of about 10–11 wt.%. The changes in the WG orientation were dependent upon β, showing larger contractions with increased β. Figure 5-7 shows the change in volume due to irradiation for graphites with varying binder-coke content. Volume decreases for up to about 11.5 wt.% binder-coke fraction, after which overall expansion takes over shrinkage, and volume expansion seems to occur beyond this dose.
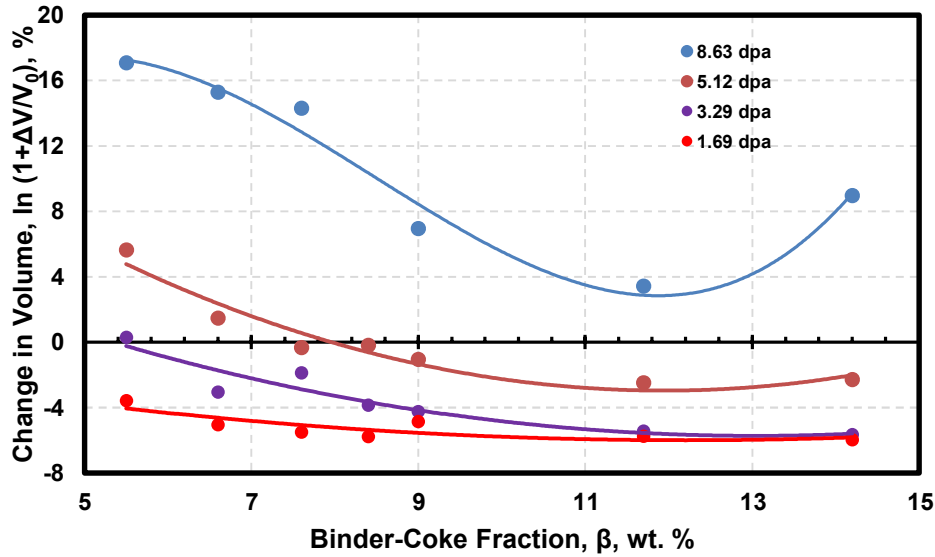
Figure 5-7 Volume change due to irradiation at 1,225 degrees C (2,237 degrees F) for indicated doses as a function of binder-coke fraction, adapted from Engle (1971a)

The shrinkage to expansion transition occurs at various dose levels, depending upon the binder-coke content. Regression analyses were conducted on the data to fit a polynomial dependence. The dose at which a zero or near-zero value results was then determined, which is the irradiation dose value at which the transition from shrinkage to expansion, or the "turn-around," occurs. Figure 5-8 shows the dependence of this turnaround dose on the binder-coke fraction. Engle (1971a) concluded, "the data suggest an optimum binder content for this series of materials of about 11 wt.%, but the optimum value may be different when other filler particles and binders are used and fabrication processes differ."
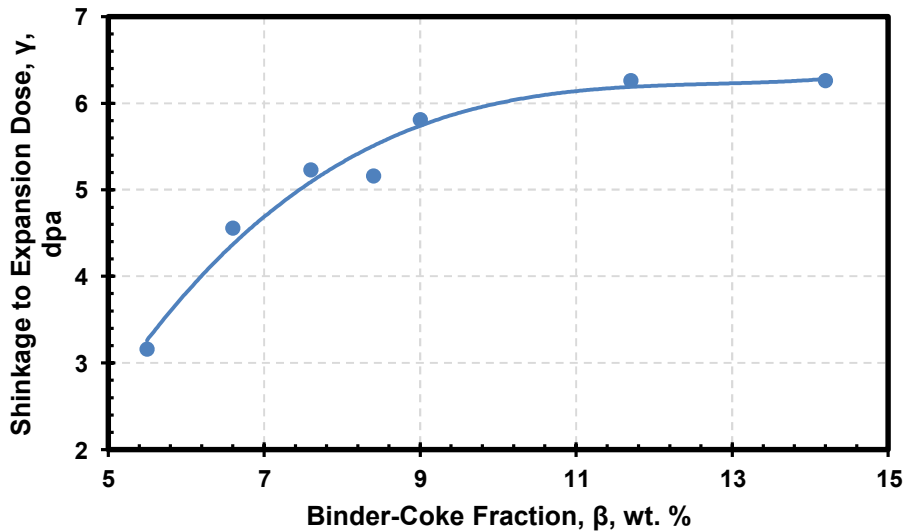
Figure 5-8 Dependence of the shrinkage to expansion crossover dose on the amount of binder-coke in the green mix for graphites (calculated from the data of Engle (1971a))

Haag (2014) also investigated the effect of binder content. The investigations involved graphite made with Gilsocoke filler. Details on the graphitization temperature and other processing details are not available. The irradiation temperature ranged from 1,060 degrees C (1,940 degrees F) to 1,280 degrees C (2,336 degrees F) (Haag, 2020). Figure 5-9 shows Haag's results, with the dose calculations using the correction suggested by Haag (2020). Apparently, the published fluence values were larger by a factor of two. The increase in binder content showed a tendency to increase the relative shrinkage in both directions. Typical binder content for nuclear graphite is around 20 percent.
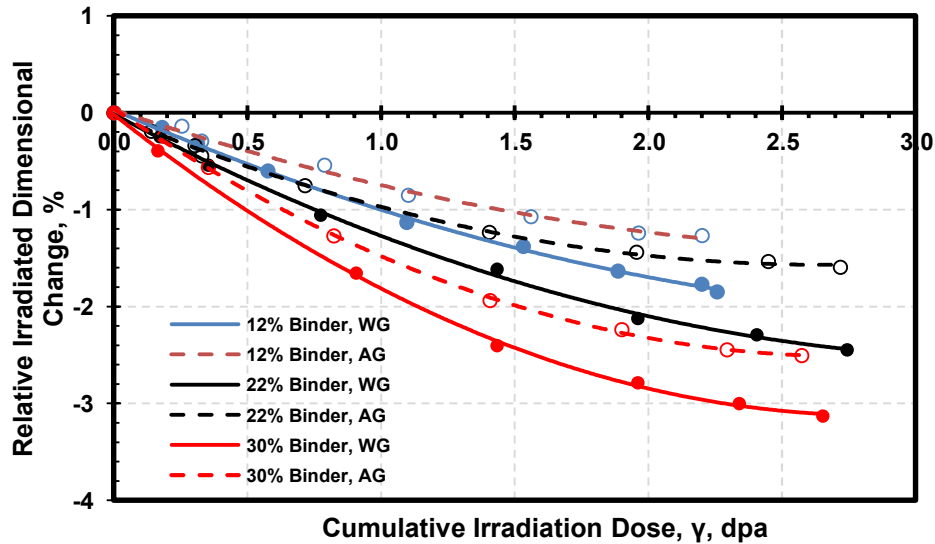
Figure 5-9 Effect of binder content on the irradiation dimensional change, adapted from Haag (2014) with the suggested correction factor from Haag (2020)

5.4   Effect of forming method

5.4.1   Effect on Young's modulus

The Dragon project in the U.K. generated a large amount of data on the effect of graphite green-processing Young's modulus changes with irradiation. Figure 5-10 shows the sonic Young's modulus dependence on irradiation dose, obtained by dynamic sonic modulus measurements on cylindrical samples for an extruded coal tar pitch coke graphite and a molded coal tar pitch graphite.
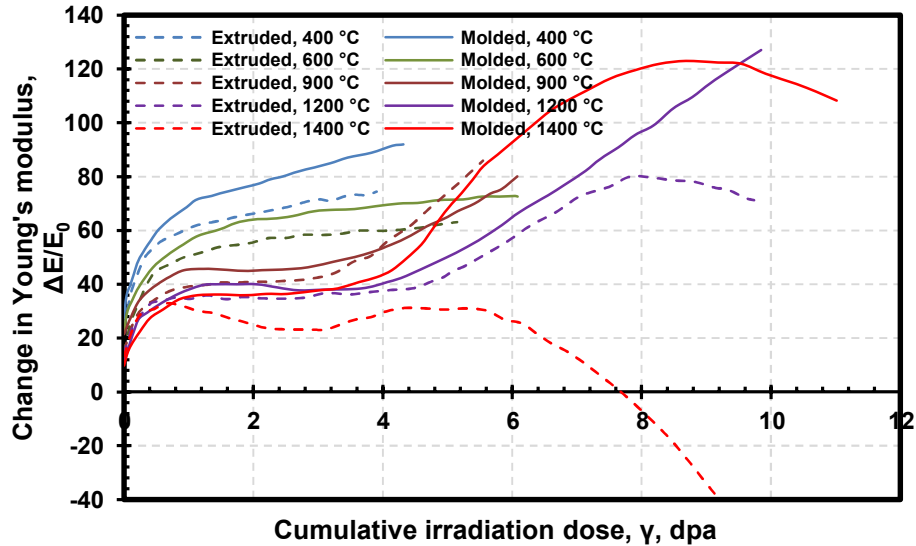
Figure 5-10 Effect of green forming method on the Young's modulus change after irradiation at indicated temperatures, data modified from Price (1975)

Price (1975) did not provide details on, for example, graphitization temperature or density. The graphs shown in Figure 5-10 represent the "generalized average" behavior of several individual datum points, as were depicted by Price. Interestingly, the sonic modulus values in the radial and axial directions for the extruded graphite were found to be located on the same curve, within the expected inherent data scatter. The Young's modulus values are always higher for the molded graphite when compared to extruded graphite, although the behavior pattern is similar. A rapid initial rise is followed by a plateau region. The value of the plateau region decreases as irradiation temperature increases. With increasing dose, a second rise occurs in relative modulus change, which decreases after passing through a peak value. The decrease can even be lower than the unirradiated value for extruded graphite irradiated at 1,400 degrees C (2,552 degrees F). Pinning of basal plane dislocations by small point defect clusters was attributed as the cause for the initial increase in Young's modulus. The progressive compaction of the structure due to the closure of microcracks was suggested as the reason for the second rise. The final decrease was attributed to the formation of new intercrystalline pores, as graphite volume expands at higher doses.

5.4.2   Effect on dimensional change

Haag (2005) also examined the irradiation behavior of near-isotropic Gilsocarbon graphites made by AGL. Pertinent to this report are two grades, unidirectionally molded IM 2-24 and extruded IE 1-24 graphites. Table 5-2 lists some of the properties of these graphites. Haag (2005) irradiated the graphite specimens at 750 degrees C (1,382 degrees F) and determined the change in irradiated dimensions, as shown in Figure 5-11.

Table 5-2 Properties of molded and extruded AGL Gilsocarbon graphites, adapted from Haag (2005)

Property	IM 2-24 (Uniaxially molded)	IE 1-24 (Extruded)
Density, Mg/m^3	1.76 (Matsuo, 1979)	1.72 (Matsuo et al., 1981)
WG CTE, 10^{-6}/°K	5.5	4.3
AG CTE, 10^{-6}/°K	5.2	5
CTE anisotropy	1.06	1.16[†]
WG thermal conductivity, W/m°K	111	122
AG thermal conductivity, W/m°K	113	123
WG Young's modulus, GPa	10.4	12.3
AG Young's modulus, GPa	10.5	10.8

[†]Exceeds ASTM specification of 1.15 maximum
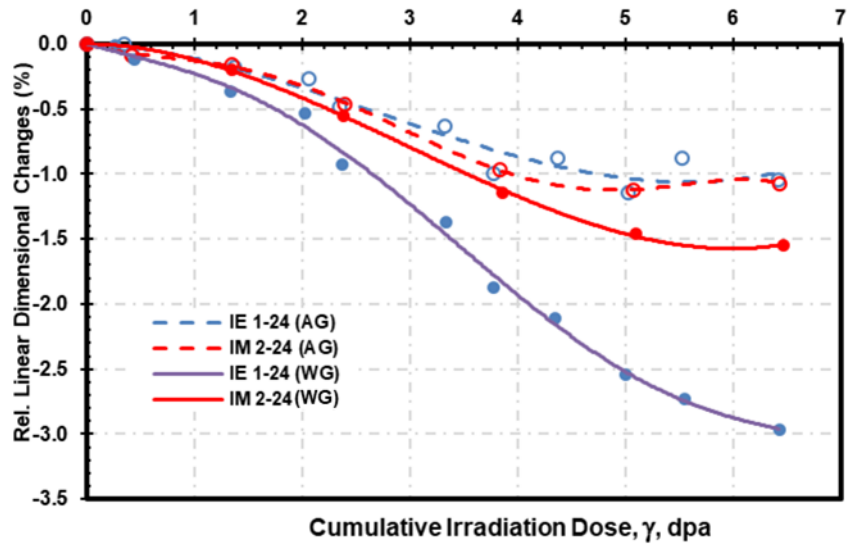
Figure 5-11 A comparison of the irradiated dimensional change behavior of molded and extruded graphites, adapted from Haag (2005)

The molded graphite with better CTE isotropy than the extruded graphite also shows closer shrinkage in the two orthogonal directions than the extruded graphite, which exhibits a large divergent behavior in the shrinkage in both orthogonal directions. These results suggest that isomolding as the green-forming technique provides superior geometry retention under irradiation when compared to the extrusion technique, due to the extreme crystalline orientation resulting from the green compaction stress distribution in the green-formed carbon article.

5.5 Graphitization temperature

5.5.1 Effect on Young's modulus

For irradiation performed at 600 degrees C (1,112 degrees F), the ratio of the irradiated Young's modulus to that of the unirradiated Young's modulus is plotted against the cumulative irradiated dose in Figure 5-12. A substantial increase in Young's modulus is observed at all dose levels as the graphitization temperature is increased to 2,800 degrees C (5,072 degrees F); additionally, the turnaround dose at which E/E_0 is the maximum and then begins to decrease is higher at this graphitization temperature. This is the case for both grain orientations and reflects the highest degree of graphitization achieved at 2,800 degrees C (5,072 degrees F).
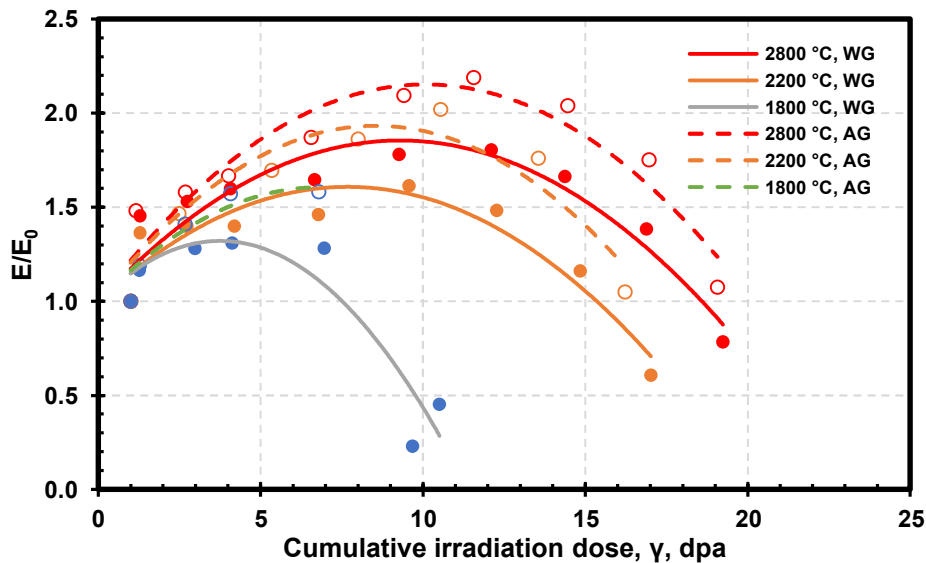
Figure 5-12 Effect of graphitization temperature on the irradiation-induced change in Young's modulus for PGA graphite, modified from Brocklehurst and Kelly (1993)

5.5.2 Effect on coefficient of thermal expansion

Microstructural changes due to irradiation affects the expansion and contraction of the graphite lattice and the bulk material. The microstructure is also a function of the graphitization temperature; therefore, a property such as CTE may be expected to be a function of the graphitization temperature. This has been demonstrated by Brocklehurst and Kelly (1993), as shown in Figure 5-13. The irradiation temperature was 600 degrees C (1,112 degrees F). The differences were attributed to the changes to the crystal dimensional change rate due to the low graphitization temperature.
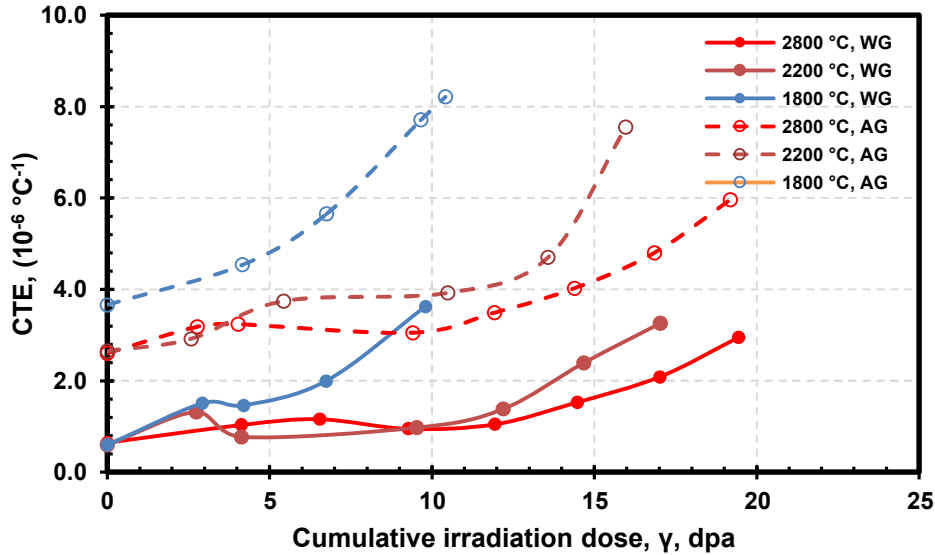
Figure 5-13 The effect of graphitization temperature on CTE behavior under irradiation at 600 degrees C (1,112 degrees F) for PGA graphite, adapted from Brocklehurst and Kelly (1993)

5.5.3   Effect on dimensional change

Microstructural changes due to irradiation affects the expansion and contraction of the graphite lattice and the bulk material. The microstructure is also a function of the graphitization temperature; therefore, a property such as irradiated dimensional change may be expected to be a function of the graphitization temperature. Fourré et al. (1976) studied the effect of the graphitization temperature on irradiation dimensional change. Their study did not offer details on the raw material mix formulation that included binder-coke content, green compaction and processing method used, impregnation and baking cycles, and density changes throughout these process steps. The irradiation temperature is not available but was reported to be similar for all samples compared, since they were irradiated close to one another (Haag, 2020). Fourré et al. (1976) also did not provide information on the irradiation temperature. Their graph designations were for "parallel" and "perpendicular" orientations, without any further guidance on whether such designations were for compacting force directions or grain orientation. Their data were interpreted by the authors of this report to mean they defined the orientation of the grains. Their results were regraphed and further analyzed, with the outcome shown in Figure 5-14.

Several inferences can be made from the behavior shown in Figure 5-14. First, the magnitude of dimensional shrinkage after irradiation decreases with increasing graphitization temperature for both the WG and AG orientations. Second, more shrinkage is observed in the AG orientation than in the WG direction, as would be expected from the graphite crystal shrinkage differences in the c- (orthogonal) and a- (basal plane) directions. Third, the difference in the shrinkage between the two orientations decreases with the increased graphitization temperature. Fourth, at the graphitization temperature of 3,000 degrees C (5,432 degrees F), the data for the two orientations overlap, due to the near-complete graphitization, which can be

achieved at this temperature. Paragraph 5.6.3 of ASTM D7219 requires a minimum graphitization temperature of 2,700 degrees C (4,892 degrees F). Therefore, from the viewpoint of keeping the irradiation shrinkage to the smallest degree possible during reactor operation, the ASTM D7219 requirement for graphitization temperature may not be considered as conservative. However, when cost and the replacement schedule are considered, the ASTM minimum graphitization temperature requirement may yet be sufficient to maintain adequate design and operational safety.
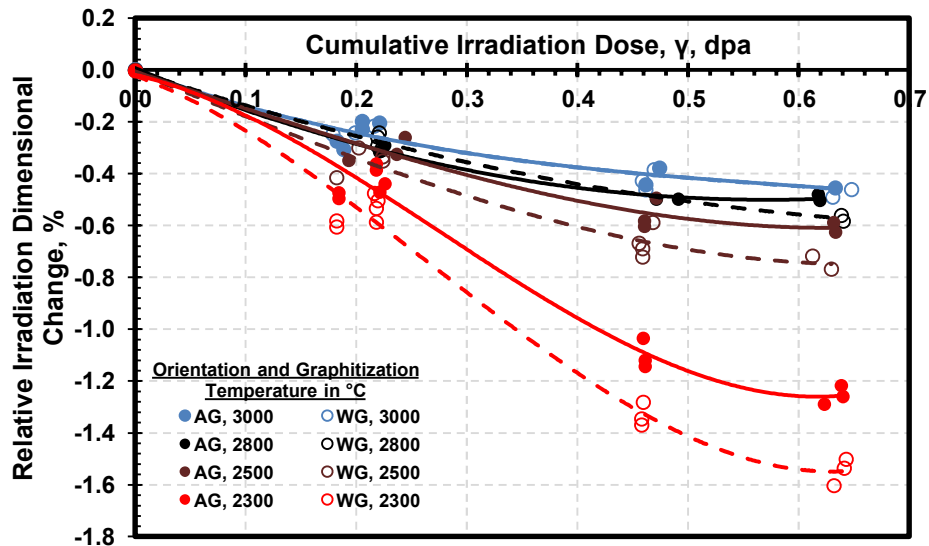
Figure 5-14 The effect of graphitization temperature on the irradiated dimensional change, data adapted from Fourré et al. (1976)

The general trend is similar for both the WG and AG orientations for the PGA graphite graphitized at the temperatures indicated. Microstructural changes due to irradiation affect the expansion and contraction of the graphite lattice and the bulk material. The microstructure is also a function of the graphitization temperature; therefore, a property such as irradiated dimensional change may be expected to be a function of the graphitization temperature. This has been demonstrated by Brocklehurst and Kelly (1993), as shown in Figure 5-15, for PGA graphite irradiated at 600 degrees C (1,112 degrees F). For the WG orientation, the shrinkage rate seems to decrease with an increasing graphitization temperature, with a concomitant increase in the dose at which turnaround might occur. The amount of shrinkage before turnaround does not seem to vary much with the graphitization temperature. For the AG orientation, a more pronounced effect is seen with increasing graphitization temperature, as shown in Figure 5-15. With increasing graphitization temperature, both the turnaround dose and the crossover dose seem to increase substantially. Here again, he graphitization temperature does not have much effect on the amount of shrinkage before turnaround. Thus, the degree of graphitization achieved plays a leading role; graphitization at a minimum temperature is indicated as a means to achieve optimum dimensional response under the irradiation of PGA graphite.
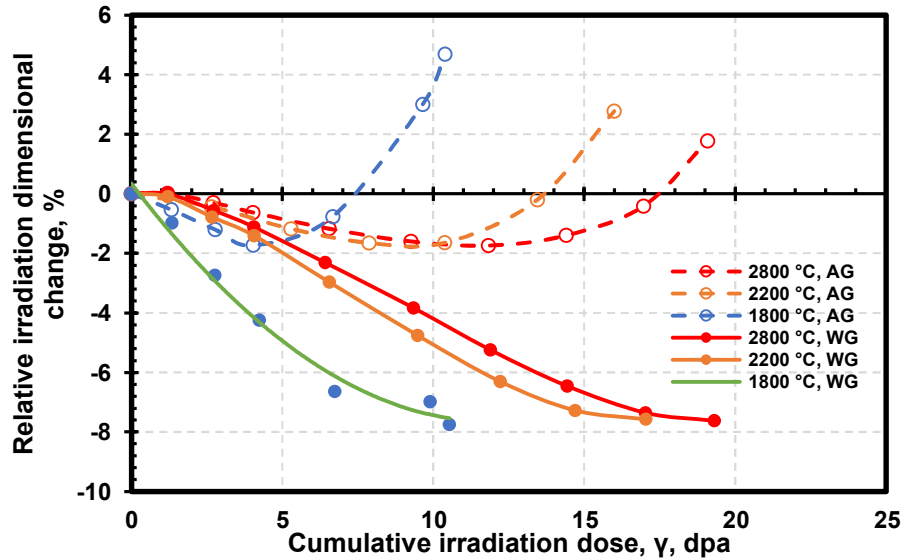
Figure 5-15 The effect of graphitization temperature on the irradiated dimensional change for PGA graphite, adapted from Brocklehurst and Kelly (1993)

5.6   Large-scale irradiation studies of recent nuclear-grade graphites

The difficulties inherent in quantifying the effect of the source material and processing methods upon irradiated properties was recently illustrated by the comprehensive INNOGRAPH (Neutron Irradiation Effects on the Microstructure of Nuclear Graphite) irradiation studies under the European Framework programs High Temperature Reactor Module (HTR-M), ReActor for Process Heat, Hydrogen And Electricity Generation (RAPHAEL), and ARCHER (Advanced Reactor for Cogeneration of Heat and Electricity R&D). Heijna et al. (2017) summarized the results of the irradiation studies. The INNOGRAPH irradiation studies characterized the impact irradiation on nine grades of modern graphites at 750 degrees C (1,382 degrees F) and 950 degrees C (1,742 degrees F). Table 5-3 describes the different graphite grades tested in the INNOGRAPH program, including their unirradiated isotropy behavior. Grain size and isotropic designations were taken from Burchell et al. (2007) and Kato et al. (2015).

Table 5-3 Table of different graphite grades tested in the INNOGRAPH program

Manufacturer	Grade	Coke	Forming method	Grain size	Isotropy
Toyo Tanso	IG-110	petroleum	isomolding	fine/superfine	isotropic
Toyo Tanso	IG-430	coal tar pitch	isomolding	fine/superfine	isotropic
SGL	NBG-10	coal tar pitch	extrusion	medium	isotropic
SGL	NBG-17	coal tar pitch	vibromolding	medium	isotropic
SGL	NBG-18	coal tar pitch	vibromolding	medium	isotropic
SGL	NBG-25	petroleum	isomolding	fine/superfine	isotropic
GrafTech	PCEA	petroleum	extrusion	medium	near-isotropic
GrafTech	PCIB	petroleum	isomolding	fine/superfine	isotropic
GrafTech	PPEA	coal tar pitch	extrusion	medium	near-isotropic

Heijna et al. (2017) observed no significant differences between the effect of irradiation on the CTE, dynamic Young's modulus, or thermal conductivity among graphite grades. Heijna et al. drew no conclusions between the type of coke, grain size, and processing method with the resulting graphite irradiation behavior, despite the comprehensive data set involved. Heijna et al. explicitly stated, "*generic conclusions cannot be drawn from the database, indicating that it would be very difficult, if not impossible, to derive graphite material properties under irradiation from manufacturing graphite process parameters or will unirradiated graphite behavior* [emphasis added]." Two key figures, volumetric change and dimensional anisotropy as a function of irradiation dose from Heijna et al. (2017), are provided below as illustrations of Heijna et al.'s conclusions, when cross-referenced against Table 5-3.
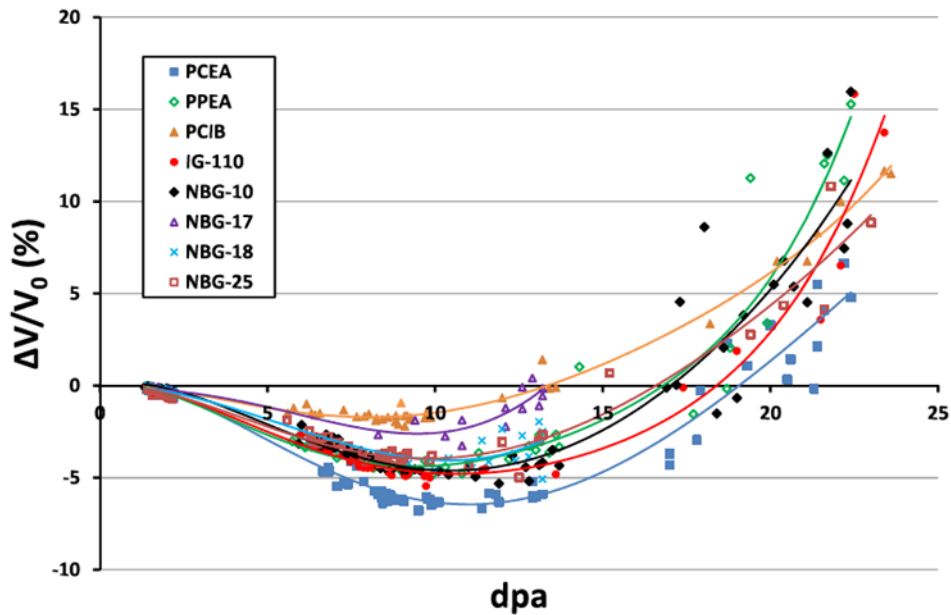
Figure 5-16 Dimensional change of graphites tested in the INNOGRAPH program as a function of dpa at an irradiation temperature of 750 degrees C (1,382 degrees F)
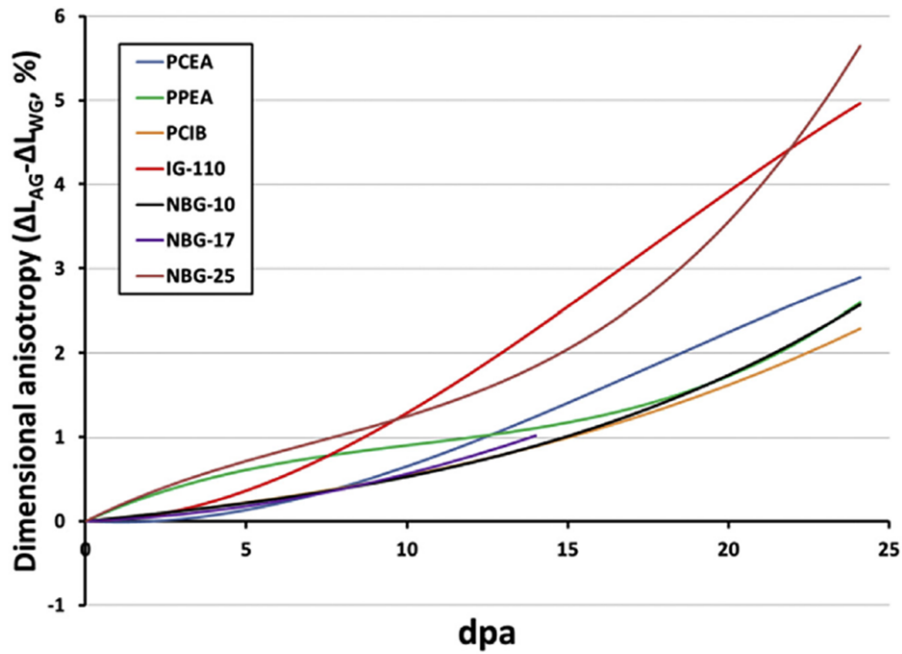
Figure 5-17 Dimensional anisotropy of graphites tested in the INNOGRAPH program as a function of dpa at an irradiation temperature of 750 degrees C (1,382 degrees F)

The conclusions of Heijna et al. (2017) are not unexpected, given Windes' (2010) summary of the Idaho National Laboratory graphite Technology Development Plan, Revision 1:

While the behavior of any given graphite can be predicted in broad terms, the exact magnitude of irradiation-induced changes cannot yet be accurately predicted using models based on previous historical data. Since each grade of graphite has a unique structure and texture, its irradiation behavior can be expected to be somewhat different.

Windes et al. (2019a) reported the longitudinal creep coefficient for several grades of nuclear graphite as part of the Advance Graphite Capsule (AGC) program at average temperatures 600–820 degrees C (1,112–1,508 degrees F) provided in Table 5-4. All creep specimens were subjected to compressive stress, and testing was performed at relatively low dose levels. The creep coefficients for the seven graphites in the AGC capsule program were normalized to a stress of 20.7 MPa and are reported in Table 5-4. H-451 is a historical grade of anisotropic, medium-grained, extruded graphite that is no longer produced. 2114 graphite is a superfine, isomolded, isotropic graphite manufactured by Mersen Inc.

Windes et al. (2019a) reported that, in general, the creep coefficients measured at 820 degrees C (1,508 degrees F) were higher than the coefficients measured at lower temperatures, demonstrating the temperature dependence of irradiation creep in graphite; no discernable trend between forming method, coke type, or grain size is observable.

Table 5-4 Creep coefficient values (K, %/ MPa*dpa) for different graphite grades at three average irradiation temperatures from the AGC capsule program

Manufacturer	Grade	Coke	Forming method	Grain size	Isotropy	Irradiation temperature		
						600 °C	625 °C	820 °C
Mersen	2114	-	isomolding	fine/superfine	isotropic	-	-	0.026
Great Lakes Carbon Company	H-451	petroleum	extrusion	medium	anisotropic	0.02	0.017	-
Toyo Tanso	IG-110	petroleum	isomolding	fine/superfine	isotropic	0.02	0.018	0.028
Toyo Tanso	IG-430	coal tar pitch	isomolding	fine/superfine	isotropic	0.032	0.016	-
SGL	NBG-17	coal tar pitch	vibromolding	medium	isotropic	0.015	0.015	0.028
SGL	NBG-18	coal tar pitch	vibromolding	medium	isotropic	0.014	0.014	0.026
GrafTech	PCEA	petroleum	extrusion	medium	near-isotropic	0.018	0.019	0.032

Windes et al. (2019a) also plotted creep data from the AGC capsule program with previous values calculated from historical creep studies. The creep coefficients measured from the AGC capsule program were within the range of historical creep coefficients.

Figure 5-18 Comparison of creep coefficients from the AGC program and historical graphites
(Windes et al., 2019a)

5.7   **Summary**

This chapter described the generalized irradiation behavior of graphites before and after the turnaround fluence. Limited experimental data would appear to indicate the following:

- The type of coke used may not influence the strength behavior of irradiated graphite at relatively low doses.

- There is an optimum binder-coke ratio for minimizing volumetric changes associated with irradiation. One study found the optimum binder content to be approximately 11 wt.%.

- Higher graphitization temperatures, which favor increased crystallinity, result in a greater improvement to the elastic modulus after irradiation, a lower CTE, and higher turnaround fluences.

- The relative irradiated elastic modulus for the same grade of graphite tends to be improved when isomolding is used as a forming method compared to extrusion.

- Generic conclusions correlating graphite processing parameters and unirradiated properties with irradiated behavior cannot be reached, given the current state of knowledge.

6 ADDITIONAL LITERATURE AND DETAILED ANALYSIS OF PROPERTIES OF SOME RECENT NUCLEAR-GRADE GRAPHITES

As part of an exhaustive literature review to correlate the source material and processing parameters on unirradiated and irradiated graphites, the authors of this report also reviewed the work of Noda and Inagaki (1962), Dahl (1963), Smith (1964), Collins et al. (1965), Hutcheon and Jenkins (1966), Kelly et al. (1966), Hutcheon (1967), Taylor et al. (1967), Cox and Helm (1969), Kasten et al. (1969), Greenstreet et al. (1969), Engle (1974), Price (1975), Price and Beavan (1975), Engle et al. (1976), Wichner (1976), Brocklehurst (1977), Brocklehurst and Kelly (1979), Maruyama (1993), Kelly (1994), Morgan (1996), Inagaki (2000), Telling and Heggie (2007), Karthik et al. (2011), Nyathi (2011), Tsai et al. (2013), Eapen et al. (2014), Ubic (2014b), Ubic (2014c), Freeman (2016), Srinivasan (2018) and Wang et al. (2019). Despite the depth of this literature review, generic conclusions regarding the source material and processing parameters upon irradiated graphite properties could not be drawn. Many of the data could not be correlated directly to graphite in other studies or did not provide sufficient information related to the variables that define source dependency, making generic conclusions impractical.

This report contains information on the limited research conducted on laboratory-scale processed graphites with variations in processing that have been irradiated and properties determined. There is no evidence, however, that the results of these experiments have played any role in optimizing graphite manufacturing on a commercial scale. To bridge this gap, the appendices contain a thorough evaluation of thermal and mechanical properties before and after irradiation for four modern nuclear-grade graphites—IG-110, and NBG-17, NBG-18, and PCEA—that have been subjected to the most research during the last two decades. Appendix A includes the information from this data collection and analysis.

7   SUMMARY OF MICROSTRUCTURAL AND PROCESSING EFFECTS ON MATERIALS PROPERTIES LISTED IN THE ASME HHA-II-2000 MATERIALS DATA SHEET

This section generally summarizes the microstructural and processing effects on the materials properties listed in the ASME HHA-III-2000 Materials Data Sheet based upon the body of the report and data provided in Appendix A, "Data Compilation of Modern Graphites," and fundamental principles of materials science and fracture mechanics. This summary should not be used to make quantifiable comparisons between different grades of nuclear graphite and only presents general guidelines on the effect of microstructure on graphite properties listed in the data sheet. This summary does not account for many significant and subtle nuances in graphite processing and microstructure; for example, heat treatments on the source coke before the formation of the graphite green body can improve electrical resistivity and reduce the mean CTE on the final graphitized product. Unless explicitly stated, these general trends are specific to unirradiated graphite.

Maximum grain size: The maximum grain size is primarily a function of the coke filler particle size.

Bulk density: Many factors influence the bulk density of the final graphite product. Bulk density increases with an increasing number of pitch impregnations; the extent of density increase decreases with an increasing number of impregnations, regardless of the green forming process. A graded coke filler size distribution is preferred to achieve relatively high green density; however, filler size distribution is also governed by the green compaction process chosen, and this information is generally proprietary to the graphite manufacturer. Anisotropy of the coke filler particles in the mix is a negative factor that reduces packing density and the consequent bulk density of the final product. Molding pressure also affects bulk density. While pressure is necessary to form the green product, increasing molding pressures beyond an optimal level (specific to the component) can have a detrimental effect on the final bulk density of the graphite. Typical binder content in the green mix is usually between 18 and 22 wt.% for manufactured products; reducing the binder-filler ratio below about 9 wt.% has been shown to significantly reduce the bulk density of the final product.

Strength—tensile: Tensile strength generally increases with decreasing grain size and decreasing mean pore size. Increasing graphite crystallinity, as a result of higher graphitization temperatures, reduces tensile strength. In principle, tensile strength increases with decreasing porosity, but most modern graphites have a similar level of porosity of 20 ± 3 volume percent (vol.%). Generally, graphites manufactured from coke with a larger-sized optical texture (needle coke) have lower strengths than graphites manufactured from coke with a smaller-sized optical texture.

Strength—compressive: Compressive strength generally increases with decreasing grain size and decreasing mean pore size. Increasing graphite crystallinity, as result of higher graphitization temperatures, reduces the compressive strength. In principle, compressive strength increases with decreasing porosity, but most modern graphites have a similar level of

porosity of 20 ± 3 vol.%. Generally, graphites manufactured from coke with a larger-sized optical texture (needle coke) have lower strengths than graphites manufactured from coke with a smaller-sized optical texture.

Elastic modulus: The elastic modulus increases with decreasing grain size and decreasing porosity, but most modern graphites have a similar level of porosity of 20 ± 3 vol.%. The elastic modulus of modern nuclear-grade graphite is generally 10 ± 1 GPa, regardless of grain size or processing method.

Coefficient of thermal expansion: The CTE increases with increasing graphite crystallinity, which is the result of higher graphitization temperatures. Generally, graphites manufactured from coke with a larger-sized optical texture (needle coke) have lower CTEs than graphites manufactured from coke with a smaller-sized optical texture. In one study, the binder-filler ratio had a minor effect on the anisotropy CTE, increasing the anisotropy as the binder-filler ratio increased.

Thermal conductivity: Thermal conductivity generally increases with increasing bulk density and decreasing porosity. Thermal conductivity also increases with increasing graphite crystallinity, as a result of higher graphitization temperatures.

Poisson's ratio: Although not explicitly discussed in the body of this report, in principle, Poisson's ratio increases with decreasing porosity. Cost et al. (1968) calculated the theoretical maximum density of isotropic graphite to be 0.31. Experimental measurements of various graphites show Poisson's ratios range between 0.14 and 0.21, but these measurements do not necessarily correlate to density measurements. Most modern graphites have a similar level of porosity of 20 ± 3 vol%. Data from modern graphite grades (Appendix A) indicate that a higher Poisson's ratio corresponds to increased anisotropy.

Anisotropy factor: Isotropy and uniformity throughout the graphite component is affected by the method to form the green body. In general, superior isotropy and uniformity across the graphite product is provided by isomolding, followed by vibrational molding, and finally extrusion, which typically produces the most anisotropic properties and nonuniformity. Needle coke favors anisotropy, but grinding, mixing, and forming processes can overcome the inherent anisotropy of needle coke and result in a highly isotropic graphite.

Critical stress intensity factor: The critical stress intensity factor (K_{Ic}) should be favored by larger grain size, decreasing porosity, and smaller mean pore size. Graphites with larger grain sizes typically have larger mean pore sizes, however. Graphite is a relatively brittle material, and regardless of processing technique and microstructure, K_{Ic} generally ranges between 0.75 and 1.5 MPa $\sqrt{\text{m}}$.

Ratio of compressive and flexural strengths to tensile strength: The ratio of compressive and flexural strengths to tensile strength is subject to a large number of parameters (e.g., the stress profile behavior around critical flaws, the volume of material tested, testing procedure). As such, generalized statements correlating these ratios to the source materials and processing parameters may be inaccurate.

Oxidation resistance/effect of weight loss: Oxidation resistance is improved by higher overall densities, larger grain sizes, lower open-pore densities, and lower levels of impurities. In addition to these microstructural and chemical characteristics, the rate of oxidation weight loss is also dependent upon oxidation temperature. At temperatures approaching the gaseous phase transition regime (≥ 850 degrees C), the oxidation rate of graphite becomes less sensitive to microstructural differences.

Limited data suggest graphite oxidized at higher temperatures (e.g., 750 degrees C (1,382 degrees F) versus 550 degrees C (1,022 degrees F)) may have higher strengths than specimens oxidized to similar mass loss levels at lower temperatures. The reduction of compressive strength for the same level of weight loss appears to be relatively insensitive to grain size and processing method, although oxidation may reduce the compressive strength of lower strength, medium-grained graphite at a slower rate than other modern nuclear-grade graphites. A similar reduction for the tensile strength and elastic modulus among other modern nuclear graphites upon oxidation is expected.

Irradiated graphite: In general, isotropic, fine-grained or medium-grained graphite with a high degree of crystallinity is the preferred choice for permanent GCCs. Limited experimental data would appear to indicate the following:

- The type of coke used does not influence the strength behavior of irradiated graphite at relatively low doses.

- There is an optimum binder content for minimizing volumetric changes associated with irradiation; in one study, the optimum binder content was approximately 11 wt.%.

- Higher graphitization temperatures, which favor increased crystallinity, also result in a greater improvement to the elastic modulus upon irradiation, as well as superior irradiation and higher turnaround fluences.

- The relative elastic modulus for the same grade of graphite tends to be improved when isomolding is used as a forming method compared to extrusion.

8   CONCLUSION

This research effort was devoted to assembling experimental data on properties important to graphite component performance for a variety of graphites used in previously operated and currently operating gas-cooled reactors and graphites proposed for the NGNP project. Assessments were made on the effects of the source material and processing parameters on strength, Young's modulus, fracture toughness, and the CTE of unirradiated graphites. This report also examined the impact of the source material and processing parameters upon graphite degradation, as manifested by the changes to properties when subjected to irradiation.

The effect of these variables on graphite properties was examined from a variety of viewpoints, which included differences in (1) a number of raw material constituents that are used for manufacturing graphite, (2) starting maximum coke filler size and the segregation of coke sizes used in the mix, (3) green processing methods and their process control variables, (4) thermal and impregnation treatments before graphitization, and (5) graphitization temperatures. Sufficient data were collected to provide trending behavior between these source and processing parameters and the resultant properties of unirradiated graphite.

The ASTM nuclear graphite specifications were examined for their adequacy to bound the variabilities in properties due to variations in raw material and other mix formulations for graphite manufacture, the processing methods used, and the purity needs for meeting particular challenges in an HTR environment. ASTM specifications addressed concerns on property variability observed between component-size billets and within billets, by including specific requirements for sampling and testing.

Data related to the irradiation-induced changes in structural safety-significant properties were collected and analyzed to understand how these changes correlated to source and processing parameters. This research uncovered reasonably sufficient data that were of value in this regard, although some were discarded because of the dearth of information related to the variables that define source dependency. For example, several significant sources did not provide any or adequate information on the coke source and type, green-forming variables, number of impregnations, graphitization temperature, test method used for the data, or the irradiation environment, namely, atmosphere and temperature.

Although this research was able to make some observations about graphite's response to irradiation, based on material and forming methods, such as the binder content and graphitization temperature, limited success, if any, has been achieved in correlating the properties of irradiated graphite with those of unirradiated graphite. This is principally due to the scarcity of statistically meaningful data on irradiated graphite and the associated uncertainties, combined with the inherent microstructural variability within graphite that extends from batch to batch, within batches, and between billets. Limited number of microstructural studies (e.g., microscopy, XRD, porosimetry) are aimed at following the changes in graphite in order to gain a mechanistic understanding of the processes involved. This problem has been further compounded by incomplete manufacturing and microstructural information in many studies, making it very difficult to discern the influence of variations in source and processing parameters on the properties of irradiated graphite.

9 REFERENCES

Acheson, E.G., "Manufacture of Graphite," U.S. Patent No. 568,323 (1896).

Adee, L.E., "Manufacture of Petroleum Coke," U.S. Patent No. 3,116,231 (1963).

Albers, T., Miller, D.J., Lewis, I.C., and Ball, D.R., "Low CTE Highly Isotropic Graphite," U.S. Patent No. 7,658,902 B2 (2010).

Al-Haj-Ibrahim, H. and Morsi, B.I., "Desulphurization of Petroleum Coke: A Review," Industrial and Engineering Chemistry Research, 31, 1835–1840 (1992).

ASTM C559, "Standard Test Method for Bulk Density by Physical Measurements of Manufactured Carbon and Graphite Articles," ASTM International, West Conshohocken, PA.

ASTM C611, "Standard Test Method for Electrical Resistivity of Manufactured Carbon and Graphite Articles at Room Temperature," ASTM International, West Conshohocken, PA.

ASTM C747, "Standard Test Method for Moduli of Elasticity and Fundamental Frequencies of Carbon and Graphite Materials by Sonic Resonance," with ASTM International, West Conshohocken, PA.

ASTM C769, "Standard Test Method for Sonic Velocity in Manufactured Carbon and Graphite Materials for Use in Obtaining an Approximate Value of Young's Modulus," ASTM International, West Conshohocken, PA.

ASTM D92, "Standard Test Method for Flash and Fire Points by Cleveland Open Cup Tester," ASTM International, West Conshohocken, PA.

ASTM D2318, "Standard Test Method for Quinoline-Insoluble (QI) Content of Tar and Pitch," ASTM International, West Conshohocken, PA.

ASTM D3104, "Standard Test Method for Softening Point of Pitches (Mettler Softening Point Method)," ASTM International, West Conshohocken, PA.

ASTM D293, "Standard Test Method for the Sieve Analysis of Coke," ASTM International, West Conshohocken, PA.

ASTM D4239, "Standard Test Method for Sulfur in the Analysis Sample of Coal and Coke Using High-Temperature Tube Furnace Combustion," ASTM International, West Conshohocken, PA.

ASTM D4292, "Standard Test Method for Determination of Vibrated Bulk Density of Calcined Petroleum Coke," ASTM International, West Conshohocken, PA.

ASTM D4326, "Standard Test Method for Major and Minor Elements in Coal and Coke Ash by X-Ray Fluorescence," ASTM International, West Conshohocken, PA.

ASTM D4422, "Standard Test Method for Ash in Analysis of Petroleum Coke," ASTM International, West Conshohocken, PA.

ASTM D4746, "Standard Test Method for Determination of Quinoline Insolubles (QI) in Tar and Pitch by Pressure Filtration," ASTM International, West Conshohocken, PA.

ASTM D4866, "Standard Performance Specification for Coal Tar Pitch Emulsion Pavement Sealer Mix Formulations Containing Mineral Aggregates and Optional Polymeric Admixtures," ASTM International, West Conshohocken, PA.

ASTM D5003, "Standard Test Method for Hardgrove Grindability Index (HGI) of Petroleum Coke," ASTM International, West Conshohocken, PA.

ASTM D5187, "Standard Test Method for Determination of Crystallite Size (L_c) of Calcined Petroleum Coke by X-Ray Diffraction," ASTM International, West Conshohocken, PA.

ASTM D6349, "Standard Test Method for Determination of Major and Minor Elements in Coal, Coke, and Solid Residues from Combustion of Coal and Coke by Inductively Coupled Plasma—Atomic Emission Spectrometry," ASTM International, West Conshohocken, PA.

ASTM D7219, "Standard Specification for Isotropic and Near-isotropic Nuclear Graphites," ASTM International, West Conshohocken, PA.

ASTM D7301, "Standard Specification for Nuclear Graphite Suitable for Components Subjected to Low Neutron Irradiation Dose," ASTM International, West Conshohocken, PA.

ASTM D7582, "Standard Test Methods for Proximate Analysis of Coal and Coke by Macro Thermogravimetric Analysis," ASTM International, West Conshohocken, PA.

ASTM E228, "Standard Test Method for Linear Thermal Expansion of Solid Materials with a Vitreous Silica Dilatometer," ASTM International, West Conshohocken, PA.

American Society of Mechanical Engineers (ASME) Boiler and Pressure Vessel Code, Section III, "Rules for Construction of Nuclear Facility Components", Division 5, "High Temperature Reactors" (2017).

Anderson, S.B., Condley, S.D., and McClure C.W., "Method for Making Graphite Electrodes," International Patent Application Number WO2002065483A1 (2002).

AREVA Inc. (AREVA), "NGNP Conceptual Design DDN/PIRT Reconciliation," AREVA Document No. 20004-015, 2009. Available from https://art.inl.gov/NGNP/Subcontractors%20Documents/AREVA/AREVA%20DDN.pdf (accessed on October 29, 2018).

Arregui-Mena J., Edmondson, P.D., Worth, R.N., Contescu, C., Burchell, T.D., and Katoh, Y., "Characterization of the Irradiation Effects in Nuclear Graphite," The Minerals, Metals & Materials Series (eds) TMS 2019 148th Annual Meeting & Exhibition Supplemental Proceedings (2019).

Barrera, M., and Sanchez, H.S., "Design of a Die for the Cold Compaction Calibration of Powdered Materials," Rev. LatinAm. Metal. Mater. S1 (1): 223–234 (2009). Available from

http://citeseerx.ist.psu.edu/viewdoc/download?doi=10.1.1.1064.8120&rep=rep1&type=pdf (accessed on August 23, 2020).

Beck, J.M. and Pincock, L.F., "High Temperature Gas-Cooled Reactors Lessons Learned Applicable to the Next Generation Nuclear Plant," INL/EXT-10-19329, Revision 1, April (2011).

Becraft, L.G, "Method for Producing Isotropic Coke," U.S. Patent No. 5,174,891 (1992).

Bhatia, G., Aggarwal, R.J., Mahur, J.S., and Bahl, O.P., "An Improved Process for the Production of Modified Green Coke Useful for Making High Density Monolithic Graphite," Indian Patent No. 215804 (2008).

Bhattacharya, D., Kumaran, S., Gupta, B.P., Kumar P., Das A., Saidulu G., Kapur, S.D., Bansal, V., Krishnan, V., Krishnan, V., Ghosh, S., Raje N., "Process for the Production of Needle Coke," U.S. Patent No. US20050284793A1 (2004).

Bisplinghoff, B., Lochny, M., Fachinger, J., and Brücher, H., "Radiochemical characterisation of graphite from Juelich experimental reactor (AVR)," Nuclear energy, 39: 311–315 (2000). Available from 20002000https://www.osti.gov/etdeweb/servlets/purl/20184301 (accessed on June 15, 2020).

Block, M.J., Kelley, A.E., and Skripek, M., "Method for Producing Needle Coke," U.S. Patent No. 5,007,987 (1991).

Bradstreet, S.W., "(U) Graphite Technology Project Report," Illinois Institute of Technology, Armour Research Foundation (1958). Available from https://apps.dtic.mil/dtic/tr/fulltext/u2/605690.pdf (accessed on August 23, 2020).

Brocklehurst, J.E., "Fracture in polycrystalline graphite," Chemistry. And Physics of Carbon, 13:145 (1977).

Brocklehurst, J.E., and Kelly, B.T., "Graphite Structure into Relation to Mechanical Engineering Design," 3rd International Working Group on High Temperature Reactors, Gif-sur-Yvette, France, June 11–13 (1979).

Brocklehurst, J.E. and Kelly, B.T., "Analysis of the dimensional changes and structural changes in polycrystalline graphite under fast neutron irradiation," Carbon, 31:155–178 (1993).

Bu, Y., Chang, Z., Dua, J., and Liub, D., "Experimental study on the thermal expansion property and mechanical performance of oil well cement with carbonaceous admixtures," The Royal Society of Chemistry Adv., 7, 29240–29254 (2017). Available from https://pubs.rsc.org/en/content/articlepdf/2017/ra/c7ra03504g (accessed on August 24, 2020).

Burchell, T., Bratton, R., and Windes, W., "NGNP Graphite Selection and Acquisition Strategy," ORNL/TM-2007/153, Oak Ridge National Laboratory (ORNL) (2007).

Burchell, T.D., Erdman, D.L., Lowden, R.R., Hunter, J.A., and Hannel, C.C., "The Fracture Toughness of Nuclear Graphites Grades," ORNL/TM-2016/678, Oak Ridge National Laboratory (ORNL) (2016).

Burchell, T.D, "Section III, Division 5 High Temperature Reactors—Subsection HH, Subpart A, Graphite Materials, GRAPHITE I—Manufacture & Application," presented at the Technical Seminar on Application of ASME Section III to New Materials for High Temperature Reactors, Ottawa, Canada (2018). Available from http://www.nuclearsafety.gc.ca/eng/pdfs/RSP-688-1-graphite-1.pdf (accessed on September 20, 2020).

Burchell, T., "HTGR Technology Course for the Nuclear Regulatory Commission, Module 9, Graphite," Idaho National Laboratory, Idaho Falls, ID, May 24–27, (2010). Available from https://art.inl.gov/NGNP/Training%20Modules%20%20HTGR%20Fundamentals/Module%209%20-%20Graphite.pdf (accessed on January 26, 2020).

Burchell, T.D., Fuller, E.L., Romanoski, G.R., and Strizak, J.P., "Graphite for the Nuclear Industry," Proceedings of a Conference (1991). Available from https://www.osti.gov/servlets/purl/5603483 (accessed on July 21, 2020).

Chen, N.Y. and Walsh, D.E., "Delayed Coking Process," U.S. Patent No. 4,302,324 (1981).

Chi, S-H. and Kim, G-C., "Mrozowski Cracks and Oxidation Behavior of IG-110 and IG-430 Nuclear Graphites," Transactions of the Korean Nuclear Society Spring Meeting, Chuncheon, Korea,
May 25–26 (2006).

Chi, S-H. and Kim, G-C., "Comparison of the oxidation rate and degree of graphitization of selected IG and NBG nuclear graphite grades," Journal of Nuclear Materials, 381:9–14 (2008).

Chi, S-H., and Kim, G-C., "Comparison of Oxidation Characteristics of Selected Nuclear Grade Graphites," KAERI/TR-4017, Korea Atomic Energy Research Institute (2010).

Collins, A.C., Masterson, H.G., and Jennings., P.P., "The Effect of Oxidation on the Compressive Strength of Graphite," Journal Nuclear Materials, 15:135 (1965).

Commissariat à l'énergie atomique (CEA), "Gas-cooled nuclear reactors," A Monograph of the Nuclear Energy Directorate, France (2006).

Contescu, C.I., Mee, R.W., Wang, P., Romanova, A.V., and Burchell, T.D., "Oxidation of PCEA Nuclear Graphite by Low Water Concentrations in Helium," Journal of Nuclear Materials, 453:225–232 (2014).

Cost, J.R., Janowski, K.R., and Rossi, R.C., "Elastic Properties of Isotropic Graphite," The Philosophical Magazine: A Journal of Theoretical Experimental and Applied Physics, 17:148, 851–854, (1968).

Cox, Jr., J.H., and Helm, J.W., "Graphite Irradiations—300–1200 °C," Carbon, 7:319–327 (1969).

Dahl, R.E., "Measuring and Correlating Neutron Exposure and Damage in Graphite," Report HW-79793, Hanford Laboratories, Hanford Atomic Production Operation, Richland, WA (1963). Available from https://www.ipen.br/biblioteca/rel/R10729.pdf (accessed on August 5, 2020).

Dickinson, E.M., "Process for the Production of Premium Coke from Pyrolysis Tar," U.S. Patent No. 4,624,775 (1986).

Doolin, P.K., Kiser, M.D., and Wombles, R.H., "High Coking Value Pitch," U.S. Patent No. 6,352,637 B1 (2002).

Eapen, J., Krishna, R., Burchell, T.D., and Murty., K.L., "Early Damage Mechanisms in Nuclear Grade Graphite under Irradiation," Mater. Res. Lett., 2:43–50 (2014).

Eatherly, W.P., and Piper, E.L., "Manufacture," 21–51, in "Nuclear Graphite," Nightingale, R.E., editor, Academic Press. (1962).

Eguchi, J., Miyasaka, H., Kinouchi, M., Ohashi, Y., Hori, T., and Yamamura, Y., "Process for Producing Petroleum Needle Coke," U.S. Patent No. 5,286,371 (1997).

El-Genk, M.S., and Tournierab, J-M.P., "Comparison of oxidation model predictions with gasification data of IG-110, IG-430 and NBG-25 nuclear graphite," Journal of Nuclear Materials, 420, 1–3, 141–158 (2012).

Engle, G.B., "Density and Structural Distributions in Artificial Graphites," Carbon, 8:485–495 (1970).

Engle, G.B., "The Influence of Pitch-Binder Coke Content on the Properties and Irradiation Behavior of Molded Graphite," Carbon, 9:383–390 (1971a).

Engle, G.B., "Irradiation Behavior of Nuclear Graphites at Elevated Temperatures," Carbon, 9: 539–554 (1971b).

Engle, G.B., and Eatherly, W.P., "High Temperature - High Pressure," 4:143 (1972).

Engle, G.B., Everett, M.R., and Eatherly, W.P., "Status of Graphite Technology and Requirements for HTGRs," Dragon Project Report, DP-REPORT-886, Paper presented at the ANS Topical Meeting on Gas-Cooled Reactors: HTGR and GCFBR at Gatlinburg, TN, on May 8–10 (1974). Available from https://www.osti.gov/etdeweb/servlets/purl/12598525 (accessed on June 15, 2020).

Engle, G.B., Price, R.J., Johnson, W.R., and Beavan, L.A., "Properties and Irradiation Behaviour of Near-Isotropic Graphites for Large HTGRs," Proceedings of the 4th London International Conference on Carbon and Graphite, 757–768, September 23–27, 1974, Society of Chemical Industry, London (1976).

Eto, M., and Growcock, F.B., "Effective Oxidizing Environment and Strength and Oxidation Kinetics of HTGR Graphites. Part I: Reactivity and Strength Loss of H-451, PGX and IG-11 Graphites," NUREG/CR-2480, September (1981).

European Carbon and Graphite Association (ECGA), "Typical Needle Coke Properties," Brussels, Belgium (2018). Available from https://www.carbonandgraphite.org/index.php/raw-materials/cokes (accessed on June 18, 2020).

Nuclear Energy Agency, "Basic Studies in the Field of High Temperature Engineering," Paris, September 27–29 (1999). Available from https://www.oecd-nea.org/science/docs/pubs/hightemp.pdf (accessed on June 15, 2020).

Fischbach, D.B., "The Graphitization Process," Tanso, 63:115–120 (1970).

Freeman, H.M., "Characterisation of Radiation Damage in Nuclear Graphite at the Nanoscale," Ph.D. Thesis, University of Leeds (2016).

Fourré J., Pernollet, A., Delle, W. and Haag, G. "Graphite fur Die Verwendung in Fortgesch Rittenen Kern Reactor Systemen," Proceedings in the International Conference of Carbon-76, Baden-Baden, Germany, 27–28, (1976).

Frohs, W., and Roeßnera, F., "Expansion of carbon artifacts during graphitization—An industrial issue," Tanso, 267:77–83 (2015).

Frolov, A.V., and Dyskina, B.S., "Influence of crushing equipment on the elementary composition of coke," Coke Chemistry. 5429:3–296 (2011).

GA Technologies, Inc., "Design Data Needs Modular High Temperature Gas-Cooled Reactor," DOE-HTGR-86-025, Revision 2, March (1987).

Gallego, N.C., Contescu, C.I., and Burchell, T.D., "XRD and SANS Evaluation of HOPG and Polycrystalline Graphite," ORNL/TM-2018/871 (2018).

General Atomics, "NGNP Technology Development Road Mapping Report," Engineering Services for the Next Generation Nuclear Plant (NGNP) with Hydrogen Production (2008). Available from https://art.inl.gov/NGNP/Subcontractors%20Documents/General%20Atomics/NGNP%20Technology%20Development%20Road%20Mapping%20Report.pdf (accessed on November 1, 2020).

Goval, S.K., Kolstad, J.J., Hauschildt, F.W., Venardos, G., and Joval, M., "Process for Producing Needle Coke," U.S. Patent No. 5,286,371 (1994).

GrafTech International Ltd., Annual Report Form 10-K (2015). Available from https://www.annualreports.com/HostedData/AnnualReportArchive/g/NYSE_GTI_2015.pdf (accessed on August 23, 2020).

Gray, R., Davies, B., van Staveren, T., Li, C., and Joyce, M., "Behaviour of Gilsocarbon Graphite Irradiated to Life Time Dose," 20th International Nuclear Graphite Specialists Meeting, Bruges, Belgium, September 16–19 (2019).

Greenstreet, W.L., Smith, J.E., Yahr, G.T., and Valachovic, R.S., "The Mechanical Behavior of Artificial Graphites as Portrayed by Uniaxial Tests," ORNL Report: ORNL-TM-2727 (1969). Available from https://www.osti.gov/servlets/purl/4739614 (accessed on September 15, 2020).

Growcock, F.B., Barry, J.J., Eto, M., J.H. Heiser, III, J.H., and Sastre, C.S., "Oxidation-Induced Strength Loss in HTGR Graphites," in Advanced Reactor Safety Research Division Quarterly Progress Report, Brookhaven National Laboratory, NUREG/CR-1505, BNl-NUREG-51217, Jan–Mar (1980). Available from https://www.osti.gov/servlets/purl/5046439 (accessed on November 20, 2020).

Haag, G., Mindermann, D., Wilhelmi, G., Persicke, H., and Ulsamer, W., "Development of reactor graphite," Journal Nuclear Materials. 171:41–48 (1990).

Haag, G., "Nuclear Graphite for the HTR Research, Development, and Industrial Production," in "Safety Assessment of the HTR Module in Germany," U.S. Nuclear Regulatory Commission, July 26 (2001). (Agencywide Documents Access and Management System (ADAMS) Accession No. ML021960060)

Haag, G., "Properties of ATR-2E Graphite and Property Changes due to Fast Neutron Irradiation," Jülich Research Centre, Jül-4183, (2005).

Haag, G., "On the Impact of Fast Neutrons on the Macroscopic Structure of Polycrystalline Graphite," 4th EDF Energy Nuclear Graphite Symposium—Engineering Challenges Associated with the Life of Graphite Reactor Cores, 187–194, Nottingham, U.K. (2014).

Haag, G., "Property Changes of Reactor Graphite Due to Fast Neutron Irradiation, Testing Our Knowledge," 20th International Nuclear Graphite Specialists Meeting, Bruges, Belgium (2019).

Haag, G., personal communication to M. Srinivasan, September 25, (2020).

Hauser, J.B., Paspek, S.C., and Adams, H.A., "Method for Determining the Thermal Expansion of Coke," U.S. Patent No. 5,143,689 (1992).

Hayashi, K., "Process for the Production of a Petroleum Pitch or Coke of a High Purity," U.S. Patent No. 4,312,742 (1982).

Heijna, M.C.R., de Groot ,S., Vreeling, J.A., "Comparison of irradiation behaviour of HTR graphite grades", Journal of Nuclear Materials 492:148–156 (2017).

Hennig, G.R., "Catalytic Oxidation of Graphite," Journal of Inorganic Nuclear Chemistry, 24:1129–1137 (1962).

Hoover, D., "Process for the Production of Premium Grade Needle Coke from a Hydrotreated SRC Material," U.S. Patent No. 4,737,261 (1984).

Hsu, H.L., Grindstaff, L.I., and Whittaker, M.P., "Making Non-Puffing Petroleum Coke by Delayed Coking," European Patent No. 0 022 854 (1984).

Hsu, H.L., Grindstaff, L.I., and Whittaker, M.P., "Non-Puffing Petroleum Coke," U.S. Patent No. 4,312,745 (1982).

Huang, W.H., Tsai, S. C., Yang, C. W., Kai, J.J., "The Relationship Between Microstructure and Oxidation Effects of Selected IG- and NBG-Grade Nuclear Graphites," Journal of Nuclear Materials, 454: 149–158 (2014).

Hutcheon, J.M. and Price, M.S.T, Proceedings of the 4th Conference on Carbon, 645 (1960).

Hutcheon, J.M., "The Specification of Materials for Use in Nuclear Reactors," Powder Metallurgy, Vol. 10, No. 20, 65–67 (1967).

Hutcheon, J.M., and Jenkins, M.J., "The Manufacture of Isotropic Graphites of High Thermal Expansion Coefficient," Proceedings of Second Conference on Industrial Carbon and Graphite, Society for the Chemical Industry (1966).

Inagaki, M., "New Carbons: Control of Structure and Functions." Oxford: Elsevier Science, Chapter 1, 6–13 (2000).

International Atomic Energy Agency, "Irradiation Damaging Graphite Due to Fast Neutrons in Fission and Fusion Systems," IAEA-TECDOC-1154, Vienna, Austria (2000).

International Atomic Energy Agency, "Characterization, Treatment and Conditioning of Radioactive Graphite from Decommissioning of Nuclear Reactors," IAEA-TECDOC-152, Vienna, Austria (2006).

International Atomic Energy Agency, "Safety of Nuclear Power Plants: Design," IAEA Safety Standards Series No. SSR-2/1 (Rev.), IAEA, Vienna, Austria (2016).

Ishihara, M., Sumita, J., Shibata, T., Iyoku T., and Oku, T., "Principle design and data of graphite components," Nuclear Engineering and Design, 233:251–260 (2004).

JAERI M-8068, "Effect of Neutron Irradiation on Physical and Mechanical Properties of SM1-24 and IG-11 graphites," Report on JAERI/KFA Jülich Graphite Irradiation Experiment HFR GG-14-, Japan Atomic Energy Research Institute (JAERI) (1979). Available from https://jopss.jaea.go.jp/pdfdata/JAERI-M-8068.pdf (accessed on October 6, 2020).

Kane, J.J., Matthews, A.C., Orme, C.J., Contescu, C.I., Swank, W.D., and Windes, W.E., "Effective gaseous diffusion coefficients of select ultra-fine, super-fine and medium grain nuclear graphite," Carbon, 136:369–379 (2018).

Karika, J.C., "Characterization of Graphitization in Coal Tar and Petroleum Pitches," Report No. AFIT/CI/NR 86-42T, M.S. Thesis Dissertation, Arizona State University (1985). Available from https://apps.dtic.mil/dtic/tr/fulltext/u2/a166942.pdf (accessed on August 28, 2020).

Karthik, C., Kane, J., Butt, D.P., Windes, W.E., and Ubic R., "In situ transmission electron microscopy of electron-beam induced damage process in nuclear grade graphite," Journal Nuclear Materials, 412: 321–326 (2011).

Karvatskii, A., Leleka, S., Pedchenko, A., and Lazarev, T., "Investigation of the current state of isostatic graphite production technology," Industrial and Material Systems, Materials Science, 2:16–21 (2017). DOI: 10.15587/2312-8372.2017.98125.

Kasten, P.R., Bettis, S., Cook, W.H., Eatherly, W.P., Holmes, D.K., Kedl, R.J., Kennedy, C.R., Kirslis, S.S., McCoy, H.E., Perry, A.M., Robertson, R.C., Scott, D., and Strehlow, R.A., "Graphite behavior and its effects on MSBR performance," Nuclear Engineering and Design, 9:157–195 (1969).

Kato, Y., Snead, M., Shih, C., Porter, W., Snead, L., Burchell, T., "Applicability and Limitations of Miniature Specimens for Properties Determination of Fine-Grained Graphite," ASTM Selected Technical Publication 1578, ASTM Symposium on Graphite Testing for Nuclear Applications, Seattle, WA, September 19–September 20, 2013, 1578:65–83 (2015).

Kelly, B.T., Martin, W.H., and Nettley, P.T., "Dimensional Changes in Pyrolytic Graphite Under Fast-Neutron Irradiation," Philosophical Transactions of the Royal Society of London, Series A, Mathematical and Physical Sciences, 260:37–49 (1966).

Kelly, B.T., "Nuclear Reactor Moderator Materials," 365–417, in Volume 10 A, Nuclear Materials, Part 1, Edited by B.R.T. Frost in Materials science and technology: a comprehensive treatment, edited by R.W. Cahn, P. Haasen, E.J. Kramer, v. 10A, Wiley-VCH (1994).

Kelly, B.T., Brocklehurst, J.E., Ashton, B.W., and Martin, W.H., "The Interaction of Radiolytic Oxidation and Fast Neutron Irradiation in CO2-Cooled Reactor Graphite Moderators," Proceedings of the 4th International Conference on Carbon London (1974), 429–437, Society of the Chemical Industry, London (1976).

Kennedy, C.R, "Graphite Having Improved Thermal Shock Resistance and Method of Preparation," U.S. Patent No. 4,190,637 (1980).

Kölling, G., Pietzka, G., Romey, I., and Tillmanns, K., "Method of Producing an Isotropic Coke," U.S. Patent No. 4,289,604 (1981).

Konishi, T., Miki, S., Salstorom, N., Sumita. J., Shibata, T., and Sawa, K., "Quality Control of Nuclear Graphite," 10th International Nuclear Graphite Specialists Meeting, West Yellowstone, MT, September 28–30 (2009).

Kunerth, D.C., McJunkin, T.R., "Nondestructive Evaluation of Nuclear-Grade Graphite," Idaho National Laboratory, Idaho Falls, ID, INL/CON-11-22123, (2011).

Lee, S.M., Kang, D.S. and Roh, J.S. (2015) "Bulk Graphite: Materials and Manufacturing Process," Carbon Letters, 16:135–146 (2015).

Lee, J.J., Ghosh, T.K., and Loyalka, S.K., "Comparison of NBG-18, NBG-17, IG-110 and IG-11 Oxidation Kinetics in Air," Journal of Nuclear Materials, 500: 64–71 (2017). Available from https://www.osti.gov/pages/servlets/purl/1423049 (accessed on October 6, 2010).

Li, K.W., "Manufacture of Petroleum Coke with Fines Recycling," U.S. Patent No. 4,082,650 (1978).

Marek, R.W., Parker, W.E., and Cox, J.H., "Effects of Some Process Temperatures on Radiation Induced Contraction of Graphite," Carbon, 6:349–358 (1968).

Marsden B.J., Hall, G.N., Wouters, O., Vreeling, J.A., and van der Laan, J., "Dimensional and material property changes to irradiated Gilsocarbon graphite irradiated between 650 and 750 °C," Journal of Nuclear Materials 381:62–67 (2008).

Marsden, B.J., and Preston, S.D., "Graphite Selection for the PBMR Reflector," OECD Proceedings, p. 19028, First Information Exchange Meeting on Survey on Basic Studies in the Field of High Temperature Engineering, Paris, September 2–29 (1999). Available from https://www.oecd-nea.org/science/docs/pubs/hightemp.pdf (accessed on June 15, 2020).

Marsden, B.J., Hall, G.N., and Jones, A.N., "Graphite in Gas-Cooled Reactors," in: Konings, R.J.M., and Stoller, R.E. (eds.), "Comprehensive Nuclear Materials," 2nd edition, 4:357–421, Oxford: Elsevier (2020).

Marsden, B.J., "Nuclear Graphite for High Temperature Reactors," U.S. Nuclear Regulatory Commission (2001). (ADAMS Accession No. ML011770379)

Marsh, H., and Latham, C.S., "The Chemistry of Mesophase Formation," in Bacha et al., "Petroleum-Derived Carbons," ACS Symposium Series, American Chemical Society, Washington, DC (1986).

Marsh, H., ed., "Introduction to Carbon Science," Butterworths: Boston (1989).

Maruyama, T., "Effect of Atmosphere on the Bend Strength of Nuclear Graphite," 177–182 in IAEA-TECDOC-690, "The status of graphite development for gas cooled reactors," Proceedings of a Specialists Meeting held in Tokai-mura, Japan, September 9–12, 1991, International Atomic Energy Agency, Vienna, Austria, (1993).

Matsuo, H., "Studies on Thermal Expansion and Neutron Irradiation Effect of Polycrystalline Graphites but," JAERI-M 8367, Japan Atomic Energy Research Institute (1979).

Hideto Matsuo, Tamotsu Saito, Yasuichi Sasaki, Effects of High Temperature Neutron Irradiation on Dimension and Thermal Expansion Coefficient of Nuclear Grade Graphites," Journal of Nuclear Science and Technology 18:863-869 (1981).

Mercuri, R.A., and Criscione, M., "Nuclear Graphite," U.S. Patent No: 4,526,834 (1985).

Miller, D.J., and Ball, D.R., "High Purity Nuclear Graphite," U.S. Patent No. 2009/0324485 A1 (2009).

Mochida, I., Nesumi, Y., and Korai, Y., "Evaluation of Petroleum Residues and Pitches as the Needle Coke Feedstock" (1985). Available from

https://personal.ems.psu.edu/~radovic/1985/papers/1985_257.PDF (accessed on August 24, 2020).

Morgan, W.C., "Nuclear Graphite Development, Operational Problems, and Resolution of these Problems at the Hanford Production Reactors," Proc. of the IAEA Specialists Meeting on Graphite Moderator Lifetime Behaviour, IAEA-TECDOC-901, 69–77, International Atomic Energy Agency, Vienna, Austria (1996).

Murakami, H., "Process for Manufacturing Needle Coke," U.S. Patent No. 4,029,749 (1977).

Murakami, T., Nakaniwa, M., and Nakayama, Y., "Process for the Preparation of Super Needle Coke," U.S. Patent No. 4,814,063 (1989).

Neighbour, G.B., "Development of the Modelling of Dimensional Change in Nuclear Graphites," OECD Proceedings, p. 19028, First Information Exchange Meeting on Survey on Basic Studies in the Field of High Temperature Engineering, Paris, September 27–29 (1999). Available from https://www.oecd-nea.org/science/docs/pubs/hightemp.pdf (accessed on June 15, 2020).

Neighbour, G.B., "Nuclear Graphite: Past and Future Perspectives." Available from http://www.indmin.com/events/download.ashx/document/speaker/8431/a0ID000000X0j50MAB/Presentation (accessed on December 19. 2019).

Nightingale, R.E., "Graphite: Advantages, Limitations, and Applications," Conference Paper, Conf–661003-2" (1966). Available from https://www.osti.gov/servlets/purl/4524408 (accessed on July 23, 2020).

Nightingale, R.E., "Nuclear Graphite," Division of Technical Information, U.S. Atomic Energy Commission, Academic Press (1962).

Nightingale, R.E., Yoshikawa, H.H., and Losty, H.H.W, "Physical Properties," Chapter 6, "Nuclear Graphite," edited by R.E. Nightingale, Academic Press, New York (1962).

Nishiwaki, T., Yasuda, M., and Ito, T., "Graphite Material," U.S. Patent No. 8,367,196 B2 (2013).

Noda, T. and Inagaki, M., "Heat Treatment of Carbon under Various Pressures," Nature, 106:772 (1962).

Nyathi, M.S., "Evaluation of Co-Cokes from Bituminous Coal with Vacuum Resid or Decant Oil and Evaluation of Anthracites, as Precursors to Graphite," Ph.D. Thesis, University of Pennsylvania, Philadelphia, PA (2011).

Önera, F.O., Yürüm, A., and Yürüma, Y., "Structural Characterization of Semicokes Produced from the Pyrolysis of Petroleum Pitches," Journal of Analytical and Applied Pyrolysis (2014).

Orac, T.H., Chang, C.F., Lewis, I.C., and Shao, R.L., "Method of Production of Solids-Free Coal Tar Pitch," U.S. Patent No. 5,843,298 (1998).

PBMR (Pvt) Ltd., "Technical Description of the PBMR Demonstration Power Plant," Revision 4 (2006). (ADAMS Accession No. ML060940293)

Peroomian, M.B., Barsell, A.W., and Saeger, J.C., "Oxide-3: A Computer Code for Analysis of HTGR Steam or Air Ingress Accidents," General Atomic Company Report No. GA-A12493 (1974).

Perruchoud, R., Fischer W., Meier M., and Mannweiler U., "Coke Selection Criteria for Abrasion Resistant Graphitized Cathodes," in Lindsay S.J. (eds), Light Metals 1067-1072 (2011).

Perruchoud the., and Letizia, I., "Measurement of the dimension changes of carbon artifacts during graphitization in a pilot LWG furnace," TANSO, 249:168–173 (2011).

Pierson, H.O., "Handbook of Carbon, Graphite, Diamond and Fullerenes," Properties, Processing and Applications, Noyes Publications, Park Ridge, NJ (1993).

POCO Graphite, Inc., "Properties and Characteristics of Graphite for Industrial Applications" (2015).

Price, R.J., "Mechanical Properties of Graphite for High Temperature Gas Cooled Reactors: A Review," General Atomics Report No. GA-A13524, UC-77 (1975).

Price, R.J., and Beavan, L.A., "Final Report on Graphite Irradiation Test, OG-2," General Atomics Report No. GA-A 13556, UC-77 (1975).

Ragoss, A., Fitzer, E., Nedopil, E., and Buhmann, A., U.S. Patent No. 3,035,308 (1962).

Sato, E., Shiwa, M., Shinagawa, Y., Ida, T., Yamazoe, S., Sato, A., "Ultrasonic Testing Method for Detection of Planar Flaws in Graphite Material," Material Transactions, 48: 1227-1235 (2007).

Sato, S., Ishihara, M., Hirakawa, K., Kiyono, S., and Inoue, Y., "Optimum Particle Size Distribution of Coke for Graphite Electrode Determined by Thermal Shock Testing" (1985). Available from https://personal.ems.psu.edu/~radovic/1985/papers/1985_452.PDF (accessed on August 23, 2020).

Sawa, K., Ueta, S., and Iyoku, T., "The High Temperature Gas Cooled Reactor Fuel," Paper 1221, GENES4/ANP2003, Kyoto, Japan, September 15–19, (2003).

Sawran, W.R., Turrill, F.H., Newman, J.W., Hall, N.W., and Ward, C., "Process for the Manufacture of Carbon Fibers and Feedstock Therefore," U.S. Patent No. 4,761,864 (1987).

SGL Group, "Investor Relations Presentation," The Carbon Company (2015). Available from https://irpages2.eqs.com/download/companies/sglcarbon/Presentations/Investor-Relations-Presentation-July-2015.pdf (accessed on June 24, 2020).

Shen, K., Yu, S., and Kang, F., "The microstructure texture of Gilsocarbon graphite," Carbon, 153:428–437 (2019).

Smith, J., "Manufacture of Petroleum Coke," U.S. Patent No. 3,173,852 (1965).

Smith, M.C., "CMF-13 Research on Carbon and Graphite Report No. 13, Summary of Progress from February 1 to April 30, 1970," Los Alamos Scientific Laboratory Report No. LA-4480-MS, July (1970).

Smith, M.C., "Effects of Temperature and Strain Rate on Transverse Tensile Properties of H4LM Graphite Tested in Helium and in Vacuum," Carbon, 1, 147 (1964).

Spahr, M., Cattaneo, A., and Stgreb, K., "Method for Producing Graphite Powder with An Increased Bulk Density," U.S. Patent 7,115,221 B1 (2006).

Srinivasan, M., "Optimizing Fracture Mechanics Specimen Design for Fine Grain Graphite and Analysis," 19th International Nuclear Graphite Specialists Meeting (INGSM-19), Shanghai, China, September 2–6 (2018).

Stiller, A.H., Zondlo, J.W., and Stansberry, P.G., "Method of Producing High Quality, High Purity, Isostatic Graphite from Coal," U.S. Patent No. 5,705,139 (1998).

Suetsugu, Y., and H. Miyazaki, "Process for Producing Needle-Shaped Coal Pitch Coke," U.S. Patent No. 3,799,865 (1974).

Tahon, B., personal communication to M. Srinivasan (2018).

Taylor, R., Brown, R.G., Gilchrist, K., Hall, E., Hodds, A.T., Kelly, B.T., and Morris, F., "The Mechanical Behavior of Reactor Graphite," Carbon, 5:519–531 (1967).

Telling, R.H., and Heggie, M.I., "Radiation Defects in Graphite," Philosophical Magazine, 87:4,797–4,846 (2007).

The Open University, Available from https://www.open.edu/openlearn/science-maths-technology/engineering-technology/manupedia/cold-isostatic-pressing (accessed on April 20, 2021).

Thrower, "Microstructure of Carbon Materials," in Proceedings of the Workshop on the Electrochemistry of Carbon, Ed. Sarangapani, S., Akridge, J.R., and Schumm, B., Proc. 84-5:40–60 (1983).

Tsai, S-C., Huang, E-W., Kai, J.J., and Chen, F-R, "Microstructural evolution of nuclear grade graphite induced by ion irradiation at high temperature environment," Journal of Nuclear Materials, 434:17–23 (2013).

U.S. Nuclear Regulatory Commission, "Guidance for Developing Principal Design Criteria for Non-Light-Water Reactors," Regulatory Guide 1.232. (ADAMS Accession No. ML17325A611)

Ubic, R., "Microstructural characterization and pore structure analysis of nuclear graphite," in "Irradiation Creep in Graphite," Final Report of Project No. 09-794, Idaho National Laboratory, Idaho Falls, ID, (2014a). Available from https://www.osti.gov/servlets/purl/1128528 (accessed on September 18, 2020).

Ubic, R., "Simulated neutron-induced damage process in nuclear graphite," in "Irradiation Creep in Graphite," Final Report of Project No. 09-794, Idaho National Laboratory (2014b). Available from https://www.osti.gov/servlets/purl/1128528 (accessed on September 18, 2020).

Ubic, R., "Irradiation Creep in Graphite," Final Report of Project No. 09-794, Idaho National Laboratory (2014c). Available from https://www.osti.gov/servlets/purl/1128528 (accessed on September 18, 2020).

UCAR Carbon Company Inc., in Chapter One, "The Manufacture of Carbon and Graphite," Industrial Graphite Engineering Handbook (2001).

Ueta, S., Aihara, J., Sakaba, N., Honda, M., Furihata, N., and Sawa, K., "Fuel performance under continuous high temperature operation of the HTTR," Journal of Nuclear Science and Technology, 51:1345–1354 (2014).

Valesquez, C., Johnson, W., Hightower, G., and Burnette, R., "The Effect of Steam Oxidation on the Strength and Elastic Modulus of Graphite H-451," General Atomic Company Report, GA-A14657 (1978).

Wang, S.M., Wang, Y., Wang, Y.X., Liu, F.P., and Cao, J., "Stresses State and Mechanical Behaviors of the Green Body During Die Compaction and Ejection Process," Acta Metallurgica Sinica (English Letters) 33:605–614 (2020).

Wang, Z., Palmer, N., Muránsky, O., Zhu, H., Karatchevtseva, I., Ionescu, M., Munroe, P., and Windes, W., "Ion irradiation induced damage in graphite and its recovery," INGSM 20, September 16–19, Bruges, Belgium (2019).

Westinghouse Electric Company LLC, "Next Generation Nuclear Plant, Conceptual Design Study, Design Data Needs (DDNs), Reconciliation against PIRTs," NGNP-CDWP TI-DDN, Revision 1 (2009b). Available from https://art.inl.gov/NGNP/Subcontractors%20Documents/Westinghouse/WEC%20DDN.pdf (accessed June 2, 2019).

White, J.L., "The Formation of Microstructure in Graphitizable Materials," Progress in Solid State Chemistry, Vol. 9, 59–104 (1975).

Wichner, R.P., "Effect of Steam Corrosion on Core Post Strength Loss: I. Low, Chronic Steam Ingress Rates," ORNL/TM-5534, Oak Ridge National Laboratory, Oak Ridge, TN 87830, (1976).

Windes, W., Burchell, T., Carroll, M., "Graphite Technology Development Plan," INL/EXT-07-13165, Idaho National Laboratory, Idaho Falls, ID, (2010).

Windes, W.E., Rohrbaugh, D.T, Swank, W.D., and Lord, J., "AGC-2 Graphite Preirradiation Data Analysis Report," INL/EXT-13-28612, Revision 1, Idaho National Laboratory, Idaho Falls, ID, August (2013).

Windes, W.E., Rohrbaugh, D.T, Swank, W.D., "AGC-3 Irradiation Creep Strain Data Analysis," Idaho National Laboratory, Idaho Falls, ID, Idaho National Laboratory, Idaho Falls, ID (2019a).

Windes, W., Matthews, A., Joshua J., and Swank, D.W., "The Degradation of Strength under Varying Oxidizing Conditions for Nuclear Graphite," INL/EXT-19-53623, Idaho National Laboratory, Idaho Falls, ID (2019b).

Wright, R., and Windes, W., "Nuclear Graphite Components," NRC HTGR Training, July 16–17 (2019). Available from https://www.nrc.gov/docs/ML1921/ML19214A096.pdf (accessed on November 1, 2020).

Yang, H., Chen, Y., Li, H., Huang, D., and Wu, H., "Nuclear Graphite Development and Neutron Irradiation Testing Programme in Sinosteel AMC," 15th International Nuclear Graphite Specialists Meeting, Hangzhou, China, September 15–18 (2014).

Yu, S., and Sun, L., "The Design of HTR-PM Graphite Internals," Nuclear Science and Engineering Institute, University of Missouri-Columbia, July 12 (2010).

Zhang, Z., and Wang, Q., "The New Method of XRD Measurement of the Degree of Disorder for Anode Coke Material," Crystals, 7, 5 (2017).

Zhou, X., "Nuclear graphite for high temperature gas cooled reactors," New Carbon Materials, 32(3):193–204 (2017).